Republic of Iraq
Ministry of Higher Education & Scientific Research
University of Babylon
College of Education for Pure Sciences
Department of Physics

Effect of Some Molecules Adsorption on the Electronic and Optical Properties of HfSSe Monolayer

A Thesis

Submitted to the Council of the College of Education for Pure Sciences, University of Babylon in Partial Fulfillment of the Requirements for the Degree of Master in Education / Physics

By

Ghufran Falah Ibrahim Hassan
B. E. Sc. (Physics)
(University of Babylon 2013)

Supervised by

Prof. Dr. Shurooq Sabah Abed Al-Abbas

2022 A.D. 1444 A.H.

بِسْمِ اللهِ الرَّحْمَنِ الرَّحِيمِ

وَإِذَا سَأَلَكَ عِبَادِي عَنِّي فَإِنِّي
قَرِيبٌ ۖ أُجِيبُ دَعْوَةَ الدَّاعِ إِذَا
دَعَانِ ۖ فَلْيَسْتَجِيبُوا لِي وَلْيُؤْمِنُوا
بِي لَعَلَّهُمْ يَرْشُدُونَ

صدق الله العظيم

سورة البقرة , الآية (186)

Dedication

This achievement is dedicated to my God (The Almighty)that through this journey has given me strength

To the lovely people who brighten my life,

To whom the most beautiful words in the world do not describe,

To the person who supported me and shared with me every moment l lived, and l had a friend ,a lover, and a family

My dear husband Hassanein

The lights of my eyes my children

(Yunus and Lara)

With all my gratitude

Ghufran

Acknowledgement

Praise be to Allah, Lord of the worlds, and prayers and peace be upon the most honorable prophet our Prophet Muhammad and all his family and companions.

I thank Allah abundantly for guiding me and helping me to complete this research, I extend my gratitude to Professor Dr. (**Shurooq Sabah Abdul-Abbas**),my special thanks go to the Professor Dr. *(***Hamad Rahman Jappor***)*, for his generosity, high morals, and distinguished style in following up with the study. I ask Allah to reward him with the best reward. Thanks to all my family members and all my friends, especially Mr. Youssef Abdel Hakim and all my classmates.

Ghufran

Abstract

The density functional theory (DFT) method have been used to study the electronic, optical and the adsorption properties of (CO,CO_2,NO,NO_2 and SO_2) gas molecules on HfSSe (Se and S) monolayer. Initially, the properties of pristine HfSSe monolayer are calculated. The band gap of HfSSe (Se and S) monolayer is estimated to be (0.620eV), which authorize the semiconducting behavior. The absorption coefficients of pristine HfSSe can reach to 10^6 cm^{-1},which are comparable to the Perovskite solar cells. The results show that the adsorption of gases occurs at different sites on the studied monolayer. However, all the adsorption energies are negative and the adsorption of gas molecules on this monolayer undergoes physisorption interaction, thus they can be used to detecting gas molecules. It has been calculateded that the interactions between above mentioned monolayer and the gas molecules are the energy band structure of the monolayer are substantially affected. In addition, band structures of HfSSe (Se,S) monolayer after the adsorption of NO gas that it is conductive. In addition, band structures of HfSSe monolayer after the adsorption of SO_2gas ,the band gaps of the adsorbed systems in HfSSe of Se is conductive and the band gap in HfSSe of S is (0.025 eV). The optical properties of this monolayer can be modified by the adsorption of gas molecules. The refractive indices of HfSSe-S monolayer are larger than that in HfSSe-Se monolayer, and reach to 2.50 and 2.31 of CO_2 and SO_2gases,respectively. On the other hand, the reflection peaks of the monolayer occur in the UV region range which agrees with the absorption coefficient. Besides, the maximum value of reflectivity in the adsorbed systems does not exceed 60%. It has been concluded that the HfSSe monolayer is more suitable as a gas sensor for CO,CO_2,NO,NO_2 and SO_2 due to the existence of the desorption process. Finally,

the calculations provide an effective method to modulate the electronic ,and optical properties of the HfSSe monolayer for optoelectronic and nanodevices applications.

Contents

List of Figures

List of Symbols

Symbol	Description
2D	Two Dimensional
$TMDC_s$	Transition Metal Di-chalcogenides
Hf	Hafnium
S	Sulfur
Se	Seleinum
MO	Molecular Orbital
MOS_2	Molybdenum Disulfide
MoSSe	Molybdenum Sulfur Seleinum
Zr	Zirconium
$ZrSe_2$	ZirconiumDiselenide
$HfSe_2$	Hafnium Diselenide
HfS_2	Hafnium Disulfide
CO	Carbon Monoxide
CO_2	Carbon Dioxide
NO	Nitrogen Monoxide
NO_2	Nitrogen Dioxide
SO_2	Sulfur Dioxide
DFT	Density Functional Theory
HfSSe	Hafnium Sulfur Seleinum
CVT	Chemical Vapor Transport
$AGNR_s$	Armchair Graphene Nanoribbons

NH_3	Ammonia
PBE	Perdew,Burke and Ernzerhof Functional
GaSe	Gallium Seleinum
H_2S	Hydrogen Sulfur
GaN	Gallium Nitride
CH_4	Methane
Ψ	Wave Function
$\hat{H}$	Hamiltonian Operator
E	Total Energy
$\hat{T}$	Kinetic Energy Operator
$\hat{V}$	Potential Energy
$\hat{T}_e$	Kinetic Energy Operator for the Electrons
$\hat{T}_n$	Kinetic Energy Operator for the Nuclei
$\hat{V}_{ne}$	Potential Energy between Electron-Nucleus
$\hat{V}_{ee}$	Potential Energy between Electron-Electron
$\hat{V}_{nn}$	Potential Energy between Nucleus-Nucleus
ħ	Planck's Constant /2π
∇^2	Laplacian Operator
$V(r,R)$	The Potential Energy of all Electrons and Nuclei
m_I	Mass of Electron
M_a	Mass of Nucleus
ε_o	Vacuum Permittivity

$Z_{a,b}$	Charge of Nuclei a and b
r_{Ia}	Distance between Electron I and Nucleus a
r_{IJ}	Distance between Electron I and Electron J
R_{ab}	Distance between a Nucleus and b Nucleus
a_o	Bohr radius=0.529177Å
$\widehat{H}_{tot}$	Total Hamiltonian Operator
Ψ_{tot}	Total Wave Function
$E_{\mathbf{\Phi}}$	Lowest Energy Eigen Value of the Trial Function
Φ	Trial Function
E_o	Ground-State Energy
SCF	Self Consistent Field
N	Normalization Factor
ε_i	The Electronic Energy
LCAO	Linear Combination Atomic Orbital
Ψ_i	Molecular Orbitals
F	Fock Operator
J_l	Coulomb Operator
K_l	Exchange Opetator
Φ_μ	Basis Functions
$C_{\mu i}$	The Expansion Coefficients
$\rho(r)$	Function of Electron Density
N	Number of Electrons

HK	Hohenberg-Kohn
$V_{ext}(r)$	External Potential
$E_{NC}[\rho]$	Non-Classical Energy
$J[\rho_0]$	Classical Coulomb Energy
$F_{HK}[\rho]$	Hohenberg-Kohn Operator
$T_S[\rho]$	Kinetic Energy of Non-Interacting Electron System
$E_{xc}[\rho]$	Exchange-Correlation Energy
δE	The Variation of E
$\phi_i(r)$	Kohn–Sham Orbital's
$V_{xc}[r]$	Exchange-Correlation Potential
φ^{λ}	Wave Function to the Hamilton Operator
ρ_{xc}	The Averaged Exchange–Correlation Density
$\bar{h}(r_1, r_2)$	The Averaged Pair Correlation Function
$\rho\,{}^{\lambda}_{2}(r_1, r_2)$	The Diagonal Part of the Two–Particle Density Matrix
E_c^{ks}	The Hartree–Fock exchange energy
Φ_P	Kohn –Sham Determinant
Ψ_{ρ}	The Exact Interacting Wave Function
$LSDA$	Local Spin Density Approximation
LDA	Local Density Approximation
ε_{xc}	The Exchange-Correlation Energy
ρ_{α}	The Density of Spin Up
ρ_{β}	The Density of Spin Down
GGA	Generalized Gradient Approximation

EHG	Homogeeous Electron Gas
ϵ_x^{PBE}	The Exchange Part of Perdew,Burke and Ernzerhof Functional
F_x^{PBE}	The Exchange Enhanceement factor to the HEG
ϵ_x^{HEG}	The Exchange Part of the homogeneous electron gas
r_s	The Local Value of the Density Parameter
$H(r_s, \zeta, t)$	Correlation enhancement factor to the HEG
$(n^{\downarrow} - n^{\uparrow})$ /n	The Spin Polarization
K_{TF}^{n}	The Thomas-Fermi screening
γ, β	Constant of PBE
CASTEP	Cambridge Sequential Total Energy Package
E_v	Valence Energy
E_c	Conduction Energy
VB	Valence Band
CB	Conduction Band
DOS	Density of States
g(E)	The Electron Density of States
3D	Three-Dimensional
L^3	System of Volum
m^*	Effective Mass
QW_s	Quantum Wells
QWR_s	Quantum Wires
QD_s	Quantum Dots

L	Length of the 1D System
PDOS	Partial Density of States
$\alpha(\omega)$	Absorption Cefficient
$\sigma(\omega)$	Conductivity
$n(\omega)$	Refractive Index
$R(\omega)$	Reflectivity
$L(\omega)$	Energy Loss Function
$\varepsilon(\omega)$	Dielectric Function
ω	The Cyclic Frequency
VBM	Valence Band Maximum
CBM	Conduction Band Minimum
$HSE06$	Heyd-Scuseria-Ernzerhof 2006
UV	UItraviolet
E_{Tot}	Total Energy
E_{ad}	Adsorption Energy
TDOS	Total Density of States
Re	Real Part
Im	Imaginary Part
IR	Infraed

List of Tables

Chapter One Introduction and Previous studies

1.1 General Introduction:

Due to its band gap tunability, atomically thick layer, unusual density of states, and mechanical strength, two-dimensional (2D) transition metal di-chalcogenides (TMDCs) have attracted a lot of attention in the field of electronics and optoelectronics in recent years [1]. Several experimental and theoretical investigations show that they might be extremely interesting materials with a reasonable band gap beyond 2D graphene for a variety of applications, electronic [2], optoelectronic [3], thermoelectric [4], gas sensing [5], water splitting [6] and piezoelectric applications[7]. These TMDCs, which have the generic formula MXY (where M=Mo, W, Hf, Zr, Pt, etc. and X,Y=S, Se, and Te), are layered materials with extremely weak Van der Waal interlayer contact, with one transition metal layer sandwiched by two chalcogen atoms layers. Recently, Ang-Yu Lu and colleagues (Ang-Yu Lu et al.) [8]. The top layer S atoms in monolayer MoS_2 were totally replaced by Se atoms, resulting in Janus monolayer MoSSe with broken in-plane inversion symmetry and out of plane mirror symmetry. Taking inspiration from experimental synthesis [8,9]. Various research on the electrical, optical, mechanical, thermoelectric, photocatylatic, gas sensing, and mechanical characteristics of Janus monolayer MoSSe have been carried out [10]. In Janus monolayer TMDCs, the lack of in-plane inversion symmetry and out-of-plane mirror symmetry results in valley polarization and Rashba spin splitting, making them attractive candidates for electronics and valleytronics [11]. The synthesis of $ZrSe_2$ and $HfSe_2$ in the lab and the construction of devices with on/off ratios more than 10^6 show that these might be viable materials for low-power electronic devices [12]. By adding structural defects and dopants, the electrical, optical, and thermoelectric characteristics may adjust, and increase thermoelectric and

optoelectronic capabilities can be exhibited in monolayer HfS_2 [13]. At this day, gas contaminations continue to be a serious stumbling block to social progress and economic prosperity [14]. These harmful gases are still being created uncontrollably in hundreds of facilities throughout the world, and the risk of contaminating gas leakage persists. The failure to remove and eradicate these harmful gases poses a serious risk to human health and the environment. In this regard, early identification and management of harmful gases are critical to preventing the damage of our ecosystem. Among 2D materials, many studies have focused on graphene [15–17], germanene [18–20], phosphorene [21,22], silicene [23,24], stanene [25,26], towards the adsorption and monitoring processes of gas or as a support for different catalysts owing to their low dimensions and large surface area. In the present work, the electronic and optical properties of gas molecules (including CO, CO_2, NO, NO_2, SO_2) adsorbed on HfSSe monolayer are inspected based on the density functional theory (DFT). Besides, further focused attention on the adsorption comportment of these molecules on HfSSe monolayer to perceive the possibility of benefit this monolayer as sensors for the gases mentioned above, which may experimental efforts in the field of gas sensor applications.

1.2 HfSSe

Due to its fascinating electrical and optical characteristics, hafnium (Hf) based chalcogenides have recently gained a lot of attention [27,28], The high mobility (1800 to 3500 $cm^2V^{-1}S^{-1}$) and broad absorption spectral range are especially appealing (1-2 eV). A few papers on the photoelectronic characteristics of HfS_2 and $HfSe_2$ have been published [29–33]. However, broadband photodetection is less effective with these dichalcogenides. In comparison to binary HfS_2-$HfSe_2$ end compounds, the HfSSe alloy has more degrees of freedom when it comes to customizing band gaps [34,35]. It is promising for broadband detection with quick

photoresponse. Recently, a 2D layered HfSSe film was reported to have been formed over a wide area of sapphire substrate using chemical vapor deposition (CVD), and the optoelectronic characteristics were dramatically modified by adjusting the S/Se ratio [36]. The van der Waals interaction between adjacent layers of hexagonal symmetry in the HfSSe compound allows easy exfoliation into monolayer HfSSe or few layered nanoflakes, which adds more variables on the tuning of electrical and optoelectronic properties for device fabrication. Although the outstanding adjustable optoelectronic capabilities of HfSSe compounds drew a lot of interest, growing high-quality single crystals with good crystallinity remains a problem, owing to the difficulty in achieving a homogenous distribution of chemical elements in single crystals [37]. The intermetallic element's incongruent melt and non-volatile nature, in particular, have ruled out single crystal development using traditional solution melt-growth procedures [38]. Chemical vapor transportation (CVT)method, It has been demonstrated that this approach may efficiently generate single crystals of complicated materials with incongruent melt behavior [38]. CVT approach provides the best potential for generating complicated chalcogenide high-quality single crystals by utilizing a thermodynamically equilibrated vapor phase chemical reaction in the presence of the right transporting agent. Fig.(1.1) Note that the charge density in the region between Hf–S and Hf–Se is relatively large, which is due to the interaction between Hf(5d)-S(3p) and Hf(5d)-Se(4p) states as mentioned above. Results may imply an important presence of the covalent chemical bond in the monolayer at hand[39].

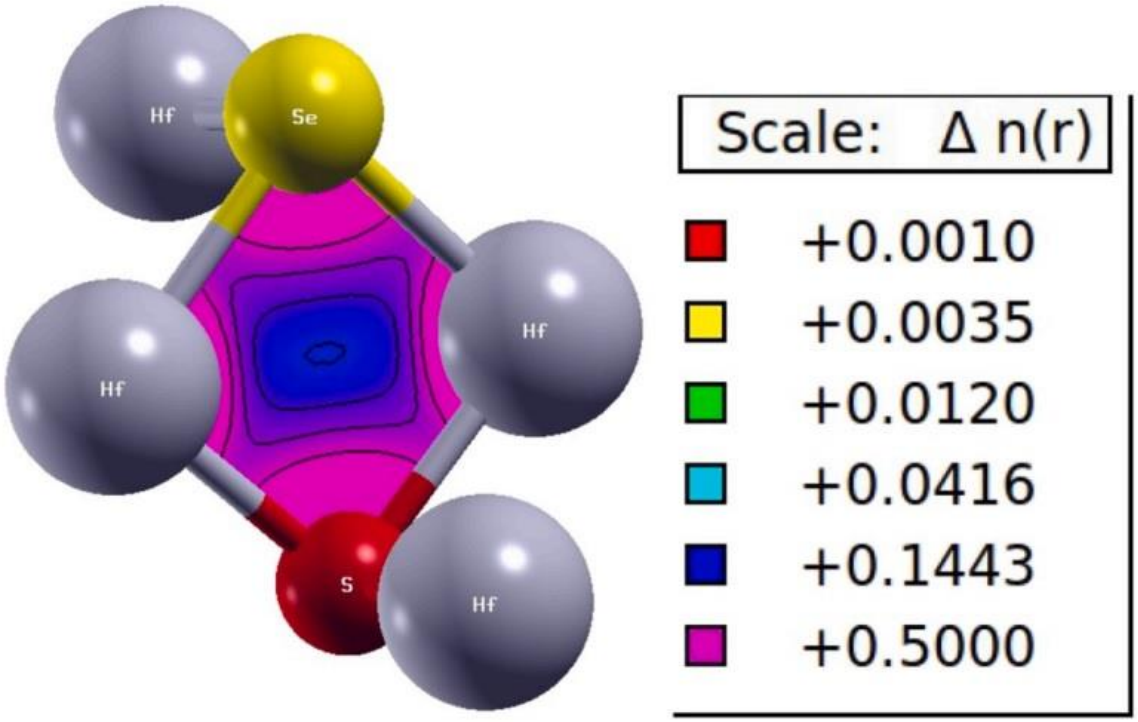

Fig. (1.1) Charge density distribution in HfSSe Janus monolayer [39].

1.3 Adsorption

The adherence of atoms, ions, or molecules from a gas, liquid, or molten solid to a surface is known as adsorption[40]. Adsorption, in other words, is the accumulation of particles (adsorbate) at a surface. The adsorption process results in the formation of an adsorbate coating on the adsorbent's surface. adsorption occurs when a fluid (the adsorbate) is dissolved by permeates, which are liquids or solids. There are two types of adsorption processes: physisorption (characterized by mild van der Waals forces) and chemisorption (characterized by strong van der Waals forces) (characteristic of covalent bonding). It might also happen as a result of electrostatic attraction.

Physisorption is a particularly efficient process that happens at temperatures near to a gas's critical temperature. Chemisorption normally takes place at temperatures much over the critical temperature [41].

1.4 Previous studies

A. Saffarzadeh *et al*. in 2010 [42] By applied the results of ab initio calculations to the single-band tight-binding approximation, a theory for studying gas molecules adsorption on armchair graphene nanoribbons (AGNRs) was proposed. They demonstrated that the states contributed by CO and NO molecules are quite localized near the center of the original band gap, implying that charge transport in such systems cannot be significantly improved, despite the fact that the adsorbed CO_2 and NH_3 molecules act as acceptor and donor, respectively. Low gas concentrations were found to be in good agreement with those derived using DFT simulations.

Q. Yue *et al*. in 2013 [43] Investigated the adsorption of several gas molecules (H_2, O_2, H_2O, NH_3, NO, NO_2, and CO) on a MoS_2 monolayer using first-principle calculations based on the density functional theory (DFT). It is possible to acquire the most stable adsorption configuration, adsorption energy, and charge transfer. The molecules (H_2, O_2, H_2O, NO, NO_2, and CO) are found to be weakly adsorbed on the monolayer MoS_2 surface and operate as charge acceptors for the monolayer, with the exception of the NH_3 molecule, which is discovered to be a charge donor. Furthermore, they demonstrated that a perpendicular electric field may considerably influence charge transfer between the adsorbed molecule and MoS_2.

Their theoretical findings are in line with recent tests, indicating that MoS_2 might be used in gas sensing applications.

C. Zhou *et al*. in 2017 [44] Used the functional density approach and the PBE approximation, investigate the influence of stress on charge transmission during the adsorption of a group of gas molecules on the GaSe monolayer. They discovered that the adsorption effects of the gas molecules under investigation were the same, and that the changes in the valence and conductivity bands were minor. The impact of two-axis stress on charge transfer was also examined. It was discovered that the stress effect had no influence on GaSe monolayer adsorption.

X. Sun *et al* in 2017 [45] Investigated the characteristics of adsorption of gas molecules (CO, NH_3, H_2S, NO_2, NO, SO_2) on the surface of single-layer indium nitride, apply first-principles calculations inside DFT (InN). To find the most sensitive adsorption site, four distinct adsorption sites (Bridge, In, N, and Hollow) were chosen. The most energetic favorable spot is varied between N site and in site for distinct gas molecules, based on adsorption energy, charge transfer, and band gap. Furthermore, the results demonstrate that InN is chemisorption or physisorption sensitive to SO_2, NO_2, H_2S, and NH_3, and that the applied electric field has a considerable influence on the adsorption process. Furthermore, most of the gas adsorptions will alter the optical characteristics of the InN monolayer.

H. Jappor and M. Habeeb in 2018[46] Used first-principles computations, explore the optical characteristics of GaS and GaSe monolayers. Up to 35 eV, the optical characteristics are investigated. The results show that the optical characteristics of the GaS monolayer were equivalent to those of the GaSe monolayer with minor information contrasts. Furthermore, absorption begins in the

visible spectrum but peaks in the ultraviolet (UV) spectrum. They discovered that both monolayers' optical characteristics are achieved in the UV range, and the results are important. As a result, it may be employed in solar cells, UV optical nanodevices, nanoelectronic, optoelectronic, and photocatalytic applications as a very promising material.

G. Chen *et al.* in 2019 [47] The structural, kinetic, electronic, and magnetic characteristics of hazardous gas molecules (H_2S, NH_3, and SO_2) adsorbed on pristine and transition metal atom (Fe, Mn) doped GaN monolayers are studied using corrected DFT. The results reveal that H_2S and NH_3 are physisorbed with low adsorption energy, charge transfer, and a long adsorption distance on virgin GaN monolayers. While it is possible to acquire the chemical adsorption character of SO_2 on GaN monolayer, this suggests that the virgin GaN monolayer is susceptible to SO_2. They discovered that adding Fe and Mn dopants to a pure GaN monolayer improves its adsorption ability. Except for SO_2 adsorbed Fe doped GaN monolayer, Fe and Mn doping can boost adsorption energy and charge transfer of adsorbed systems.

V. Ye *et al.* in 2019 [48] DFT computations are used to explore the interaction between gas molecules (CO, CO_2, O_2, NO, NH_3, SO_2, and NO_2) and the SnSe monolayer. They discovered that the SnSe monolayer had a higher affinity for SO_2 and NO_2, as well as adequate adsorption energies (-6.000 eV and -0.759 eV) and higher charge transfers (-0.239 e and -0.328 e). Also, chemical adsorption of NO_2 was seen on the SnSe monolayer, however physically adsorbing SO_2 was shown to be more suited for the adsorption mode of SO_2 sensors, since the adsorption quantity of SO_2 is 6 times that of NO_2. As a result, adsorption of SO_2 is more

frequent than adsorption of other gas molecules. The SnSe monolayer might also be a good choice for high selectivity and sensitivity SO_2 sensors.

V. Tian *et al.* in 2019 [49] Studied the adsorption behavior of five typical gas molecules (CH_4, N_2, H_2, CO, and H_2S) on the surface of monolayer GeP_3, we used a first-principles computation. According to their calculations, the GeP_3 monolayer may adsorb these gas molecules directly. There are also significant adsorption energies and charge exchanges between the GeP_3 monolayer and the gas molecules. The electrical behavior of the GeP_3 monolayer can be substantially modified after adsorbing these gas molecules. Furthermore, at 300 K, the predicted recovery time of a monolayer GeP_3-based sensor is appropriate for CH_4, N_2, and H_2. Their findings show that monolayer GeP_3 might be useful in molecular sensors for CH_4, N_2, and H_2.

V. Kumar and D. R Roy in 2019 [50] The influence of gas adsorption (NO_2, SO_2, CO_2, and NH_3) on the structural, electrical, and vibrational characteristics of stanane monolayer was studied in detail using DFT. These gas molecules' most stable configuration, electrical characteristics, adsorption energies, and charge transfer on stanane are all researched and explained in detail. After contact with gas molecules, the band gap of pure stanane (0.52 eV) is shown to shift. Adsorption of NO_2, SO_2, NH_3, and CO_2 gas molecules on p-type stanane-based material results in changes in the energy band gap and charge density. The findings indicate that the selectivity of hydrogenated stanane-based gas sensors is critical for improving their sensitivity. In this experiment, it was discovered that all gas molecules function as charge donors.

N.ghobadi *et al* .in 2020 [51] The electrical and spin characteristics of mono- and bilayer HfSSe are investigated in the presence of a vertical electric field in this research. Their characteristics are investigated using the density functional theory. There are fifteen distinct stacking orders of bilayer HfSSe that are taken into account. The bandgap of the monolayer and bilayer is indirect, however the bandgap of the bilayer may be efficiently modulated by the electric field. While the bandgap of a bilayer closes at strong electric fields, resulting in a semiconductor to metal transition, the influence of a normal electric field on the bandgap of monolayer HfSSe is rather small. In both monolayer and bilayer structures, spin-orbit coupling induces band splitting in the valence band and Rashba spin splitting in the conduction band. The band splitting in the valence band of a bilayer is lower than in a monolayer, but the vertical electric field enhances it in bilayer one.

X.Zhao *et al*. in 2022[52] Based on the first-principles calculations, we studied the structure and electronic properties of HfSSe/Graphene (HfSSe/Gr) and Graphene/HfSSe (Gr/HfSSe) van der Waals heterostructures (vdWHs) under the effects of external electric field and interlayer distance. The results show that the electronic properties of HfSSe/Gr and Gr/HfSSe heterostructures are not sensitive to interlayer distance, and the heterostructures always maintain n-type Schottky contact when the interlayer distance changes. Under the different applied electric field, the Schottky barrier of heterostructures can be regulated from n-type Schottky contact to p-type Schottky contact, and it can be further adjusted to Ohmic contact. In summary, these results are useful in nanoelectronic and optoelectronic devices in the future experiments.

1.5 Aims of the study

1-The primary aim of this research is to fully understand, by first principles, the Structural, electronic, and optical properties of 2-D structures based nanostructures for nanoelectronic devices and gas sensors.

2-Detection of toxic gases through their adsorption on HfSSe monolayer.

3-The electronic and optical properties of gas molecules (including NO, NO_2, CO, CO_2 and SO_2,) adsorbed on HfSSe monolayer are inspected based on the density functional theory (DFT).

4- Finding materials with unique characteristics for different applications

symmetry, which is aided by the electric field.

Chapter Two
Theoretical Background

2.1 Introduction

The study and understanding of natural systems are the main aims of physics theories. Since the structure on a microscale is responsible for the macroscale character of matter; the understanding and exploiting the properties of electrons and atomic-nuclei systems interacting is a primordial step in materials science. Through quantum theory, the fundamental properties of matter, and especially, in the condensed case are well known. Full describing of the atomic system requires the solving of Schrödinger's equation for the concerned system. Unfortunately, there are analytical solutions of this equation for very few simple system, and accurate numerical solutions for just a little number of atoms and molecules. However, in most cases, the use of approximations and assumptions is absolutely necessary [53].

2.2 Schrödinger Equation

One of the most important goals of physics is to characterize the physical characteristics of interacting many-particle systems using computational physics and chemistry. Quantum mechanical law can solve any difficulty in the electrical structure of any system.

The Schrödinger equation, which is written as, is used to explain the movements of atomic and subatomic systems, electrons, and nuclei [54].

$$\widehat{H}\Psi = E\Psi \qquad (2.1)$$

Here Ψ is the wave function, $\widehat{H}$ is the Hamiltonian operator, and E is the total energy of the system.

The Hamiltonian operator has kinetic energy ($\hat{T}$) and potential energy ($\hat{V}$) for all particles, is given by [55].

$$\widehat{H} = \hat{T} + \hat{V} \qquad (2.2)$$

$$\hat{T} = \hat{T}_e + \hat{T}_n \quad , \quad \hat{V} = \hat{V}_{ne} + \hat{V}_{ee} + \hat{V}_{nn} \qquad (2.3)$$

Theoretically, the kinetic energy is the sum of the kinetic energies of electrons ($\hat{T}_e$) and nuclei ($\hat{T}_n$), while the potential energy is the sum of three components, the coulomb attraction between the nuclei and electrons ($\hat{V}_{ne}$), the Coulomb repulsion between electrons ($\hat{V}_{ee}$), the Coulomb repulsion between nuclei ($\hat{V}_{nn}$).

The kinetic energy operator is given as [56].

$$\hat{T}_e = -\frac{\hbar^2}{2m_I}\sum_I \nabla_I^2 \qquad (2.4)$$

$$\hat{T}_n = -\frac{\hbar^2}{2\,M_a}\sum_a \nabla_a^2 \qquad (2.5)$$

Here: m_I and Ma are the electron and nuclear mass, respectively.

Where $\nabla^2 = \frac{\partial^2}{\partial x^2} + \frac{\partial^2}{\partial y^2} + \frac{\partial^2}{\partial z^2}$ is the Laplacian operator of i electrons and a nuclei.

The potential energy operators are given as [54].

$$\hat{V}_{ne} = -\frac{1}{4\pi\varepsilon_o}\sum_a \sum_I Z_a \ \frac{e^2}{r_{Ia}} \qquad (2.6)$$

$$\hat{V}_{ee} = \frac{1}{4\pi\varepsilon_o}\sum_{I<J}\frac{e^2}{r_{IJ}} \qquad (2.7)$$

$$\hat{V}_{nn} = \frac{1}{4\pi\varepsilon_o}\sum_{a<b} Z_a Z_b \ \frac{e^2}{R_{ab}} \qquad (2.8)$$

$$\hat{H} = \hat{T} + \hat{V} = -\frac{\hbar^2}{2}\sum_{a=1}^{K}\frac{1}{M_a}\nabla_a^2 - \frac{\hbar^2}{2m}\sum_{I=1}^{n}\nabla_I^2 + V(r,R) \qquad (2.9)$$

$$\hat{V} = \frac{e^2}{4\pi\varepsilon_o}\left[\sum_{a<b}^{K}\frac{Z_a Z_b}{R_{ab}} - \sum_{a=1}^{n}\sum_{I=1}^{K}\frac{Z_a}{r_{Ia}} + \sum_{I<J}^{n}\frac{1}{r_{IJ}}\right] \qquad (2.10)$$

Where $\vec{r}_{IJ} = \left|\vec{r}_I - \vec{r}_J\right|$ and Z_a is the charge of nuclei, a, Z_b are the charge of nuclei b, $\vec{r}_{IJ}$ are the distance between I electron and J electron, $r_{Ia} = \left|\vec{r} - R_a\right|$, r_{Ia} is the distance between nucleus and electron, $R_{ab} = \left|R_a - R_b\right|$, R_{ab} is the distance between a nucleus and b nucleus.

The so-called atomic unit is widely used in theoretical molecular and atomic physics to avoid dealing with constant factors in lengthy computations and to make integrals and equations more visible. They are attained by the definition of [55].

Note that in equating (c= e= ħ= m_e=1), the dimensions of these quantities are disregarded. Hence, equations written in atomic units are not dimensionally correct in the usual sense.

The atomic unit of length, 1 Bohr, equals the radius a_o of lowest Bohr orbit in the hydrogen atom. In SI units [57].

$$a_o = \frac{4\pi\varepsilon_o}{me^2} \approx 0.05\ nm$$

The atomic unit of energy, 1 Hartree, is defined to be twice the ionization energy of hydrogen atom (= $-E_{pot}$ for the electron in the lowest Bohr orbit with n=1). In SI units,

$$E_{pot} = -\frac{me^4}{(4\pi\varepsilon_o)\hbar^2 n^2} \approx 27.2114\ eV \quad for \quad n = 1$$

Then the total Hamiltonian for a molecule in atomic units is given by [54].

$$\hat{H}_{tot} = -\frac{1}{2}\sum_{I=1}^{n}\nabla_I^2 - \frac{1}{2}\sum_{a=1}^{k}\frac{1}{M_a}\nabla_a^2 + \sum_{a=1}^{K-1}\sum_{b=a+1}^{K}\frac{Z_a Z_b}{R_{ab}} - \sum_{a=1}^{K}\sum_{I=1}^{n}\frac{Z_a}{r_{Ia}} + \sum_{I=1}^{n-1}\sum_{J=I+1}^{n}\frac{1}{r_{IJ}} \qquad (2.11)$$

The Schrödinger equation may be written more compactly as [57].

$$\hat{H}_{tot} = \hat{T}_n + \hat{T}_e + \hat{V}_{ne} + \hat{V}_{nn} + \hat{V}_{ee} \qquad (2.12)$$

2.3 Born-Oppenheimer Approximation

Although a molecule contains both electrons and nuclei, nuclear and electronic movements may be treated separately since nuclei are significantly heavier than electrons and have more restricted mobility. The Born-Oppenheimer Approximation describes the reparability of nuclear and electronic motion. Born and Oppenheimer used a rigorous but sophisticated mathematical analysis to develop the reparability of nuclear and electronic motion in 1927. As a result, a molecule's wavefunction may be separated into two halves.

$$\Psi_{tot} = \Psi_{electronic} \times \Psi_{nuclear} \quad (2.13)$$

The kinetic energy of nuclei is taken away, while the potential energy of nuclei-nuclei is fixed. The kinetic energy of nuclei and the potential energy of nuclei-nuclei may be omitted from the Hamiltonian operator in this case, and the Hamiltonian operator $\hat{H}$ can be reduced as follows,

$$\hat{H} = \hat{T}_e + \hat{V}_{ne} + \hat{V}_{ee} \quad (2.14)$$

In the simplified equation, only three energy operators are left. They are electron kinetic energy $\hat{T}_e$, electron-nuclear interaction energy $\hat{V}_{ne}$ and electron-electron interaction energy $\hat{V}_{ee}$. The system can actually be described as all electrons moving in a potential field of nuclei with fixed positions[55, 58].

2.4 Hartree–Fock Equations

As known, to solve the Schrödinger equation for all electrons in systems requires solving many of simultaneous differential equations. The calculations are very difficult and need simplifying the methods and the problem itself. In 1928, Hartree simplified the problem by making an assumption about the form of the many-electron wave functions from the product of a set of single-electron wave functions. Considering this assumption, it was possible to proceed using the

variational principle. According to the variational principle, the lowest energy eigenvalue E_{Φ} of the trial function Φcan be expressed as [59].

$$E_{\Phi} = \frac{\langle \Phi | \hat{H} | \Phi \rangle}{\langle \Phi | \Phi \rangle} \geq E_o \qquad (2.15)$$

The ground-state energy is denoted by E_0. The precise ground-state wave function is estimated using this theorem from the trial function with the lowest energy. Hartree discovered the Hamiltonian equation for the many-electron system, allowing each electron to be treated as a distinct particle.

The Slater determinant may be used to express the wave function of the Hartree-Fock method. The Pauli Exclusion Principle and the spin of all electrons are taken into account in this determinant [60].

$$\Psi = \frac{1}{\sqrt{N!}} \begin{vmatrix} \Psi_1(1)\alpha(1) & \Psi_1(1)\beta(1) & \Psi_2(1)\alpha(1) & \Psi_2(1)\beta(1) & \dots & \Psi_N(1)\alpha(1) & \Psi_N(1)\beta(1) \\ \Psi_1(2)\alpha(2) & \Psi_1(2)\beta(2) & \Psi_2(2)\alpha(2) & \Psi_2(2)\beta(2) & \dots & \Psi_N(2)\alpha(2) & \Psi_N(2)\beta(2) \\ . & & . & & & . & \\ . & & . & & & . & \\ \Psi_1(N)\alpha(N) & \Psi_1(N)\beta(N) & \Psi_2(N)\alpha(N) & \Psi_2(N)\beta(N) & \dots & \Psi_N(N)\alpha(N) & \Psi_N(N)\beta(N) \end{vmatrix} \qquad (2.16)$$

Where $\frac{1}{\sqrt{N!}}$ is the normalization factor.

The main step in Hartree-Fock methods is to introduce the molecular orbital expansion and determine the corresponding coefficients based on the variational principle. The molecular orbitals Ψ_i(r) solving the Hartree-Fock equation using the iterative process of the self-consistent field (SCF) producer yields [61-63].

$$\hat{F}\Psi_i(\vec{r}) = \varepsilon_i \Psi_i(\vec{r}) \qquad (2.17)$$

Here ε_i is the electronic energy of the electron in orbital, and F represents the Fock operator. For closed-shell systems,

$$\hat{F} = \hat{h} + \sum_{l=1}^{n/2} \left(2\hat{j}_l - \hat{k}_l\right) \qquad (2.18)$$

With $\hat{j}_l$ and $\hat{k}_l$ are the coulomb operator and the exchange operator, respectively,

$$\hat{j}_l\Psi(\vec{r}) = \int \frac{\Psi_l^*(\vec{r})\Psi_l(\overrightarrow{r'})}{\left|\vec{r} - \overrightarrow{r'}\right|} dV'\Psi(\vec{r}) \tag{2.19}$$

$$\hat{k}_l\Psi(\vec{r}) = \int \frac{\Psi_l^*(\vec{r})\Psi_j(\overrightarrow{r'})}{\left|\vec{r} - \overrightarrow{r'}\right|} dV'\Psi(\vec{r}) \tag{2.20}$$

This correction takes into account the effects of spin correlation. Another correction involves expanding the molecular orbital (MO) in terms of the linear combination atomic orbital (LCAO) [60,62], thus an individual molecular orbital Ψ_i is defined as,

$$\Psi_i(x) = \sum_{\mu=1}^{N} C_{\mu i}\Phi_\mu(x) \qquad \mu = 1,2,\dots,N \tag{2.21}$$

The basic functions Φ_μ are selected to be normalized, N number of the basis functions, and $C_{\mu i}$ represents the molecular orbital expansion coefficients. For orbital expansion, an appropriate set of basis functions has to be selected, with that the coefficients $C_{\mu i}$ may then be adjusted to minimize the total electronic energy calculated from the many-electron wave function. The resulting value of the energy will then be as close as possible to the exact energy E_0 of the ground state of the system in the selected limitations, i.e. the exact solution of the Schrödinger equation [63]

$$E(\Phi_1, \Phi_2, \dots\dots, \Phi_N) \geq E_o \tag{2.22}$$

The equality sign shall be applied only in case Ψ is the exact ground state function.

2.5 Density Functional Theory

The quantum mechanical approach of density functional theory (DFT) is frequently used in physics and chemistry to analyze the electronic structure of many-electron systems. Density Functional Theory is currently the most successful

and promising method for computing matter's electrical structure. It may be used to atoms, molecules, and solids, as well as nuclei and quantum and classical fluids. It is now one of the most essential tools for computing metal, semiconductor, and insulator ground state parameters. In computational physics and computational chemistry, DFT is one of the most used and useful approaches [64].

The DFT's goal is to use solely the electron density idea to identify the parameters of the ground state of a system with a fixed amount of electrons in a Coulomb interaction with point nuclei.

The Thomas-Fermi model, published in 1927, calculated the energy of an atom by representing its kinetic energy as a function of the electron density and combining this with the classical expressions for the nuclear-electron and electron-electron interactions, both of which can be expressed in terms of the electron density [54]. DFT assumes that the density function instead of the wave functions Ψ (r_1, r_2, r_3...) [65].

The fundamental concept of the density functional is that the energy of an electronic system may be expressed as a function of electron density ρ(r), which minimizes the energy of the system. In general, the electron density ρ(r) is the number of electrons N per unit volume for a given state. It is dependent only on three coordinates independently of the number of electrons of the system. Therefore, the electron density is sufficient to the complete determination of the properties for an atomic system [54,66].

$$N = \int \rho(\vec{r}) d\vec{r} \qquad (2.23)$$

The DFT calculations are based on the Kohn-Sham-equations; Hohenberg–Kohn (HK) crossed this problem by presenting two basic results. **First**, the ground-state electron density uniquely determines the Hamiltonian, so, the ground states electronic wave function, and all properties of the system. **Second**, the correct

density functional for the electronic energy supposes its minimum for the correct ground state density [66].

2.5.1 Hohenberg –Kohn Theorem

In 1964, Hohenberg and Kohn formulated the fundament for DFT with the central idea to substitute many-body problems with an equation for the electron density $\rho(\vec{r})$.

The Hamilton operator of the n-electron system within the Born-Oppenheimer approximation which can be written by [66].

$$\hat{H} = \hat{T} + \hat{V}_{ext} + \hat{V}_{ee} \quad (2.24)$$

The external potential $\hat{V}_{ext}$ is uniquely defined by the electron density $\rho(\vec{r})$. The total energy can be written as [67].

$$E_0 = T[\rho_0] + \int V_{ext}(r)\rho_0(r)dr + J[\rho_0] + E_{NC}[\rho_0] \quad (2.25)$$

where $T[\rho_0]$ is the kinetic energy, $E_{NC}[\rho_0]$ is the non-classical, electron-electron interaction energy and $J[\rho_0]$ is the classical Coulomb energy defined as,

$$J[\rho_0] = \frac{1}{2}\iint \frac{\rho_0(r_1)\rho_0(r_2)}{|r_1 - r_2|} dr_1 dr_2 \quad (2.26)$$

V_{ext} (r) directly depends on the system, which is the Coulomb potential of the nuclei. Thus, the total energy can be written as,

$$E_0 = \int V_{ext}(r)\rho_0(r)dr + F_{HK}[\rho_0] \quad (2.27)$$

where F_{HK} is a universal functional of the electron density ,

$$F_{HK}[\rho] = T[\rho] + J[\rho] + E_{NC}[\rho] \quad (2.28)$$

HK theorem assumes that F_{HK} exists, but the real form of F_{HK} is not known and must be approximated. HK theorem reduced the problem of solving the Schrödinger equation for many bodies to the problem of minimizing a density functional [66].

2.5.2 Kohn-Sham Theory

In the real system with the ground state density ρ($\vec{r}$), there exists a non-interacting system with the same ρ($\vec{r}$). Equation (2.28) can rewrite as [66].

$$F[\rho] = T_S[\rho] + J[\rho] + E_{NC}[\rho] \quad (2.29)$$

Here T_S [ρ] is the Kinetic energy of the non-interacting electron system. The electron density of the non-interacting system is described by a single Slater determinant of orbitals.

The DFT exchange-correlation energy $E_{xc}[\rho]$ of interacting electron system defined in the form

$$E_{xc}[\rho] = T[\rho] - T_S[\rho] + E_{NC}[\rho] \quad (2.30)$$

By applying the variation principle, δE/δρ(r)=0, to Kohn–Sham functional [62].

$$E[\rho] = \int \rho_{(r)}\, v_{(r)} dr + T_S[\rho] + J[\rho] + E_{xc}[\rho] \quad (2.31)$$

The density $\rho(r)$is represented by,

$$\rho(r) = \sum_{i=1}^{n} \left| \phi_i\,(r) \right|^2 \quad (2.32)$$

This result in the Hartree-type of one–electron equation [67].

$$\left[-\frac{1}{2}\nabla^2 + V_{(r)} + \int \frac{\rho(r)}{\left| r - \bar{r} \right|} d\bar{r} + V_{xc}(r) \right] \phi_i(r) = \varepsilon_i \phi_i(r) \quad (2.33)$$

where $V_{xc}(r)$ is the exchange –correlation potential, $\phi_i(r)$ is Kohn–Sham orbitals, and ε_i is Kohn –Sham orbital energies [67].

$$V_{xc}(r) = \frac{\delta E_{xc}[\rho]}{\delta \rho_{(r)}} \quad (2.34)$$

Equations (2.32)–(2.34) known as the Kohn-Sham equations, are formally precise and contain only one unknown term,$E_{xc}[\rho]$. Kohn–Sham approach is the famous work that was embraced in many aims [56].

2.5.3 Exchange–Correlation Energy

The term "correlation" refers to interactions between electrons in the same molecule [68]. Hohenberg, Kohn, and Sham's density functional theory is based on the notion that the total of a uniform electron gas's exchange and correlation energies can be determined using just its density [69]. The Kohn-Sham exchange and correlation functional is [70].

$$E_{xc}[\rho] = T[\rho] - T_S[\rho] + V_{ee}[\rho] - J[\rho] \quad (2.35)$$

The Hamilton operator has multiplied by a scaling factor λ. for λ=0, a system of non-interacting electrons which could be obtained, while for λ=1, a system of completely interacting electrons will be obtained. From HK theorem, the non-interactive ρ can be obtained,

$$F_{\lambda=1}[\rho] = F[\rho] = T[\rho] + V_{ee}[\rho] \quad (2.36)$$

$$F_{\lambda=0}[\rho] = T_s[\rho] \quad (2.37)$$

Thus, equation (2.35) will be,

$$E_{xc}[\rho] = F_{\lambda-1}[\rho] - F_{\lambda-0}[\rho] - J[\rho] \quad (2.38)$$

$$E_{xc}[\rho] = \int_0^1 d\lambda \frac{\partial F_\lambda[\rho]}{\partial \lambda} - J[\rho] \quad (2.39)$$

Using Hellmann – Feynman theorem [62].

$$\frac{\partial F_\lambda[\rho]}{\partial \lambda} = < \varphi^\lambda \mid V_{ee} \mid \varphi^\lambda > \quad (2.40)$$

Where φ^λ represents the wave function to the Hamilton operator. Equation (2.39) will be,

$$E_{xc}[\rho] = \int_0^1 d\lambda < \varphi^\lambda \mid V_{ee} \mid \varphi^\lambda > -J[\rho] \quad (2.41)$$

$$E_{xc}[\rho] = \frac{1}{2}\iint \frac{1}{r_{12}}\rho(r_1)\bar{\rho}_{xc}(r_1, r_2)dr_1 dr_2 \qquad (2.42)$$

The averaged exchange-correlation $\bar{\rho}_{xc}$ is defined as [70].

$$\bar{\rho}_{xc}(r_1, r_2) = \rho(r_2)\bar{h}(r_1, r_2) \qquad (2.43)$$

Where $\bar{h}(r_1, r_2)$ is the averaged pair correlation function,

$$\int_0^1 d\lambda\, \rho\,{}_2^{\lambda}(r_1, r_2) = \frac{1}{2}\rho(r_1)\rho(r_2)\left[1 + \bar{h}(r_1, r_2)\right] \qquad (2.44)$$

Where $\rho\,{}_2^{\lambda}(r_1, r_2)$ is the diagonal part of the two-particle density matrix. The exchange–correlation energy depends only on a spherically average$\bar{\rho}_{xc}(r_1, r_2)$.

$$E_{xc}[\rho] = \frac{1}{2}\int dr\, \rho(r) \int_0^{\infty} 4\pi s ds \rho_{xc}^{SA} \qquad (2.45)$$

Here

$$\rho_{xc}^{SA}(r, s) = \frac{1}{4\pi}\int \bar{\rho}_{xc}\,(r, \bar{r})d\bar{r} \qquad (2.46)$$

From the Kohn–Sham density functional theory, the exchange –correlation functional E_{xc} is separated into correlation E_c^{ks} parts and the exchange E_x^{ks} [71].

$$E_{xc}[\rho] = E_x^{ks}[\rho] + E_c^{ks}[\rho] \qquad (2.47)$$

Where $E_c^{ks}$is the HF exchange energy calculated with Kohn-Sham determinant Φ_ρ,

$$E_x^{ks}[\rho] = < \phi_\rho \,|\, \hat{V}_{ee} \,|\, \phi_\rho > - J[\rho] \qquad (2.48)$$

$$E_c^{ks}[\rho] = < \Psi_\rho \,|\, \hat{V}_{ee} \,|\, \Psi_\rho > - < \phi_\rho \,|\, \hat{V}_{ee} \,|\, \phi_\rho > \qquad (2.49)$$

Where Ψ_ρ is the exact interacting wave function. The correlation energy is a coulomb interaction of electrons with a neutral charge distribution.

2.6 The Local (Spin) Density Approximation (L(S) DA)

The local density approximation (LDA), proposed by Hohenberg and Kohn in their initial DFT work, is the oldest, simplest, and probably most significant functional [72]. The LDA is the simplest approximation to E_{XC} [ρ(r)], which

assumes the system is a homogeneous electron gas and E_{XC} [ρ(r)] depends only on the local value of electron density. Therefore, E_{XC}[ρ(r)] can be written in a simple form [58], 73] .

$$E_{xc}^{LDA}[\rho] = \int \rho(\vec{r})\varepsilon_{xc}\left(\rho(\vec{r})\right)d\vec{r} \qquad (2.50)$$

Where ε_{xc} is the exchange-correlation energy per particle. Compared to LDA, LSDA defines the exchange-correlation potential in terms of the density of α and β spins (i.e., spin up and spin down respectively) and was developed for calculating the properties of open-shell systems [74].

$$E_{xc}^{LSDA}\left[\rho_\alpha, \rho_\beta\right] = \int \rho(\vec{r})\varepsilon_{xc}\left(\rho(\vec{r})_\alpha, \rho(\vec{r})_\beta\right)d\vec{r} \qquad (2.51)$$

For some features like as equilibrium structures, vibrational frequencies, and dipole moments, the LSD approximation outperforms the HF approximation; nonetheless, it is unable to generate the very exact energy data that many computational chemists require.

In general, the LSDA provides reliable data for systems that closely resemble a uniform electron gas, i.e., those in which density varies slowly with position. However, in actuality, atomic and molecular systems do not have uniform electron densities, necessitating the use of more complex models.

2.7 The General Gradient Approximation (GGA)

The electron density of a real molecule fluctuates a lot from one place to the next. The functions do not only incorporate electron density, but also gradient electron density, in order to provide a more precise approximation of exchange correlation energy.

Therefore, one can have [41].

$$E_{XC}^{GGA}\left[\rho_\alpha, \rho_\beta\right] = \int f\left(\rho_\alpha, \rho_\beta, \nabla\rho_\alpha, \nabla\rho_\beta\right)\overrightarrow{dr} \qquad (2.52)$$

In general, these functions show improvement over LSDA because it takes the density variation with positions into account. To simplify the problem (E_{XC}) often can be written as a sum of exchange term (E_X) term and correlation term (E_C) as follows [75].

$$E_{XC} = E_X + E_C \tag{2.53}$$

The exchange-energy functional can then be gained from the HF exchange term with the Kohn-Sham orbitals in place of the HF orbitals and approximate solutions for E_c. Different exchange and correlation functions have developed independently and can be combined in various ways. For example, one popular GGA functional is PBE, Perdew, Burke and Enzerhof (PBE) [76].

2.8 Perdew-Burke-Ernzerhof (PBE)

There are several instances of GGA functions, such as PBE's GGA [76]. The exchange part is given by [77].

$$\epsilon_x^{PBE} = \epsilon_x^{HEG} F_x^{PBE} \tag{2.55}$$

$$F_x^{PBE} = 1 + K - \frac{K}{1 + \left(\frac{\mu s^2}{K}\right)} \tag{2.56}$$

Where F_x^{PBE} would be the exchange enhancement factor to the HEG, Where k = 0.804 and μ = 0.21951. While the correlation part is chosen as.

$$\epsilon_{xc}^{GGA} = \epsilon_c^{HEG} + H(r_s, \zeta, t) \tag{2.57}$$

Where H would be the correlation enhancement factor to the HEG, H is given by [77].

$$H = \frac{e^2 \gamma \phi^3}{a_\circ} log(1 + \frac{\beta t^2}{\gamma} \frac{1 + At^2}{1 + At^2 + A^2 t^4}) \tag{2.58}$$

$\phi(\zeta) = [(1+\zeta)^{\frac{3}{2}} + (1-\zeta)^{\frac{3}{2}}]/2$ is a spin scaling factor, $\zeta = (n^{\downarrow} - n^{\uparrow})$ /n is the relative spin polarization, r_s is the local value of the density parameter, $t = |\nabla_n|$ /

$(2\phi K_{TF^n})$ is a dimensionless gradient, K_{TF^n} is the Thomas-Fermi screening, β = 0.066725 is a constant and $\gamma = \frac{(1-log\,2)}{\pi^2}$ is a constant. The function A represents

$$A = \frac{\beta}{\gamma}\left[e^{\frac{-a_\circ\ \epsilon_x^{HEG}}{e^2\,\gamma\,\phi^3}} - 1\right]^{-1} \qquad (2.59)$$

2.9 CASTEP Package

CASTEP (Cambridge Sequential Total Energy Package) is an ab initio quantum mechanical software that uses density functional theory (DFT) to model the characteristics of solids, molecules, interfaces, and surfaces for a variety of materials classes including ceramics, semiconductors, and metals. Without any experimental input, first principle calculations let researchers to examine the nature and genesis of a system's structural, electrical, and optical features. CASTEP is an ideal simulation tool for studying problems in solid-state physics, materials science, molecules, and chemical engineering that lack empirical models and experimental data. CASTEP can help researchers save a lot of time and money by reducing the number of tests they have to run. CASTEP can compute a wide range of electrical, optical, and physical characteristics. It can forecast electrical characteristics like band gaps, density of states, and Schottky barriers, as well as optical properties like reflectivity, absorption, IR spectra, and dielectric functions. It can even predict physical properties like elastic constants. CASTEP employed a total energy plane-wave pseudopotential approach. Core electrons were substituted with effective potentials that solely affect on the valence electrons in the system to minimize computation complexity. The contact, exchange, and correlation effects of electrons in the system were calculated using LDA or GGA after the electronic wave functions were enlarged using a plane-wave basis set. Geometry optimizations of

molecules, solids, surfaces, and interfaces are efficient thanks to the use of pseudopotentials and plane-wave basis sets [78].

2.10 Electronic Properties

2.10.1 Energy Band Gap

The energy band gap is defined as the minimum energy required for an electron to jump from its bound state into its valence state where it can engage in conduction [79].

Energy valence (E_v) is the lower energy level, and energy conduction (E_c) is the state of energy where the electron is considered to be free.

The energy band gap is the difference between these two energies and represents the lowest energy necessary to excite an electron from the valence band into the conduction band [80]. The electrons are directly cognizant of the band gap. An electric current is formed when a group of electrons all travel in the same direction. An atom's electrons are organized into states, shells, momentum, spin, and energy levels [81]. Some electrons have the same energy level as others, whereas others have different levels. The band refers to the set of feasible electron states, whereas the band gap refers to the set of electron states that are not possible. Core levels are bands that are closest to the nucleus. The valence band is the band that is farthest away from the nucleus. The conduction band follows, in which electrons are free to flow. The VB and CB overlap in metals, allowing electrons to freely flow and making them strong conductors of electricity. Insulators are another type of material in which the VB and CB are separated by a significant distance. Moving an electron to the CB is quite difficult [82]. Semiconductors are materials with an extremely thin gap between the VB and CB gaps. In some circumstances,

they behave as both conductors and insulators. Because of their varied nature, semiconductors were of little interest when they were originally discovered and prior to scientists discovering the enigma of the band gap. The concept of an energy band inspired scientists to research semiconductor applications in optoelectronic devices [82]. When the electron is hit by light energy called the photon, it can help the electron to jump across the band gap. In the conduction band, the electron is free to flow, thus producing an electric current [83]. Measuring the band gap is important in the semiconductor and nanomaterial industries. The band gap energy of insulators is large (> 4 eV), but lower for semiconductors (< 3 eV). A diagram illustrating the bandgap is shown in Figure (2.1) [80]. Direct and indirect energy band gaps, as shown in Figure (2.2) are the two variants in semiconductors. The top of the valence band and the bottom of the conduction band both occur at the same momentum in a semiconductor with a direct band gap, but the maximum in the valence band occurs at a different momentum than the minimum of the conduction band energy in a semiconductor with an indirect band gap [80].

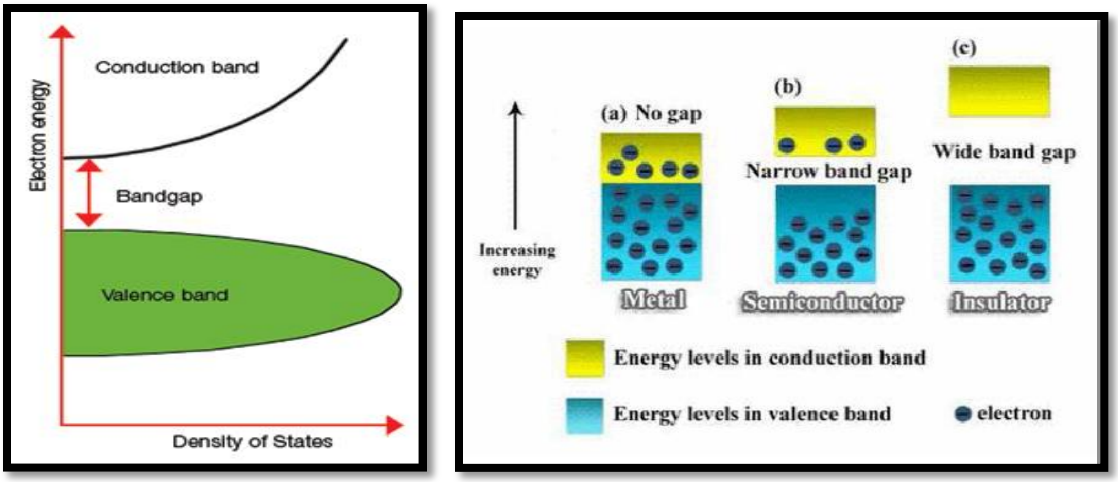

(i) **(ii)**

Fig. (2.1): (i) Explanation of the band gap, (ii) Schematic electron occupancy in allowed energy bands for (a) metal, (b) semiconductor and (c) insulator which are showing no gap, narrow and wide-band gap respectively. The metal's conduction band is half-filled, the insulator's conduction band is empty, and the semiconductor's conduction band has a very tiny population of electrons [84].

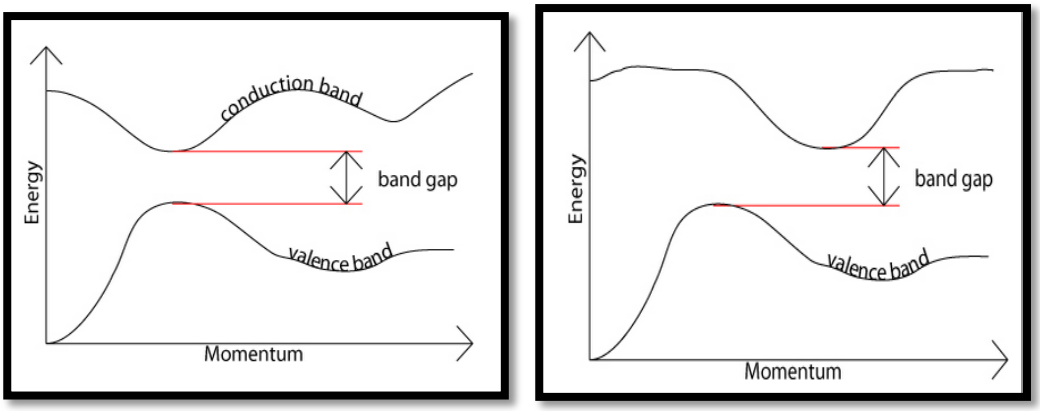

(a) **(b)**

Fig.(2.2): (a) Direct band gap, and (b) Indirect band gap [80].

2.10.2. Density of states

The electronic density of states (DOS), which is defined as the number of states available to be filled at each energy level, is one of the most important electronic characteristics for any material. The idea of the DOS is crucial to present here since it serves to emphasize the influence of quantum confinement on the electrical characteristics of a low-dimensional system [85]. The electronic transport, electrical, thermal, optical, and mechanical characteristics of a crystalline solid are all described by the DOS [86]. Semiconductor nanostructures can be classified into three groups based on their dimensionality. The electron density of states, g(E), for a three-dimensional (3D) system of volume L^3 is directly proportioned to the square root of the energy [87].

$$g(E) = \frac{1}{2\pi^2}\left(\frac{2m^*}{\hbar^2}\right)^{3/2}\sqrt{E} \qquad (2.64)$$

As a result, the electron may exist in a wide range of energy levels. The DOS displays a step-like dependency when the dimensionality of the system is reduced to 2D, which is known as quantum wells (QWs) because an electron is restricted in one direction but free to travel in the other two spatial dimensions. The DOS is broken down into steps, each of which is explained as follows [88].

$$g(E) = \frac{m^*}{\pi\hbar^2} \qquad (2.65)$$

In the direction of confinement, these equal-height stairs correspond to quantized electrical states. In one-dimensional systems, such as quantum wires (QWRs), where the electron may only flow in one direction, such as Nanowires, the density of states resembles an array of spikes, each indicating a quantized electronic state in the confinement direction.

$$g(E) = \frac{1}{\pi\hbar}\sqrt{\frac{m^*}{2E}} \qquad (2.66)$$

When an electron is contained in three spatial dimensions in a 0D system, such as quantum dots (QDs). The most public semiconductor nanostructures can be classified in terms of dimensionality. This classification, is in fact, supposed according to the number of orthogonal directions x, y, z in which the structure patterns have dimensions L_x, L_y, L_z smaller than, the so-called characteristic length (L_0) can be defined as the description of the behavior of electrons in semiconductors. Figure (2.3) shows how the density of states changes with energy for semiconductor structures with different geometries[89].

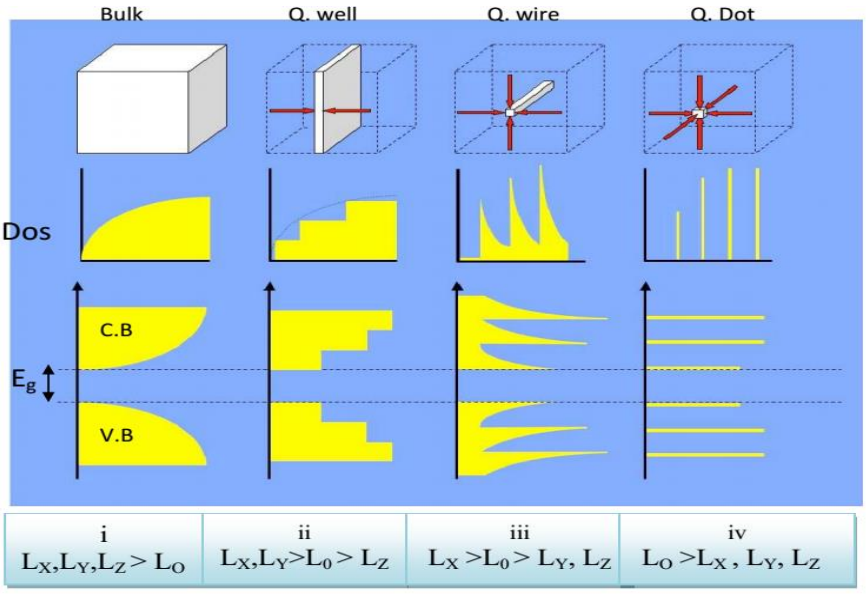

Fig. (2.3): Classification of nanostructures: (i) Bulk material, (i) Quantum well, (iii) Quantum wire, (iv) Quantum Dot [90].

2.10.3 Partial Density of States

The partial density of states (PDOS) analysis approach is invalid for high-energy levels in the conduction band because the partial density of states representation frequently decays to zero at around 20 eV above the Fermi level.

This is due to the fact that expanding an essentially free-electron state in terms of a small number of atomic-like basis functions is hard to do with any

precision. In the partial density of states, only the valance band and the bottom half of the conduction band are relevant [91].

The angular momenta that should be included in the partial density of states can be modified using the s, p, d, and f variables. For evaluating electronic structure, partial density of states are valuable semi-qualitative tools. These results are further qualified by PDOS, which rotates these contributions according to the angular momentum of the states. It's frequently used to determine if the DOS's primary peaks are of the s, p, or d character [92].

2.11 The Optical Properties

The optical parameters are investigated by density functional perturbation theory. These properties include the absorption coefficient $\alpha(\omega)$, conductivity $\sigma(\omega)$, refraction index $n(\omega)$, reflectivity $R(\omega)$, the energy loss function $L(\omega)$, the dielectric function $\varepsilon(\omega)$, where term ω represented the frequency. The dielectric function of the material points out the linear spectral reaction of the system to the electromagnetic radiation. The complex dielectric function is formed by summation the real and imaginary parts as follow [61].

$$\varepsilon(\omega) = \varepsilon_1(\omega) + i\varepsilon_2(\omega) \qquad (2.67)$$

Where the real $\varepsilon_1(\omega)$ part and imaginary part $\varepsilon_2(\omega)$ are given by the well-known relations [93].

$$\varepsilon_1(\omega) = 1 + \frac{2}{\pi} P \int_0^{\infty} \frac{\omega' \varepsilon_2(\omega')}{\omega'^2 - \omega^2} d\omega' \qquad (2.68)$$

$$\varepsilon_2(\omega) = \frac{e^2 \hbar}{\pi m^2 \omega^2} \sum_{v,c} \int_{BZ} |\langle u_{cv} | u. \nabla | u_{ck} \rangle|^2 \, \delta[\omega_{cv}(k) - \omega] d^3k \qquad (2.69)$$

where P stand for the principal value of the integral, m and e denote respectively for the mass and charge of electron, u is the unit vector, v and c indicate matrix

elements of the transitions to conduction band states $u_{ck}(r)$ from valence band states ($u_{vk}(r)$). Besides, the complex refraction index with the real part so-called refraction index (n) as well as the imaginary part named extinction coefficient (k) can be expressed as [94].

$$n^*(\omega) = n(\omega) + ik(\omega) \tag{2.70}$$

$$n(\omega) = \left[\frac{\varepsilon_1(\omega)}{2} + \frac{\sqrt{\varepsilon_1^2(\omega) + \varepsilon_2^2(\omega)}}{2}\right]^{\frac{1}{2}} \tag{2.71}$$

$$k(\omega) = \left[\frac{\sqrt{\varepsilon_1^2(\omega) + \varepsilon_2^2(\omega)}}{2} - \frac{\varepsilon_1(\omega)}{2}\right]^{\frac{1}{2}} \tag{2.72}$$

The conductivity is dependent on the imaginary part of the dielectric function. On the other hand, the absorption coefficient is related to complex refraction index according to the following equation [94] .

$$\sigma(\omega) = \frac{\omega}{4\pi}.\varepsilon_2(\omega) \tag{2.73}$$

$$\alpha(\omega) = \frac{2\omega}{c}.k \tag{2.74}$$

Here c is the light speed in the vacuum. In addition, the reflectivity can be obtained by studying the normal incidence on the plane surface and the energy loss function of the material represents the energy lost by the electrons that pass through the material, these quantities can be given in the following equations [95].

$$R(\omega) = \frac{(n(\omega) - 1)^2 + k^2(\omega)}{(n(\omega) + 1)^2 + k^2(\omega)} \tag{2.75}$$

$$L(\omega) = \frac{\varepsilon_2(\omega)}{{\varepsilon_1}^2(\omega) + {\varepsilon_2}^2(\omega)} \tag{2.76}$$

Chapter Three

Results And Discussion Part One

3.1 Computational Methods

DFT techniques, which were run using the CASTEP program with leveraging the PBE and ultrasoft pseudopotentials and exchange-correlation energy functionals, were used to examine the electronic and optical characteristics of monolayer HFXY (XY= S, Se) [97,98].

A 8×8×1 k-mesh Monkhorst-Pack grid is used to evaluate the Brillouin zones. The optical characteristics were computed with 30×30×1 Monkhorst pack k-mesh, while the density of state computations were done with 24×24×1 .This k-point level is critical for displaying the optical spectrum of materials, particularly the imaginary component of the dielectric function. All calculations are done on a plane wave basis with a kinetic energy cut-off of 470 eV. All atoms in these Janus structures are totally relaxed, with convergence criterion of for total energy and force acting on atoms, respectively. In the Z-direction10^{-6} eV and 0.01 eV/Å, a vacuum gap of 30 Å was employed to avoid contact between the consecutive monolayer. Nonetheless, the optical properties are investigated by the density functional perturbation theory within an energy range between 0 and 25 eV. These properties include the absorption coefficient α(ω), the energy loss function L(ω), imaginary (Im(ε(ω)) and real (Re(ε(ω)) parts of dielectric function ε(ω), refraction index n(ω), the reflectivity R(ω), where ω denoted the frequency of incident photons.

3.2 Electronic Structure of Monolayer

Figure (3.1) shows the structure of HfSSe monolayer that are used in the present study, one can see from the figure that each simulated system consists of a 4× 4×1 supercell. These materials are arranged in hexagonal structures comprised of layer cemented together using VdW connections, and all of the layers contain monoatomic furnace blades in a D_3h symmetry configuration [98]. HfSSe has a

hexagonal crystal structure with the space group P_3m_1 [99]. These materials are better for dissociating water from electro-optical sampling, optoelectronic devices, and non-linear optics like photocatalysis, photodiodes, photoresistors, field-effect transistors, phototransistors, photovoltaics, and photodetectors[14]. The HfSSe monolayer has been described as a thermally stable semiconductor with an indirect energy gap spanning a broad optical spectrum [15–17]. In the bulk form, hafinum telluride has a moderate direct bandgap of about 0.62 eV [18,19]. This leads to the production of excitons and the enhancement of photon absorption. The energy band gap in the region of (1.5 to 2.5) eV is very important for photovoltaics, as this is where the majority of the Sun's light falls. The band gap of the HfSSe material, on the other hand, is substantially influenced by its thickness or layer count. Long carrier lifetimes and photoresponsivity exceeding 10^4 A/W are seen in the HfSSe monolayer [20], significant photoluminescence [21,22], photodetectors with a 6 ms reaction time and high excitonic emission and absorption [23]. As a result, HfSSe monolayer are thought to be a potential material for thermoelectric devices, photocatalysis, phototransistors, solar energy, and radiation detectors (including X-ray). Even though the observed charge carrier mobility is extremely low, the photoresponsivity of HfSSe multilayered flakes is significantly higher than that of graphene photodetectors (0.13 A/W) and MoS_2 monolayer (880 A/W) [100, 101, 102]. Many research groups have been interested in the characteristics of vdW heterostructures based on HfSSe, however the optical properties of the HfSSe monolayer have not been fully understood and are mostly unexplored, and need to be examined further. In this paper, we use first-principles calculations based on DFT simulations to analyze the optical and electrical characteristics of HfSSe monolayer in depth . The table (3.1) shows that the smallest value in bond length is 2.584 between (Hf – S) and Bond angel between (Hf – S – Hf) is 91.961.

Table (3.1) : Bond length Å and the bond angle of HfSSe monolayer.

Bond length Å		Bond angle (degree)	
Hf – Se	2.693	Hf – Se – Hf	87.240
Hf – S	2.584	Hf – S – Hf	91.961
Hf – Hf	3.716	Hf – Se – S	43.643
Se – S	3.743	Hf – S – Se	46.006
S – S	3.716	S – Hf – Se	90.35
Se - Se	3.716		

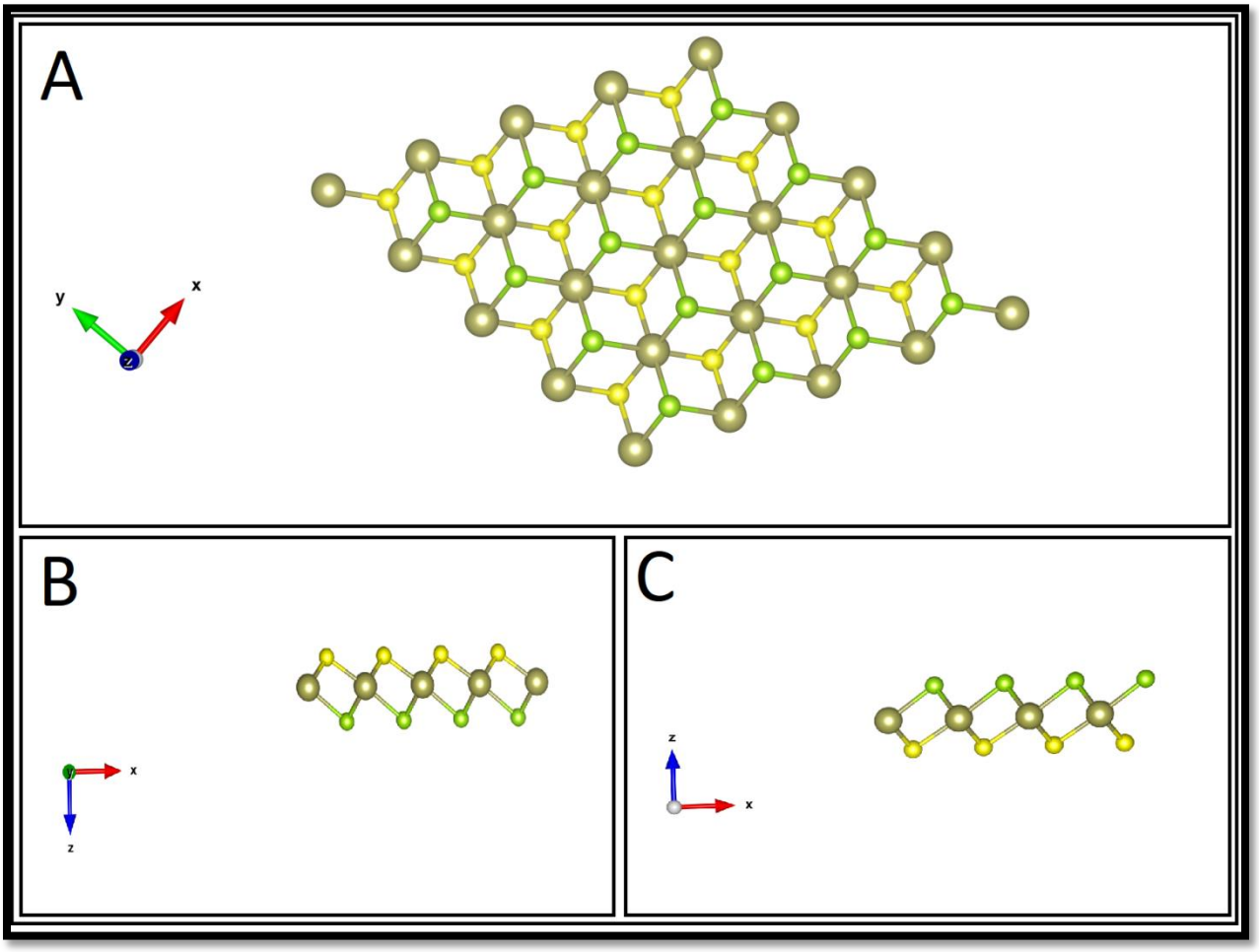

Fig. (3.1): A top view ,B and C side view of HfSSe monolayer, sulfur yellow color, selenium green color and hafnium brown color.

3.2.1 Band Structure

The energy ranges that an electron within a solid can travel are referred to as bands, permitted bands, or simply bands in the electronic band structure of the solid. Band gap or forbidden bands are energy ranges that do not have an electron within the material. Due to the limiting widths of the energy bands, band gaps are basically residual regions of energy that are not covered by any band. The widths of the bands vary depending on the degree of overlap in the atomic orbitals from which they emerge**.** It is of interest to see from Fig. (3.2) that the band structures of HfSSe monolayer indirect band gap, essentially because the VBM lying among the Γ and K points, while the CBM is located at the M point. The indirect band gap feature of HfSSe monolayer have been proved using first principles calculations [103,104]. The calculated indirect gap (ΓK–M) of HfSSe monolayer by PBE functional is 0.620eV as shown in the figure (3.2).

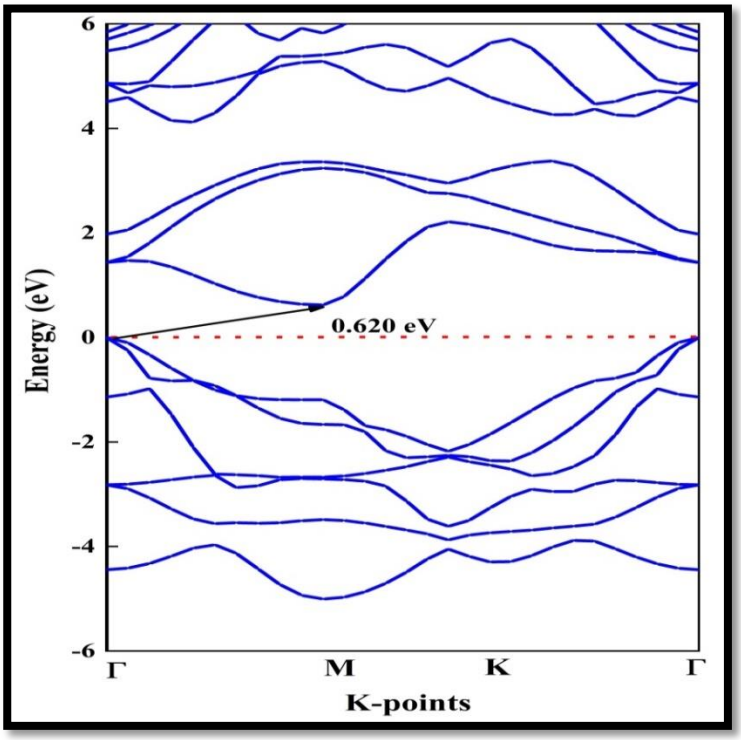

Fig. (3.2): Band structure of HfSSe monolayer.

3.2.2 Density of States

Determine which of the following components should be plotted in the density of states. Different densities of states for electrons with spin up and spin down can be formed in a spin-polarized system. As a consequence, a graph-total density of states is obtained by adding all energy bands together. Their difference yields the spin density of states, while their addition yields the overall density of states. The density of state is a valuable notion since it allows integration to be done with regard to electron energy rather than over the Brillouin zone. Furthermore, the density of state is frequently employed for fast electron structure investigation. External pressure can also create changes in electrical structure, which can be explained using density of state (DOS) analysis [104]. The partial density of states (PDOS) analysis approach is invalid for high-energy conduction band states; partial density of states representation will frequently degenerate to zero at roughly 20 eV above the Fermi level. This is due to the fact that expanding the basically free electron state in terms of a finite number of atomic-like basis functions is hard to do accurately. In a partial density of states plot, only the valance band and the bottom half of the conduction band are relevant**.** The angular momenta that should be included in the partial density of states can be modified using the s, p, d, and f variables. For evaluating electronic structure, partial density of states are valuable semi-qualitative tools. These results are further qualified by PDOS, which rotates these contributions according to the angular momentum of the states. It's frequently used to figure out where the DOS's primary peaks are of the s, p, or d character as shown in the figure(3.3) .

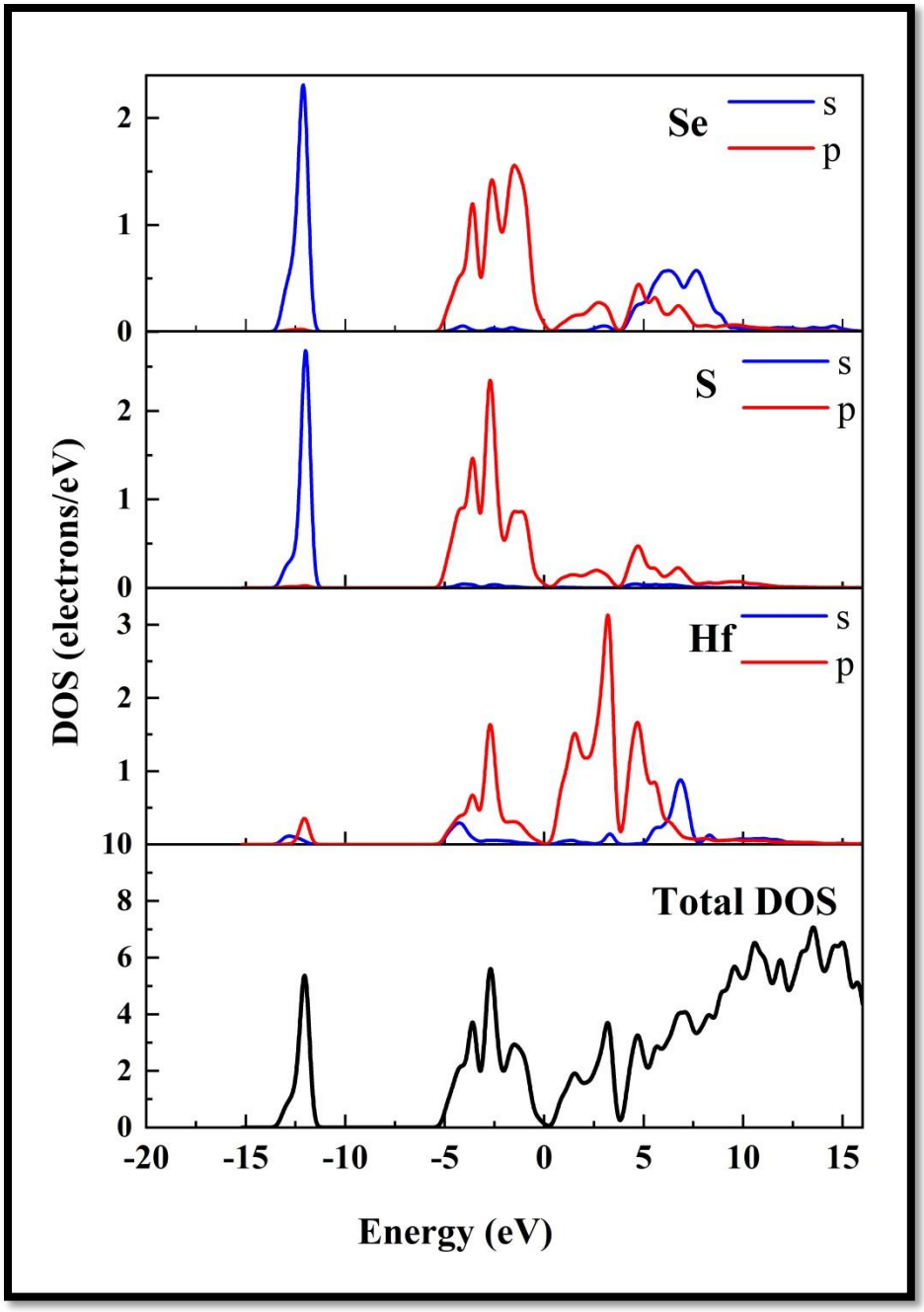

Figure (3.3) shows the electronic total density of states (DOS) of Se, S, and Hf monolayer.

3.3 Optical Properties

The optical characteristics of materials play a critical role in basic research and current applications, it is self-evident. The dielectric constants are calculated, as well as the accuracy with which the refraction index and dielectric constants can be determined using a combination structure. As a result, the optical characteristics of reflectivity, absorption coefficient, conductivity, refraction index, dielectric function, and loss function have been determined. These optical characteristics were determined for a range of energies from 0 to 25 eV.

3.3.1 Dielectric Function

The optical properties can evaluated from the knowledge of the complex dielectric function $\varepsilon(\omega) = \varepsilon_1(\omega) + i\varepsilon_2(\omega)$. The primary optical features of materials are linked to their imaginary portion in the dielectric function; for HfSSe monolayer, there is just one prominent peak for both the real and imaginary parts of the dielectric function, which occurs at (3.48 and 3.25) eV, respectively. The transitions of the direct electron from the valence band to the conduction band account for the majority of the peaks. The primary peaks in the real and imaginary components of the dielectric constant are seen to shift towards the lower energy region, indicating that input photons are entirely reflected here. This is referred to as redshift. It's worth noticing that the primary peaks of this monolayer imaginary parts are comparable to the main peaks of their real-part counterparts, as seen in Fig (3.4). It is generally known that the imaginary component of the dielectric function has a significant impact on the medium's absorption. The presence of several peaks in the imaginary region relates to the transition from one band to the next. As a result, a single peak in the imaginary section indicates the presence of a single inter-band transition between the valence and conduction bands. John and Merlin's

primary peak of the actual portion of stanene matches the main peak of the HfSSe monolayer rather well [105].

At zero photon energy limitations, the estimated static dielectric function is 2.65 monolayer . The static dielectric constant of HfSSe monolayer is lower than that of layered GaSe, which is equivalent to 4.7, as determined by Heyd-Scuseria-Ernzerhof (HSE06) [106]. Along the parallel polarization direction, however, the static dielectric constant values of HfSSe monolayer are equivalent to those of graphene and less than those of well-known 2D materials [105]. The dielectric constant is a necessary factor in determining the capacitance, so it is possible to benefit from the large of static dielectric constant to manufacture the capacitor.

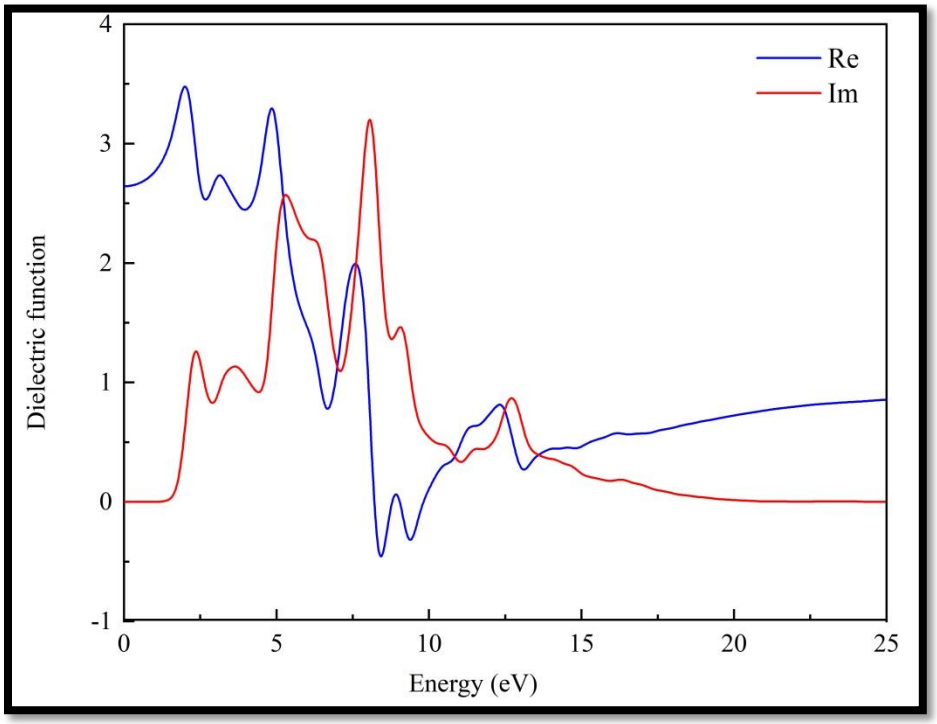

Fig (3.4): Dielectric function of HfSSe monolayer.

3.3.2 Absorption Coefficient

If the frequency of the light is resonant with the transition frequencies of the atoms in the medium, absorption occurs by propagation. The beam will be lessened as it develops in this situation. Because only unabsorbed light is conveyed, the medium's transmission is plainly connected to its absorption. The coloring of many optical materials is caused by absorption. Ruby is red because it absorbs blue and green light but not red light. The absorption of light by an optical medium is quantified by its absorption coefficient. This is defined as the fraction of the power absorbed in a unit length of the medium. When light traverses through a material, some energy is absorbed. To measure the extent of radiation energy absorption by a material**,** absorption coefficient α is determined as shown in equation (3.1).

$$\alpha=2\omega k/c=4\pi k/\lambda \qquad (3.1)$$

Where c is the speed of light in a vacuum, ω is the cyclic frequency, λ is the radiation wavelength and k is the extinction coefficient.

The absorption coefficient (α) represents the linear optical response valence from the bands to the lowest conducting bands [107]. The dielectric function is used to calculate the absorption [107,25]. The optical absorption spectrum is crucial for determining the optical characteristics of a material that will be employed in optoelectronic devices. When a light wave propagates per unit distance in a particular material, the absorption coefficient is the proportion of light intensity that is attenuated. The primary peaks of absorption coefficients are positioned at 8.321eV in the absorption coefficients seen in Fig. (3.5). This indicates that monolayer absorb UV light in a considerable way. The absorption peaks of the HfSSe monolayer are extremely comparable to those of single-layer GeP, SiP, and GeP, which exhibit prominent absorption peaks in the UV region [49]. This suggests that the HfSSe monolayer has more potential for use in photoelectric

devices, particularly in the UV area. The absorption and the imaginary component of the dielectric function are virtually inextricably linked. The imaginary component revealed that the absorption edge for HfSSe monolayer occurs at 1.81eV, putting the absorption edge in the visible light spectrum. This absorption edge is quite similar to the UV–vis absorption maximum of silicene functionalized with phenyl and bigger aromatic molecules [108]. The absorption edge of visible light is particularly important for photocatalytic activity in practical applications.

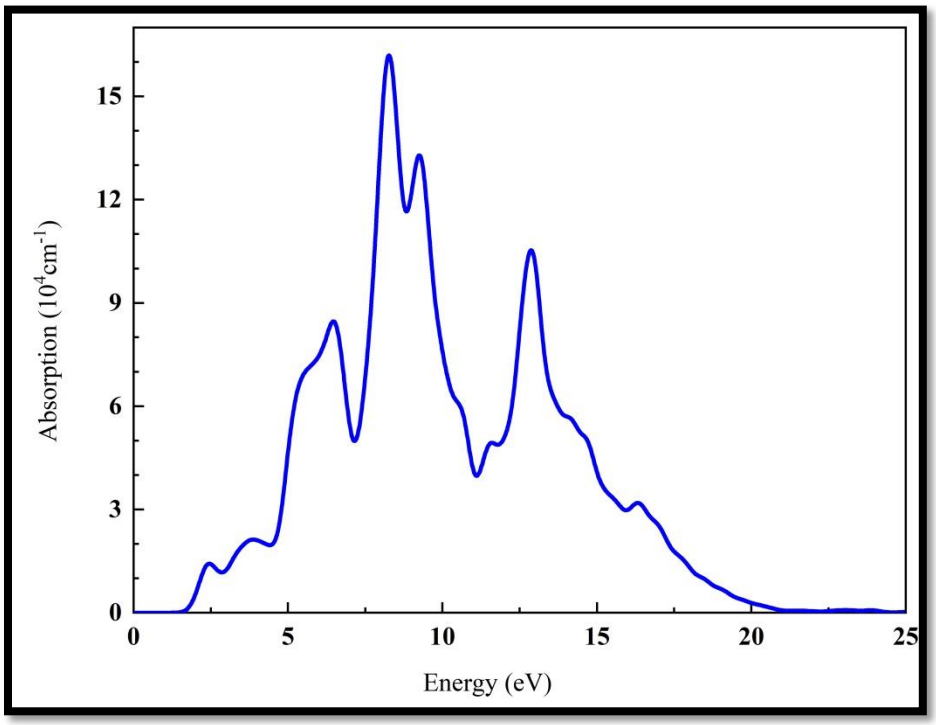

Fig. (3.5): Absorption of HfSSe monolayer.

3.3.3 Conductivity

Figure (3.6) depicts the estimated optical conductivity as a function of energy across the energy range of (0–25) eV. For HfSSe monolayer, conductivity begins at an energy of 2.18 eV. Nonetheless, for HfSSe monolayer, the curves rise to the maximum optical conductivity at peak 7.91eV. The optical conductivity of graphene, silicene, and germanene honeycomb crystals is greater than this.

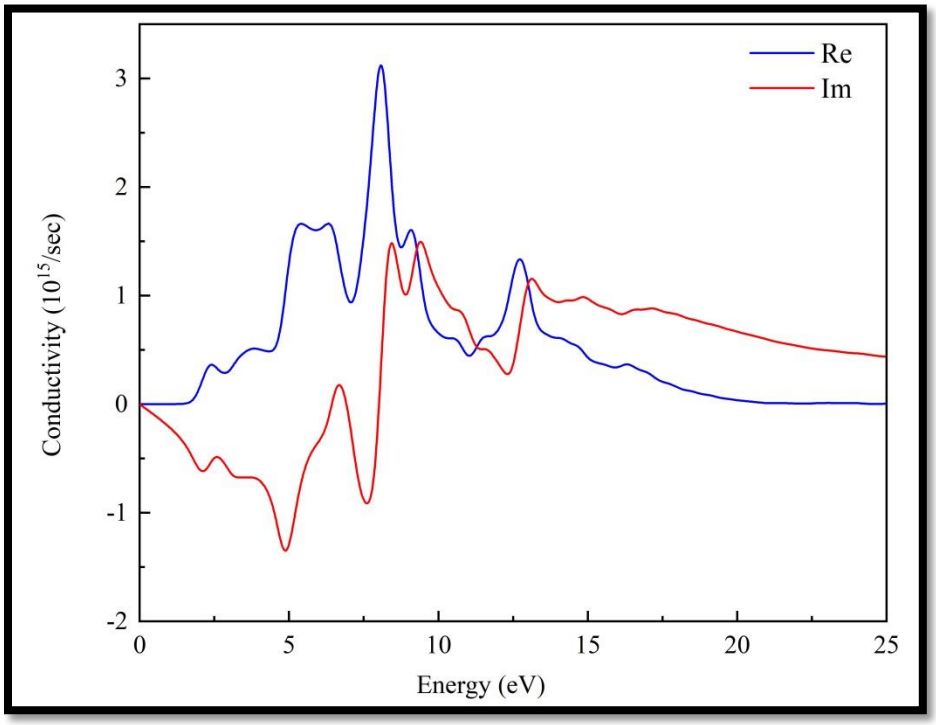

Fig (3.6): Conductivity of HfSSe monolayer.

3.3.4 Loss Function

The loss function, which is a vital characteristic representing the unadaptable disseminating of high accelerated electrons moving through the material and characterizing the plasma frequency associated to it, is another key function of optical properties that has been clarified in this work. The material operates as a dielectric beyond the plasma frequency and exhibits metallic nature below it. The peaks of energy loss describe the mixing of plasma frequency in addition to their

corresponding resonance. The major sharp peak for HfSSe monolayer is located at 11.13 eV, whereas the peak of energy loss for HfSSe monolayer is located at 11.13 eV. This energy denotes the point when this monolayer metallic to dielectric properties change; following these values, energy loss reduces as photon energy increases, as seen in Fig (3.7). This monolayer highest energy loss functions occur in the UV range. As a result, this monolayer can be effective absorbers of low-medium and low-ultraviolet wavelengths. As a result, the current monolayer can be used in solar cell applications. As is customary, the energy loss peaks depict the plasma frequency; plasma frequency is the boundary between the material's behavior as a dielectric and as a metallic; in more precise terms, any material behaves as a dielectric at lower values than plasma frequency and as a metallic material beyond this frequency. The apex of the loss function occurs in the UV zone, as previously stated.

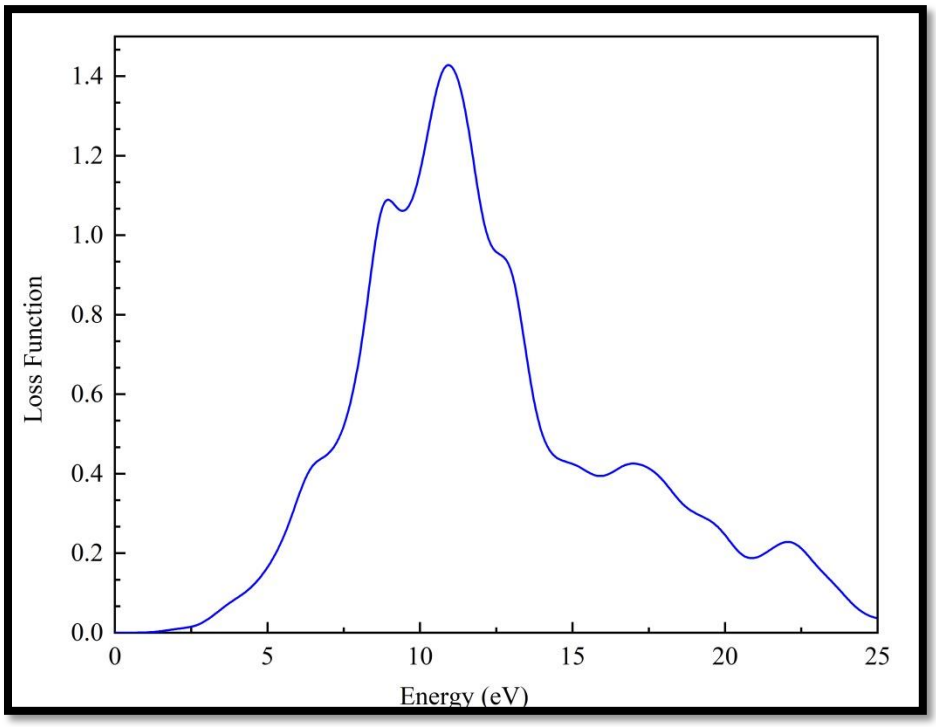

Fig. (3.7): Loss functions of HfSSe monolayer.

3.3.5 Reflectivity

The computed reflectivity as a function of energy is shown in Fig. (3.8), and it is discovered that the static reflectivity is 5.82eV monolayer, which occurs around zero frequency and when the free carriers are dominant. Above this point, the curve of displays increases in reflectance as photon energy increases.

The highest reflectivity values are 28% and occur in the middle UV, indicating that the maximum reflectivity value does not exceed 28% in all circumstances.

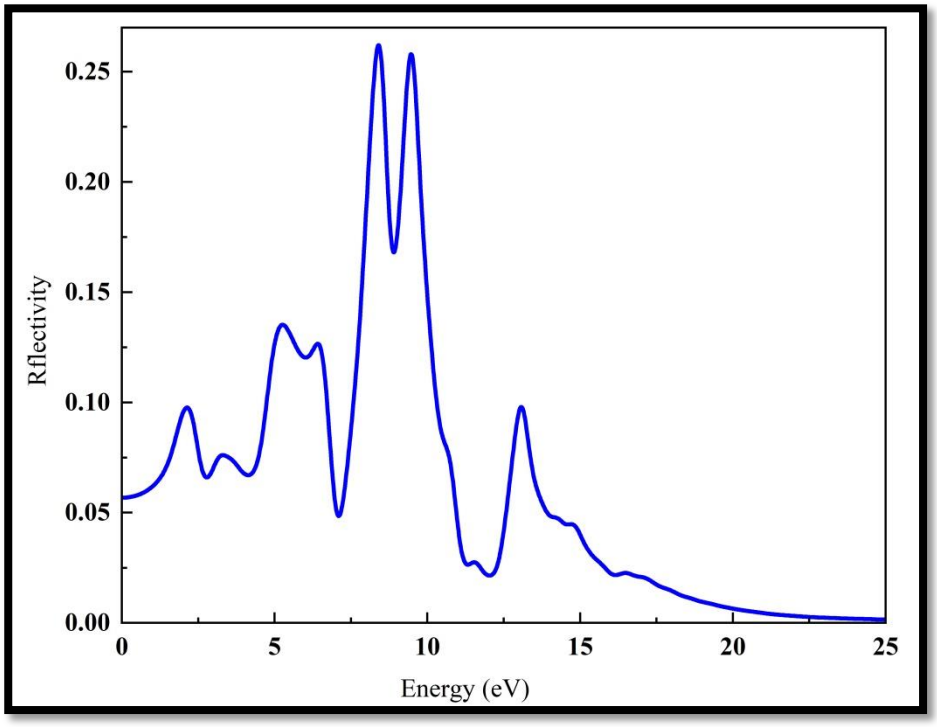

Fig. (3.8): Reflectivity of HfSSe monolayer.

3.3.6 Refractive Index (n)

The refractive index n describes the propagation of a beam through a clear material. The ratio of the velocity of light in free space to the velocity of light in the medium is defined as this. The frequency of the light beam determines the refractive index. Dispersion is the term for this effect. As a result, it denotes the speed at which light travels through a substance. The refractive index increases with the frequency of incoming light under normal dispersion. When a material absorbs a large amount of radiation energy, its true refractive index deviates from normal dispersion and suffers a decrease, known as anomalous dispersion, as the frequency of the radiation increases. In the optoelectronic characteristics of materials, the refraction index is very important. At zero photon energy, the static real part refractive indices for HfSSe monolayer are equal to 1.644. The greatest value of the refractive index (real portion) for HfSSe monolayer is 1.910, which occurs at almost 3.383 eV. The refractive index steadily drops beyond this point. This monolayer can be used as an internal layer coating between the substrate and the UV absorption layer due to their high refractive indices. In this monolayer, the refractive index is anisotropic. The extinction coefficient (imaginary component) of the HfSSe monolayer in the UV region, on the other hand, rapidly decreases with increasing photon energy and becomes constant after 24 eV as shown in the figure (3.9).

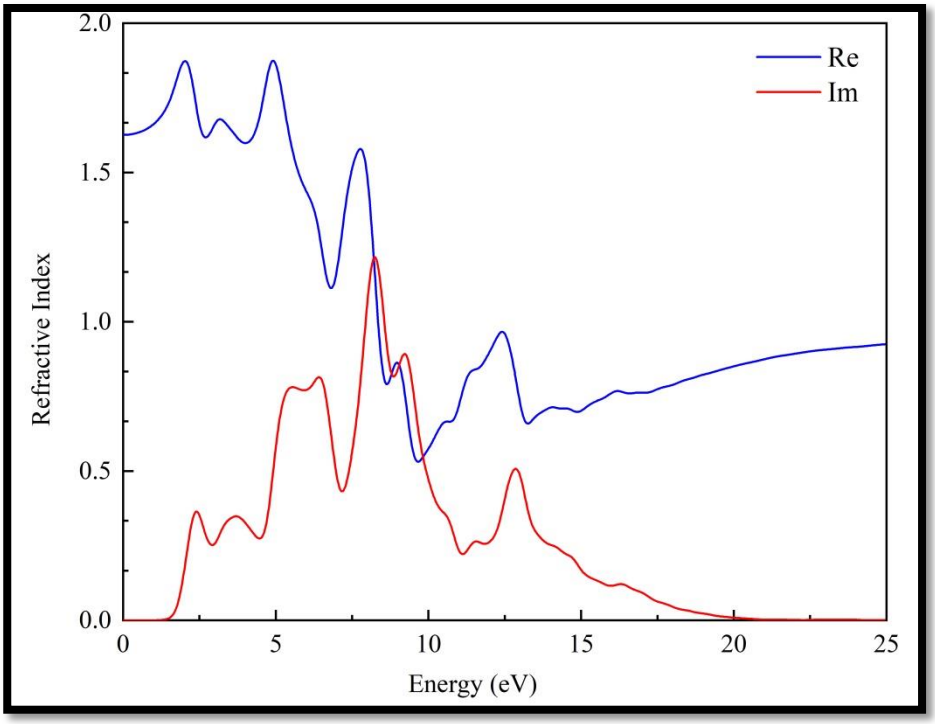

Fig. (3.9): Refractive index of HfSSe monolayer**.**

Chapter Four
Results And Discussion
Part Two

4.1 Adsorption Energy

For the study of structural, electronic, and optical properties, a comprehensive study is carried out for adsorption of gas molecules at different sites using adsorption locator module to find the sites of low energy absorption of gas molecules adsorbates. The adsorption energy (E_{ad}) can be calculated according to [109],

$$E_{ad} = E_{tot} - \left(E_{Hfsse} + E_{gas}\right) \quad (4.1)$$

Where E_{Hfsse} is the energy of monolayer (Se and S), E_{gas} is the energy of isolated gas molecules, and E_{tot} is the total energy of the system (Gas + monolayer). According to this definition, a negative value of E_{ad} indicates that the adsorption is exothermic and energetically favorable. Contrarily, positive adsorption energy implies the opposite situation.

Table (4.1). The calculated adsorption energy (E_{ad}), the bond length between atoms in gas molecules (d) Å, between the gas molecules (CO, CO_2, NO, NO_2,and SO_2) and HfSSe (Se and S) monolayer.

Gas molecules	Bond length(d) Å	E_{ad}(ev)
CO	CO-Se=3.632 CO-Hf=5.880 CO-S=5.342	CO-Se=-0.10354 CO-S=-0.10292
CO_2	CO_2-Se=4.458 CO_2-Hf=5.637 CO_2-S=5.512	CO_2-Se=-0.24137 CO_2-S=-0.24236
NO	NO-Se=5.562 NO-Hf=5.562 NO-S=5.321	NO-Se=-0.26926 NO-S=-0.26926

NO_2	NO_2-Se=4.397 NO_2-Hf=5.645 NO_2-S=5.469	NO_2-Se=-1.46403 NO_2-S=-1.46403
SO_2	SO_2-Se=4.576 SO_2-Hf=5.926 SO_2-S=5.899	SO_2-Se=-1.97503 SO_2-S=-1.88768

To begin with, the adsorption energy is a sign of stability of the system. The higher the adsorption energy, the more stable the system under study. Of course, the adsorption energy is fundamental importance to the properties of material behavior, such as physisorption or chemisorption. In addition, our outcomes portend that all the adsorption energies are negative values that infer the exothermic nature energetically favorable upon adsorption gas molecules. In this work, we take an attempt to examine the adsorption of several common pollutant gas molecules, CO, CO_2, NO, NO_2 and SO_2 which are of great importance for industrial and environmental, on HfSSe (Se and S) monolayer based on DFT.

Thus, we regularly investigated the adsorption distances (d), adsorption energies (E_{ad}), the partial density of states (PDOS), and optical properties of the adsorbed molecules on HfSSe (Se and S) monolayer.

4 .2 Adsorption of CO gas on HfSSe of Se and S Monolayer

The adsorption of carbon monoxide (CO) on monolayer is one of the most fascinating issues in surface science study. CO is a kind of hazardous gas molecule that is used in environmental monitoring, chemical process control, space missions, agricultural, and medicinal applications. CO is a non-irritating, colorless gas that, when it enters a human's body, mixes with blood hemoglobin, preventing the union of oxygen and hemoglobin, resulting in hypoxia and suffocating of bodily tissues

[110]. Figure (4.1) shows the most advantageeous configurations of CO adsorbed on HfSSe on Se and S monolayer, this monolayer deforms to some extent, and some atoms shift exterior the plane after relaxation. The most stable scenario for the monolayer-gas molecules system is when the carbon atom of CO is located in the center of the monolayer and the atoms in the monolayer surface lie in the plane and do not migrate outside after relaxing.

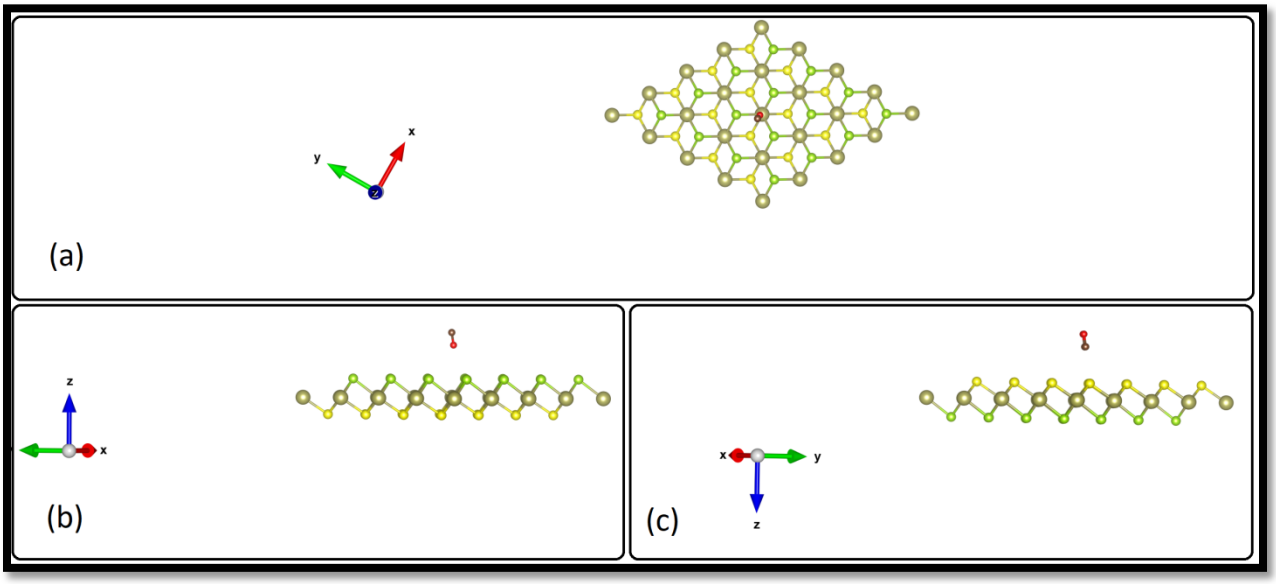

Fig. (4.1): (a) Top view of the adsorbed molecule CO on the HfSSe (b) side view Se and (c) side view S monolayer, sulfur yellow color, selenium green color and hafnium brown color.

The bond length between (Hf–CO) of HfSSe monolayer are 5.880 Å and (Se-CO) are 3.632 Å and (S-CO) are 5.342 Å, respectively. Furthermore, the low adsorption energy,becouse the large adsorption distance indicate that CO (Se-S)is physically adsorbed on monolayer via VdW interactions [48]. The E_{ad} of the CO on the HfSSe-Se monolayer shows comparable value to HfSSe-S which means that CO molecule may chemically adsorb, acting as a donor. After adsorption, the band gaps of the adsorbed systems in CO HfSSe on Se (0.618 eV) and S (0.617 eV) show a little change as shown in Fig. (4.2)

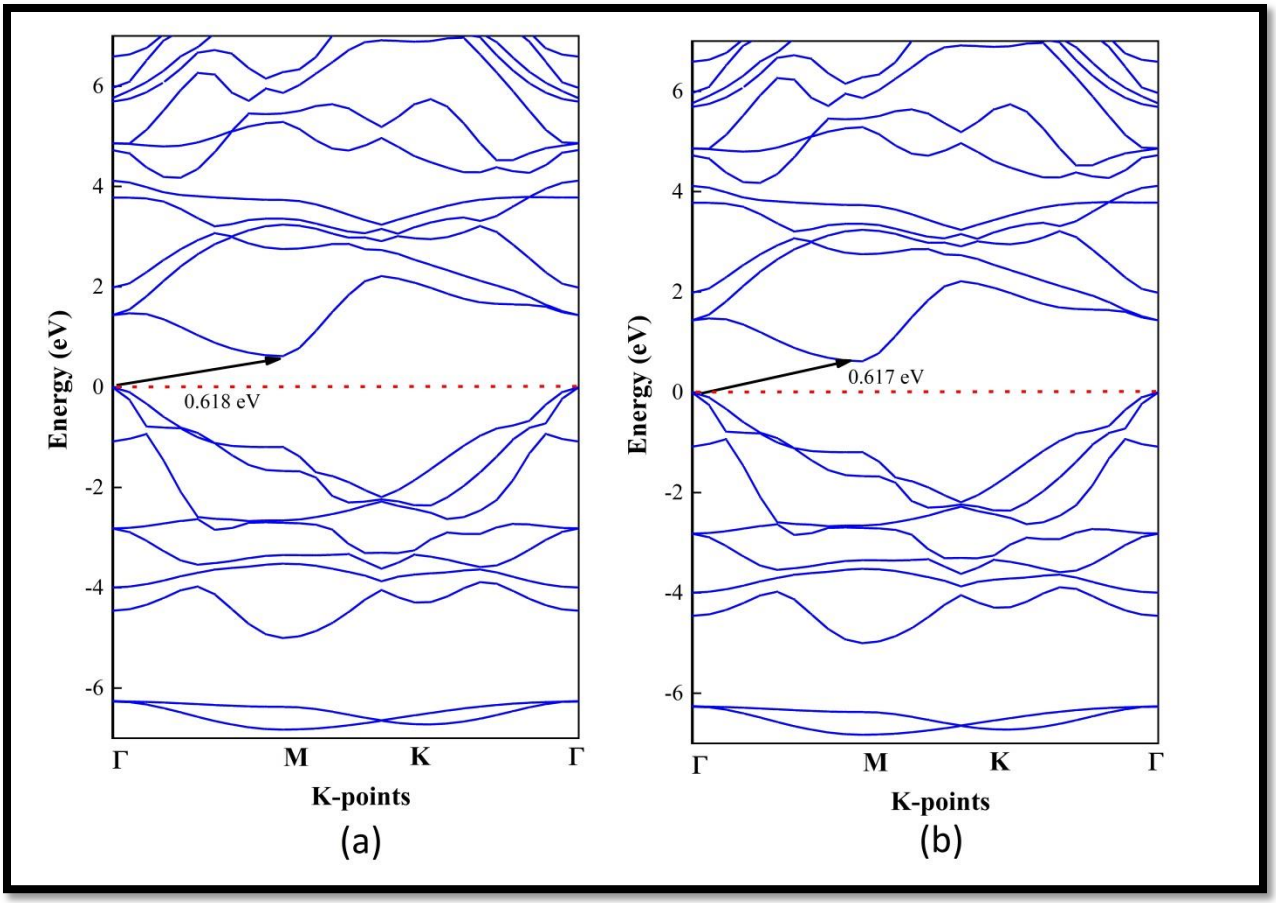

Fig. (4.2): Band Structures of HfSSe (a) Se and (b) S monolayer after the adsorption of CO gas.

the band gaps of the adsorbed systems are smaller; shrink as compared to that of pristine monolayer. Also, the electrons in full bands can be incited into the empty band with small energy. All in all, the VBM positions as noticed, do not remain along the M-Γ path as indicated in the band structure diagram, except in the state of HfSSe,Se monolayer (Fig. (4.2)). In order to further illustrate the interactions of the CO molecule on the different monolayer systems, their total and partial densities of states (DOS and PDOS) of the adsorption systems are calculated and presented in Fig. (4.3). It is found that the DOS of the CO on monolayer shows a little change after the adsorption and the contribution of the CO electronic levels to the total DOS is located between(1.3-2)eV in the VBs and around (-3-4.2) eV in CBs,

which is far away from the Fermi level. This behavior is similar to the adsorption of CO on phosphorene [17], stanene [102], graphene-like ZnO [111]and germanene [45] and further confirming the weak interaction of CO molecule on monolayer system.

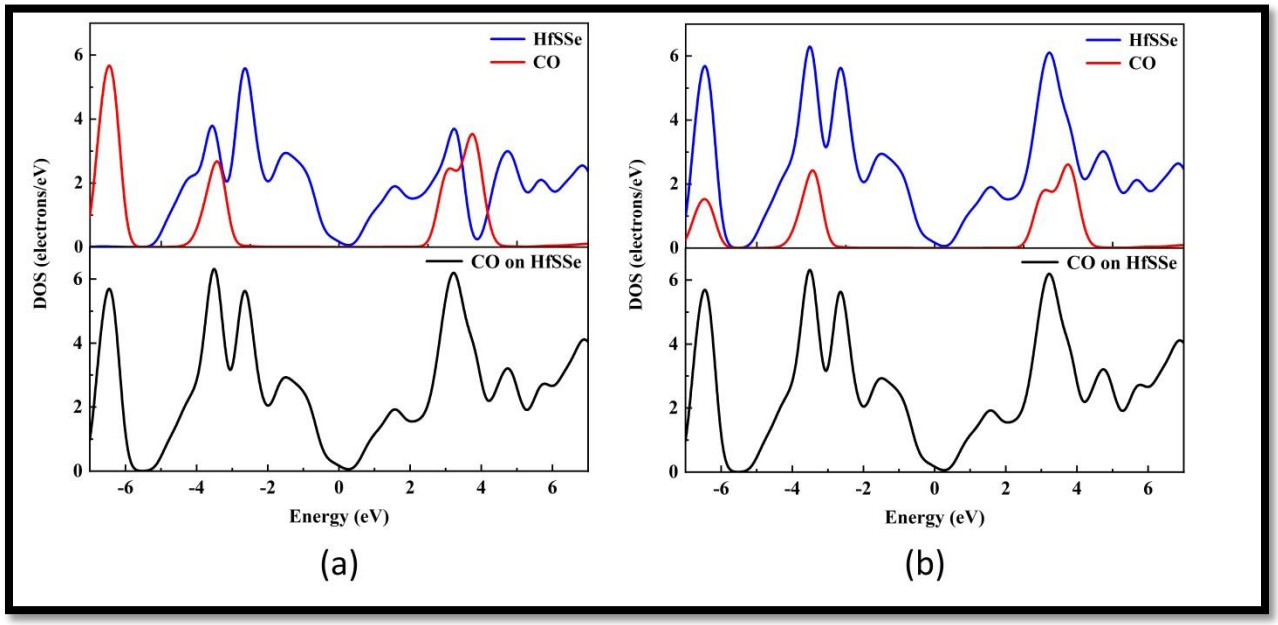

Fig. (4.3): DOS of HfSSe (a) Se and (b) S monolayer after the adsorption of CO gas.

4.3 Adsorption of CO_2 gas on HfSSe of Se and S Monolayer

Carbon dioxide (CO_2) concentrations in the atmosphere continue to grow, posing a serious danger to humanity's long-term security. As a result, it has risen to the forefront of global concerns. CO_2 reduction is regarded as the most difficult challenge in environmental conservation. The search for acceptable materials (with the best cost and efficiency) capable of detecting CO_2 in order to include them in the manufacture of devices such as sensors is one example of a solution to this challenge [106].

The most stable configuration of CO_2 adsorbed on HfSSe is discovered in Fig. (4.4), which demonstrates that the bond lengths between Hf-CO_2 of (5.637) Å,

which essentially decrease with the increase of electrons in the elements, are comparable to CO adsorption on HFXY monolayer. Furthermore, our findings suggest that all adsorption energies are negative, implying an exothermic character that is energetically advantageous to adsorption gas molecules. This monolayer are suitable as a sensor for CO_2. Besides, the adsorption of CO_2 molecule on HfSSe-S has the lowest adsorption energy (-0.24236 eV) compared to the other molecules which make it less feasible for CO_2 sensor with less binding between the molecule and monolayer. On the other hand, the E_{ad} of HfSSe-Se is almost the same without charge transition. the adsorbed CO_2 on HfSSe is a physisorption.

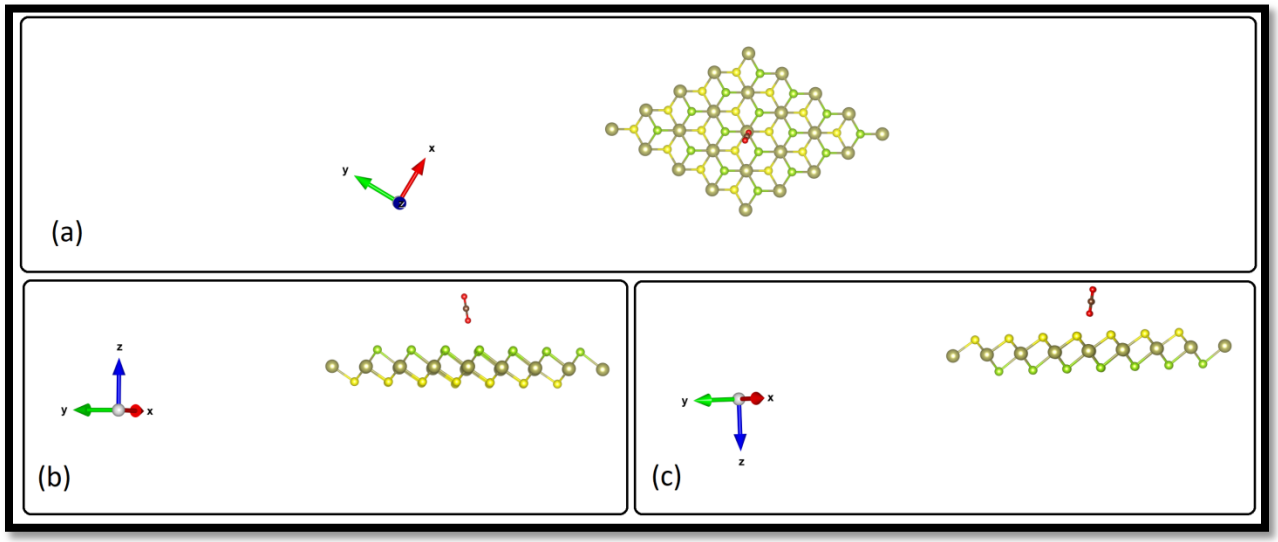

Fig. (4.4): (a) Top view of the adsorbed molecule CO_2 on the HfSSe (b) side view Se (c) side view S monolayer, sulfur yellow color, selenium green color and hafnium brown color.

The band gaps of the adsorbed systems in HfSSe,Se (0.628 eV) and HfSSe,S (0.627 eV) exhibit a minor modification after adsorption, as illustrated in Fig. (4.5). Clearly, the energy gap in the case of HfSSe,Se monolayer increases by a very tiny amount, but the band gap in the case of HfSSe,S monolayer decreases due to CO_2 adsorption. Kumar and Roy describe single layer stanane as having a similar behavior [50]. In addition, electrons in full bands can be incited into an empty band

with a modest amount of energy. In general, the VBM locations, as seen in the band structure diagram, persist along the Γ-M path as shown in the figure (4.5).

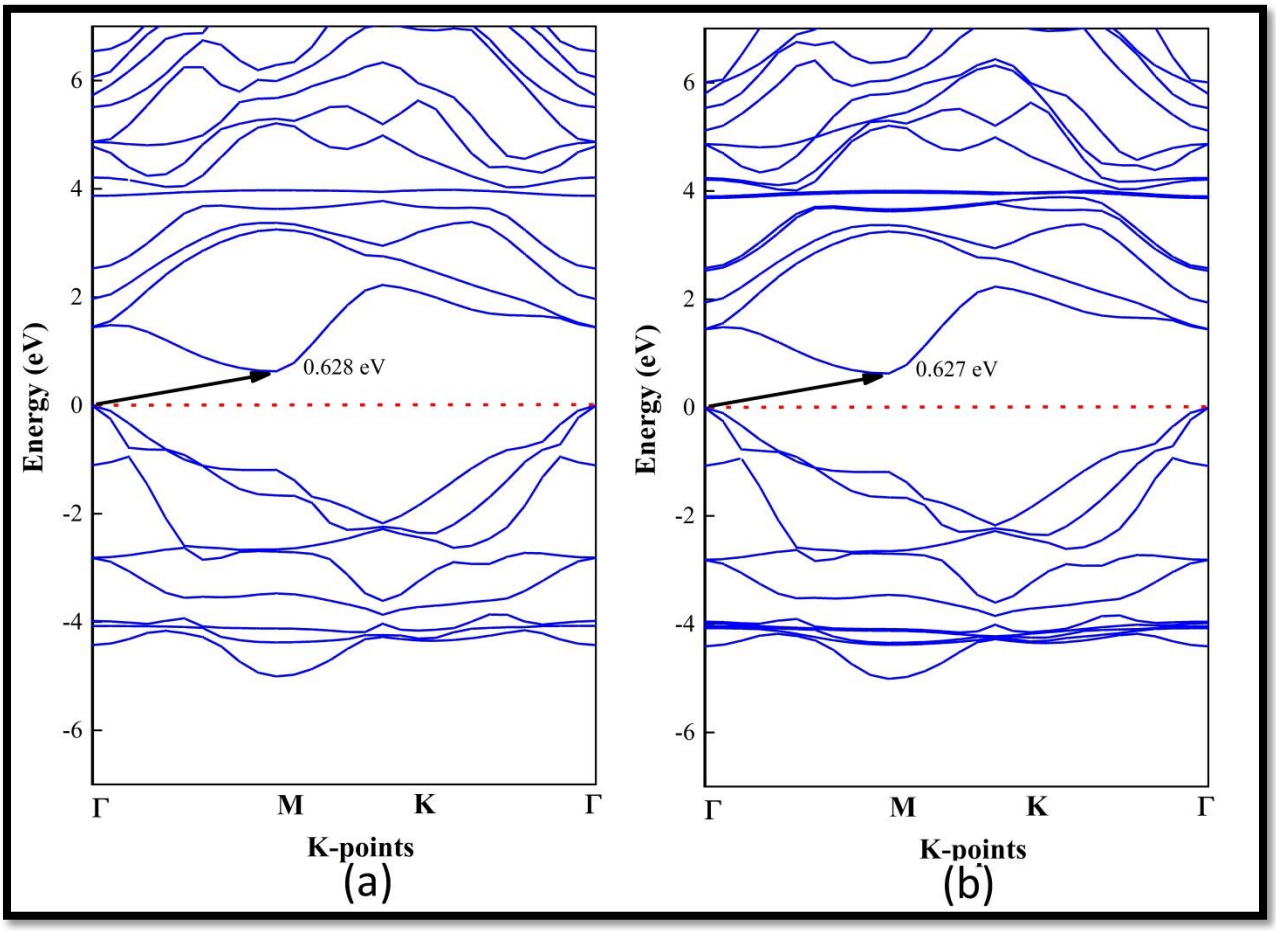

Fig. (4.5): Band structures on HfSSe of (a) Se and (b) S monolayer after the adsorption of CO_2 gas.

When gas molecules are adsorbed on monolayer, the DOS in the valence and conduction bands of the molecules are drastically changed. Gas molecules have a significant role in the electronic states of a molecular monolayer system. All gas molecules have distinct and strong contributions, with the exception of CO_2, which has a simple gas contribution in DOS but may be clearly identified. Also, the adsorption of molecules on the HfSSe monolayer lead to several peaks in the valance band and in the conduction band, these peaks were different from gas to another due to the nature of gas molecules. However, the most contribution is in

the conduction band, in particular, in the region between 3 and 6.5eV, which is consistent with the reduction of the energy gap in the adsorption systems. DOS of HfSSe monolayer as shown in Fig (4.6).

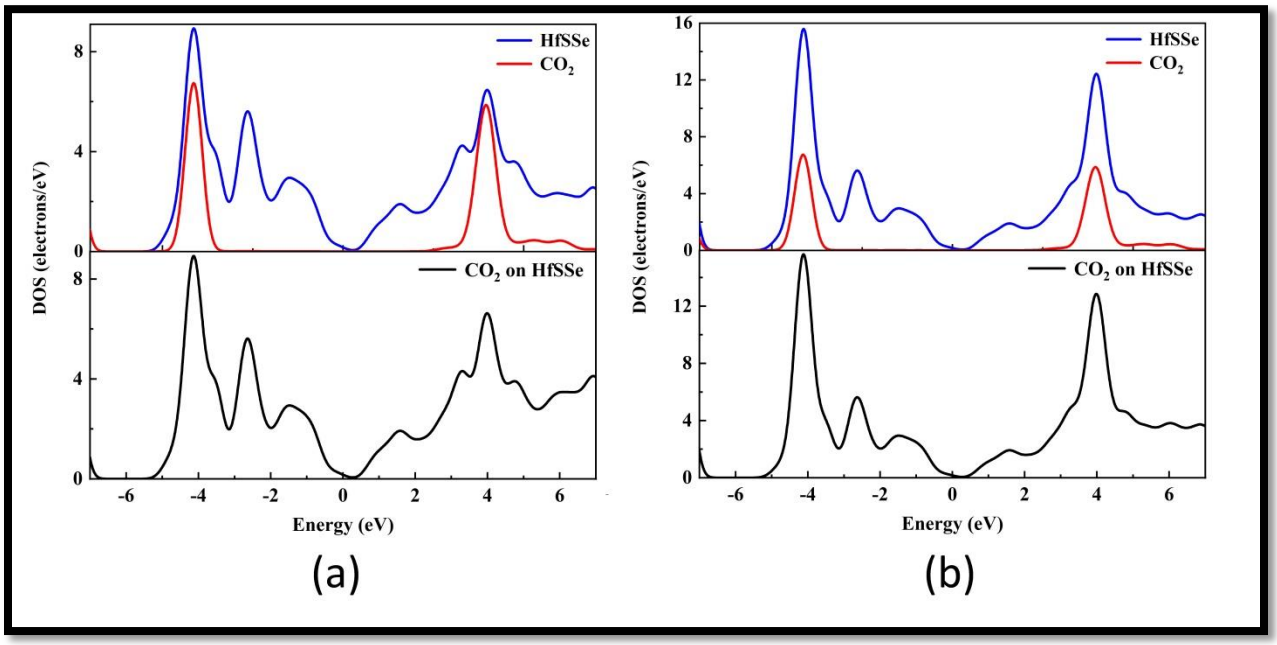

Fig. (4.6): DOS of HfSSe of Se and S monolayer after the adsorption of CO_2 gas.

4.4 Adsorption of NO gas on HfSSe of Se and S monolayer

The gas nitric oxide (NO) is colorless. Non-combustible, yet helps combustible materials burn faster. Inhalation and skin absorption are both extremely dangerous [15]. We want to investigate the influence of this gas on the structural and electrical characteristics of these monolayer after it has been absorbed. Figure (4.7) shows the optimal adsorption structure of adsorbed NO on HfSSe of Se and S monolayer. The distance between Hf and NO is 5.562 Å, while S-NO and Se-NO, are (5.321and 5.464) Å respectively, this means that NO closer to S, which is mean that this distance decrease with increasing of the number of electrons in the elements. The larger adsorption energies and shorter distance between the gas

molecules and monolayer lead to a larger interaction. The adsorption energies for HfSSe-Se and HfSSe-S are(-0.26926eV) . Because of the weak connections between the electrons of the monolayer and the NO gas molecules, the adsorption of each gas molecule on the monolayer is modest. The middle of the monolayer is occupied by the NO molecule. The monolayer strong interaction with NO results in a substantially stronger. The fact that these interactions are physisorbed interactions is clear from the outcome. On the other hand, it's clear that the distance between gas molecules and monolayer matters a lot. The low adsorption energy and wide separation height clearly suggest that the NO gas molecules investigated in this work are physisorbed on the HfSSe of the Se and S monolayer.

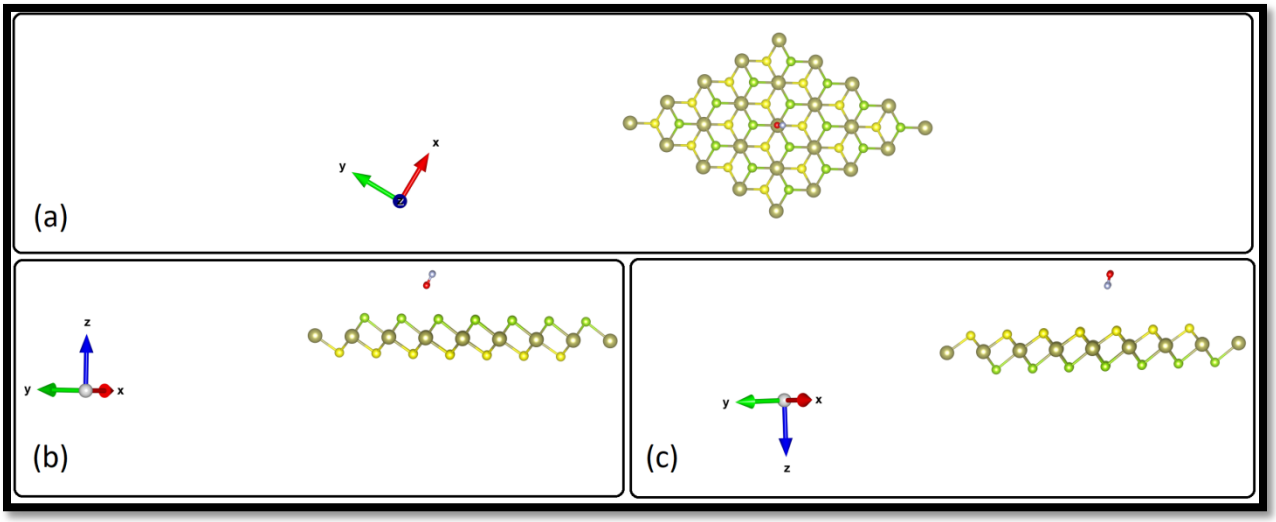

Fig. (4.7): (a) Top view of the adsorbed molecule NO on the HfSSe (b) side view Se and (c) side view S monolayer, sulfur yellow color, selenium green color and hafnium brown color.

In general, HfSSe monolayer can share electrons with the gas molecules. The band structures of the molecule-monolayer systems were calculated to evaluate the influence of the adsorption of various gas molecules on the electronic properties of monolayer HfSSe of Se and S monolayer. By comparing with the pristine monolayer HfSSe of Se and S in Fig. (4.8), there is no energy gap due to the

interference of the valence beam with the conduction beam at the Fermi level for HfSSe of Se and S monolayer and this means that it is conductive. The effect of NO adsorption on the partial density of state (PDOS) and total density of state (TDOS) of NO-HFXY systems are calculated and analyzed. Fig. (4.9) displays the PDOS and TDOS of NO molecule interacts with the surface of HFXY after NO molecule adsorbed. The TDOS of the NO-HFXY system shows a noticeable change near the Fermi level and a strong orbital hybridization. It is evident that there are states available for the occupation at high DOS for a specific energy level and no states can be occupied at a zero- DOS for energy level. We can see that the states above Femi energy disappear after the NO adsorbed on, due to the fix of N atom on the S atoms, which is similar to the previous report [112]. We can see from Fig. (4.9) that the large overlap at Fermi level evident for HfSSe of Se and S monolayer.

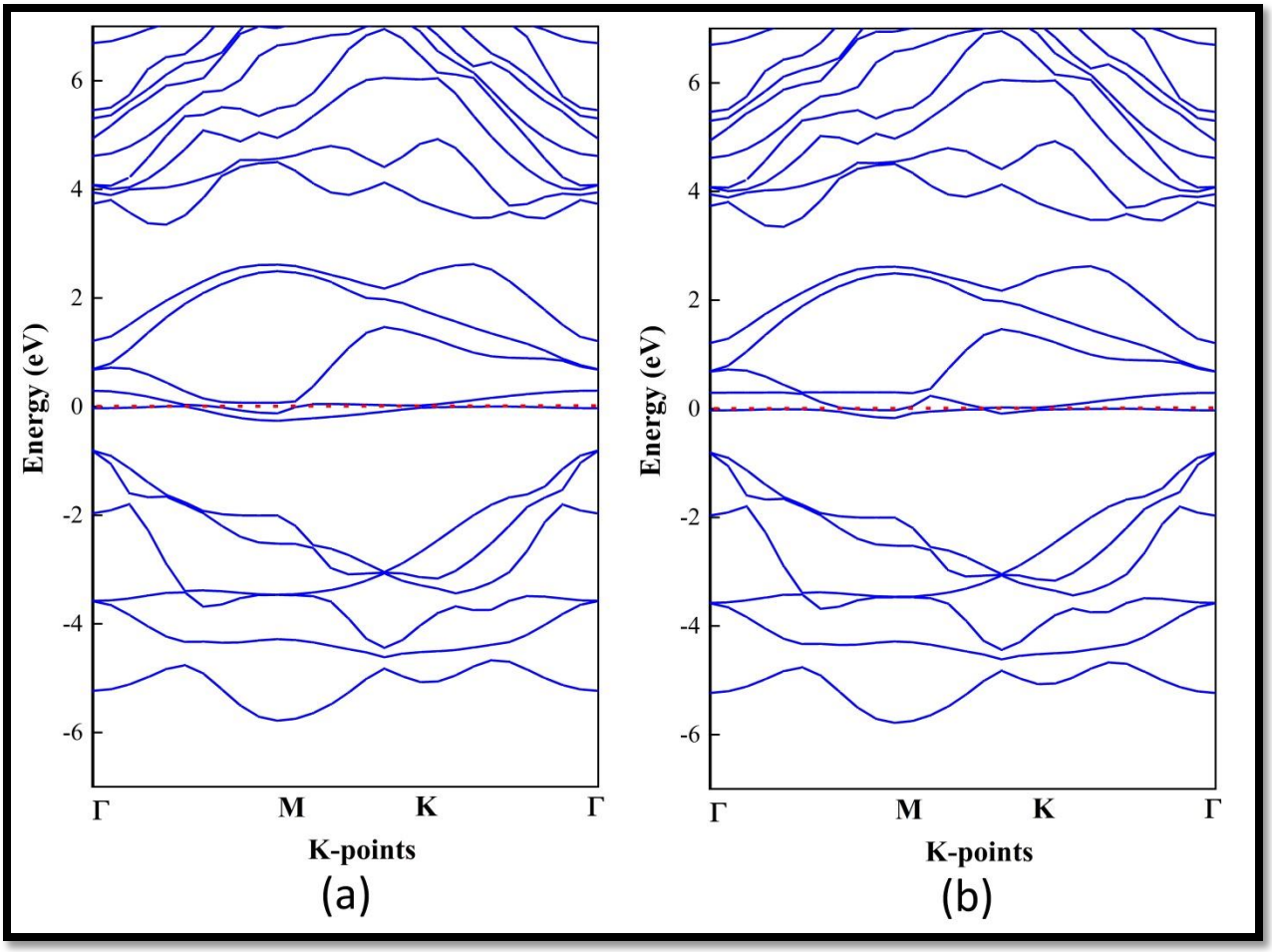

Fig. (4.8): Band structures of HfSSe (a) Se (b) S monolayer after the adsorption of NO gas.

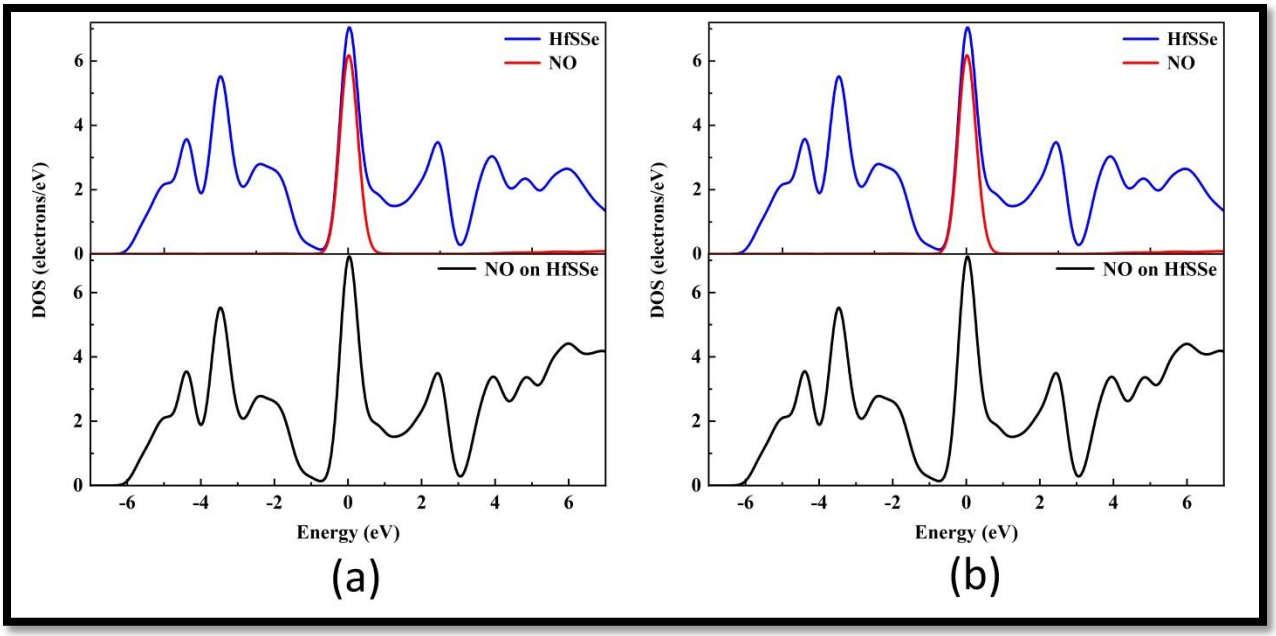

Fig. (4.9): PDOS and TDOS of HfSSe (a) Se and (b) S monolayer after the adsorption of NO gas.

According to our calculations, the two types of states in HFXY can increase the bonding energy between the adsorbed NO molecule and the HFXY monolayer greatly. The adsorbed HFXY (X = S, Se) is more appropriate for NO detection than pure HFXY.

4.5 Adsorption of NO_2 gas on HfSSe of Se and S Monolayer

Nitrogen dioxide (NO_2) is a caustic and powerfully oxidizing reddish-brown, smelly, acidic gas. The burning of fossil fuels (coal,853. gas, and oil), particularly in automobiles, is the primary source of nitrogen dioxide produced by human activity. NO_2 is a trace gas in the Earth's atmosphere, where it absorbs sunlight and regulates the chemistry of the troposphere, particularly in determining ozone concentrations, according to these sources [73]. Fig. (4.10) shows top and side views of the adsorbed molecule NO_2 on the HfSSe of Se and S monolayer. The distance between NO_2 gas and (Hf,Se,S)are (5.645,4.397,5.469)Å, respectively, NO_2 can be physically adsorbed on monolayer with high adsorption energies (-

1.46403) eV. NO_2 shows the strongest affinity with E_{ad} of −1.46403 eV for HfSSe, It can be noticed that the NO_2 molecule distorts significantly After the adsorption.

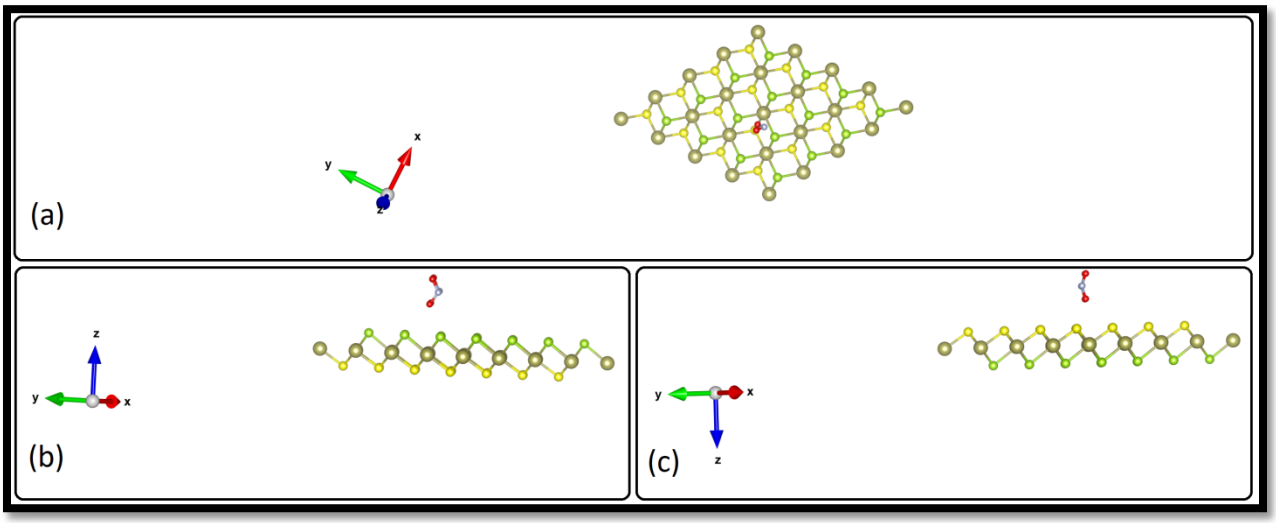

Fig. (4.10): (a) Top view of the adsorbed molecule NO_2 on the HfSSe (b) side view Se (c) side view S monolayer, sulfur yellow color, selenium green color and hafnium brown color.

Figure (4.11) shows the electronic properties of adsorbed NO_2 gas molecules on monolayer. Compared with the band structure before adsorption that presented, it is noted that after the adsorption of the NO_2 gas molecules, band gap varying is (0.628 and 0.639) eV for HfSSe of Se and S monolayer, respectively, as can be observed in Fig. (4.11). This monolayer band structure is sensitive to lattice symmetry, and the adsorption of NO_2 gas molecules leads to out-of-plane distortion of the monolayer lattice. Therefore, a gap varying is resulted, and well agrees with results of previous investigators.

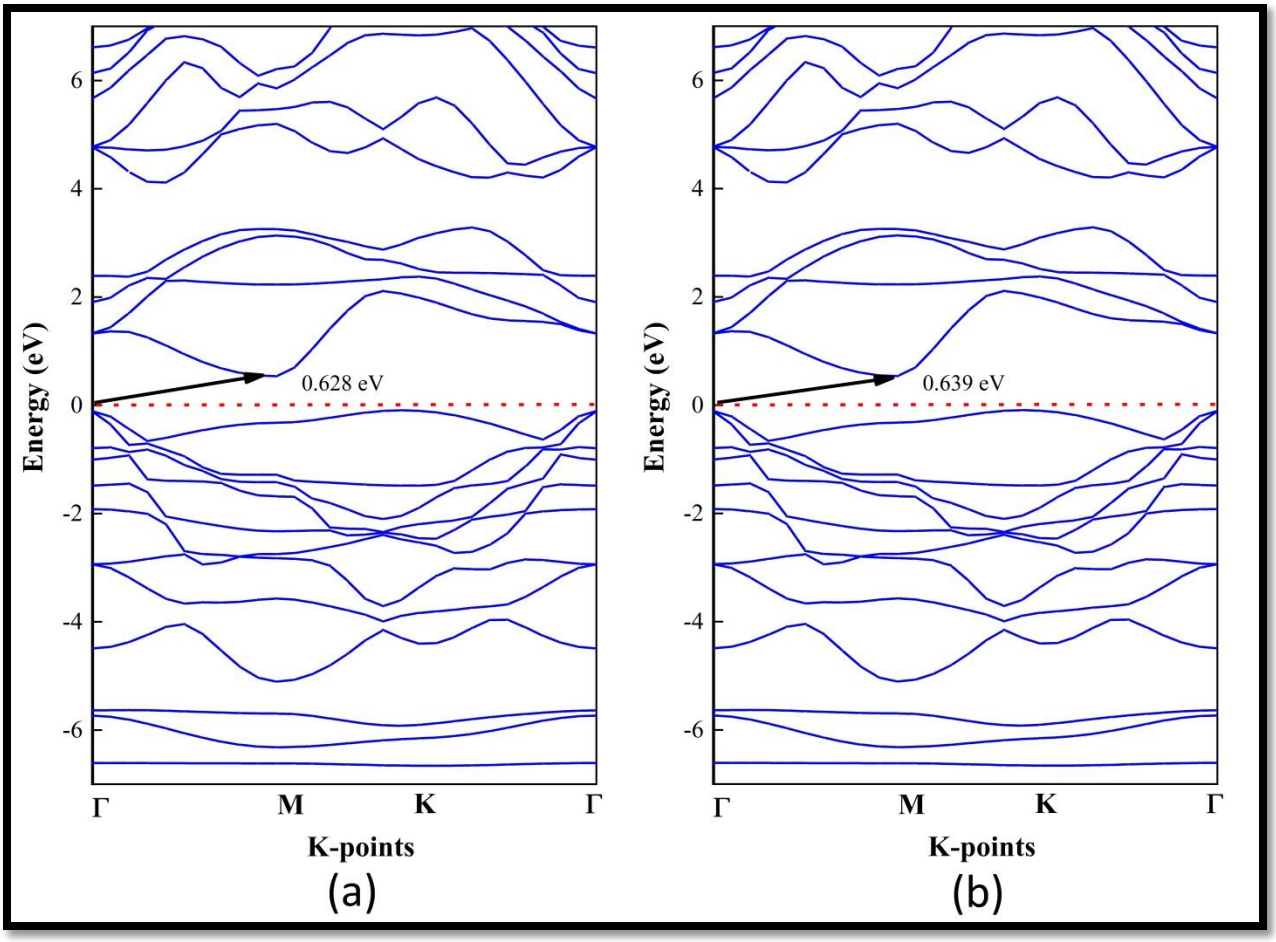

Fig (4.11): Band structures of HfSSe (a) Se and (b) S monolayer after the adsorption of NO_2 gas.

The symmetry break that transforms a monolayer from a semiconductor to a semimetal can be attributed to regularly ordered hybridization [113]. This finding may be explained by a substantial quantity of electron transfer and the creation of strong chemical interactions between the electron cloud and the orbitals of gas molecules [103]. In order to further verify the mechanisms of NO_2 adsorption interaction, the DOS and the PDOS of monolayer and molecules system are presented in Fig. (4.12). The adsorption of NO_2 on HfSSe causes a clear change in the DOS in the vicinity of the Fermi level because of the contribution of NO_2 electronic levels and NO_2 orbital is dominating.

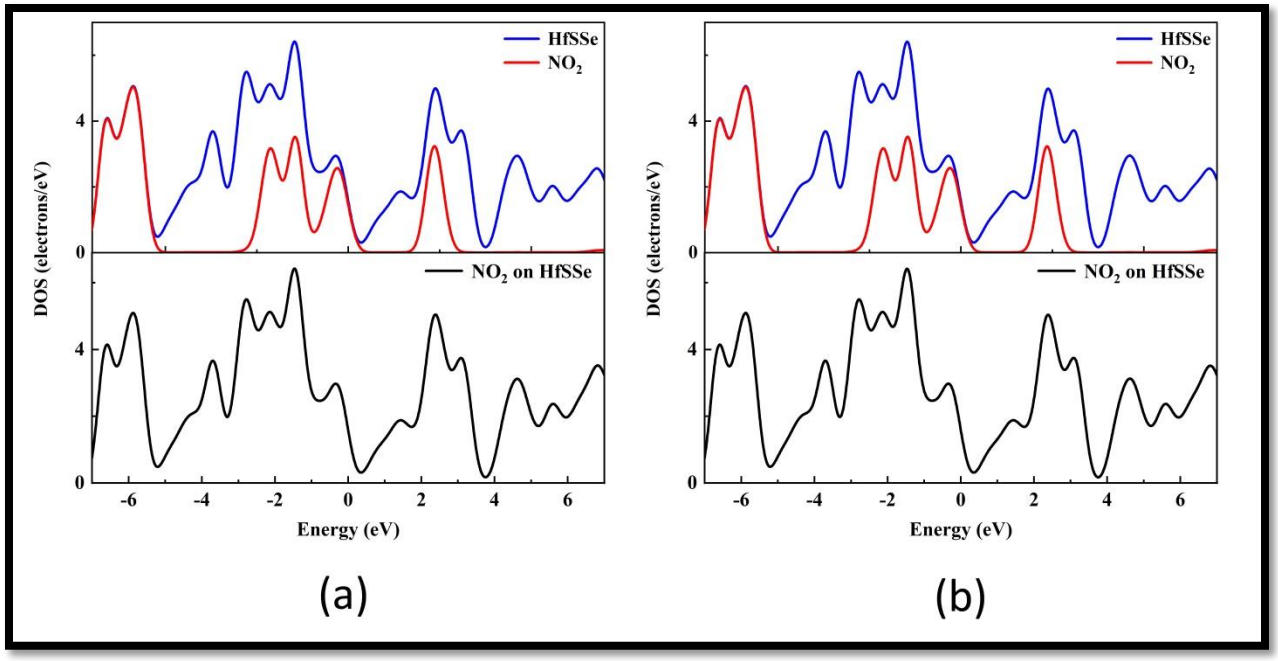

Fig (4.12): DOS of HfSSe (a) Se and (b) S monolayer after the adsorption of NO_2 gas.

4.6 Adsorption of SO_2 gas on HfSSe of Se and S Monolayer

Sulfur dioxide (SO_2), a poisonous gas, is still one of the most significant gaseous pollutants discharged into the atmosphere as a result of the combustion of sulfur-bearing fossil fuels in automotive engines, industrial complexes, power plants, and homes. The following interaction of SO_2 with air results in acidic showers, which can acidify rivers and lakes, degrade soil and forests, and corrode metals and structures [114]. SO_2 is a colorless gas that is caustic and has a pungent odor. Furthermore, sulfurous acid rain is produced when SO_2 is dissolved in bodies of water, which is damaging to the environment. When SO_2 is dissolved in water, it can produce sulfuric acid, which can irritate the mucous membranes of the eyes and nose [110]. Fig. (4.13) show the top and side views of the adsorbed molecule SO_2 on the HfSSe of Se and S monolayer. When adsorbed of the SO_2 molecule on the monolayer, the E_{ad} of the most favorable adsorption configuration are respectively

(-1.97503, -1.88768) eV for HfSSe-Se and HfSSe-S monolayer with the d(Hf−SO_2) of 5.926 Å, d(SO_2−Se) of 4.576 Å, d(SO_2-S) of 5.899 Å.

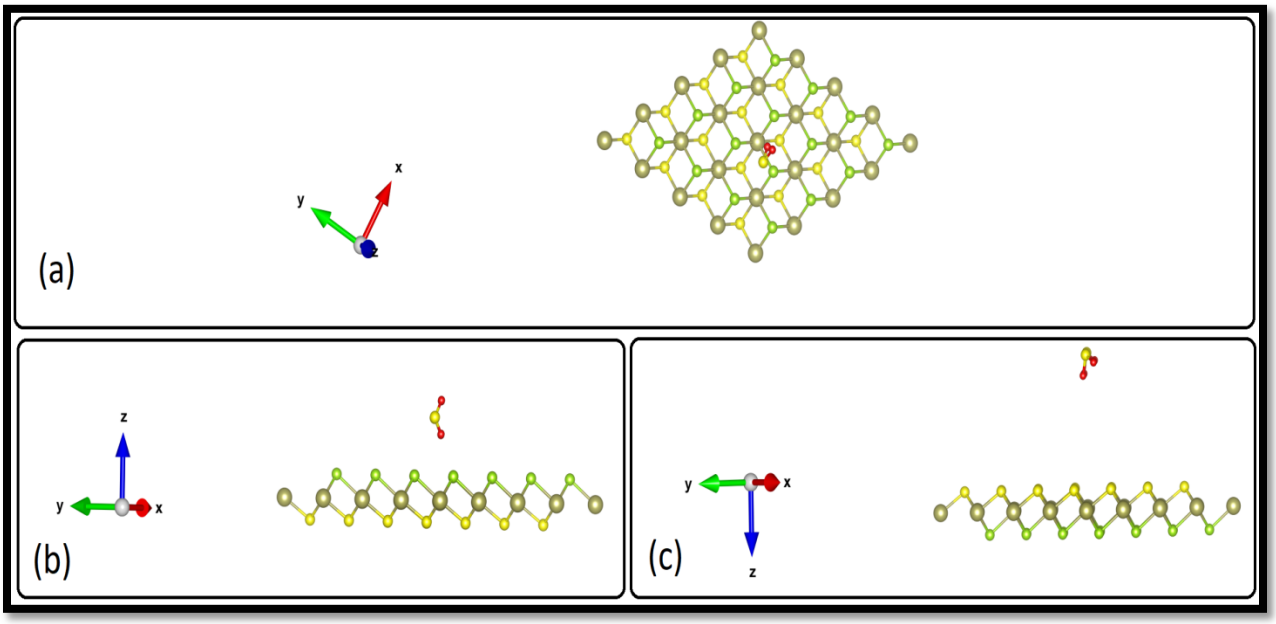

Fig. (4.13): (a) Top view of the adsorbed molecule SO_2 on the HfSSe(b) side view Se and (c) side view S monolayer, sulfur yellow color, selenium green color and hafnium brown color.

Nevertheless, this also means that the desorption of SO_2 from the HfSSe will encounter greater obstacles by means of UV irradiation [115], or electric field [116]. The distinct deformation is also observed in this configuration, suggesting that the molecule SO_2 interaction is slightly stronger than that of the monolayer adsorption which shows little deformation. The band gaps of the adsorbed systems in HfSSe of Se is no energy gap due to the interference of the valence beam with the conduction beam at the Fermi level and this means that it is conductive and the band gap in HfSSe of S is (0.025 eV) show a prodigious change as shown in Fig. (4.14). Generally, the band gaps of SO_2 adsorbed systems are much smaller; undergoes large shrink as compared to that of pristine HfSSe monolayer. Also, the

electrons in full bands can be provoked into the empty band with small energy. Overall, the VBM positions as noticed, remain along the M-Γ path as indicated in the band structure diagram. In contrast, the CBM locations change depends on the type of monolayer. Most importantly, the energy gap in the case of SO_2 adsorbed on HfSSe transfer to a direct energy gap along the M-Γ path. Accordingly, the variations in the energy gap denote to the modification in the conductivity in this monolayer, which can be efficaciously utilized to perceive the existence of the studied molecules employing a simple two-probe method. The density of states (DOS) near the Fermi level appears to be mixed. Figure (4.15) shows that this mixed states are caused by SO_2 adsorption. The p orbitals of S and O atoms have a large overlap with the orbitals of S and Se atoms, and it demonstrates that SO_2 can strongly hybridize with S and Se [22]. This has significant effect on the frontier orbital of the adsorption system, which changes orbital formation, causing the change in the DOS.

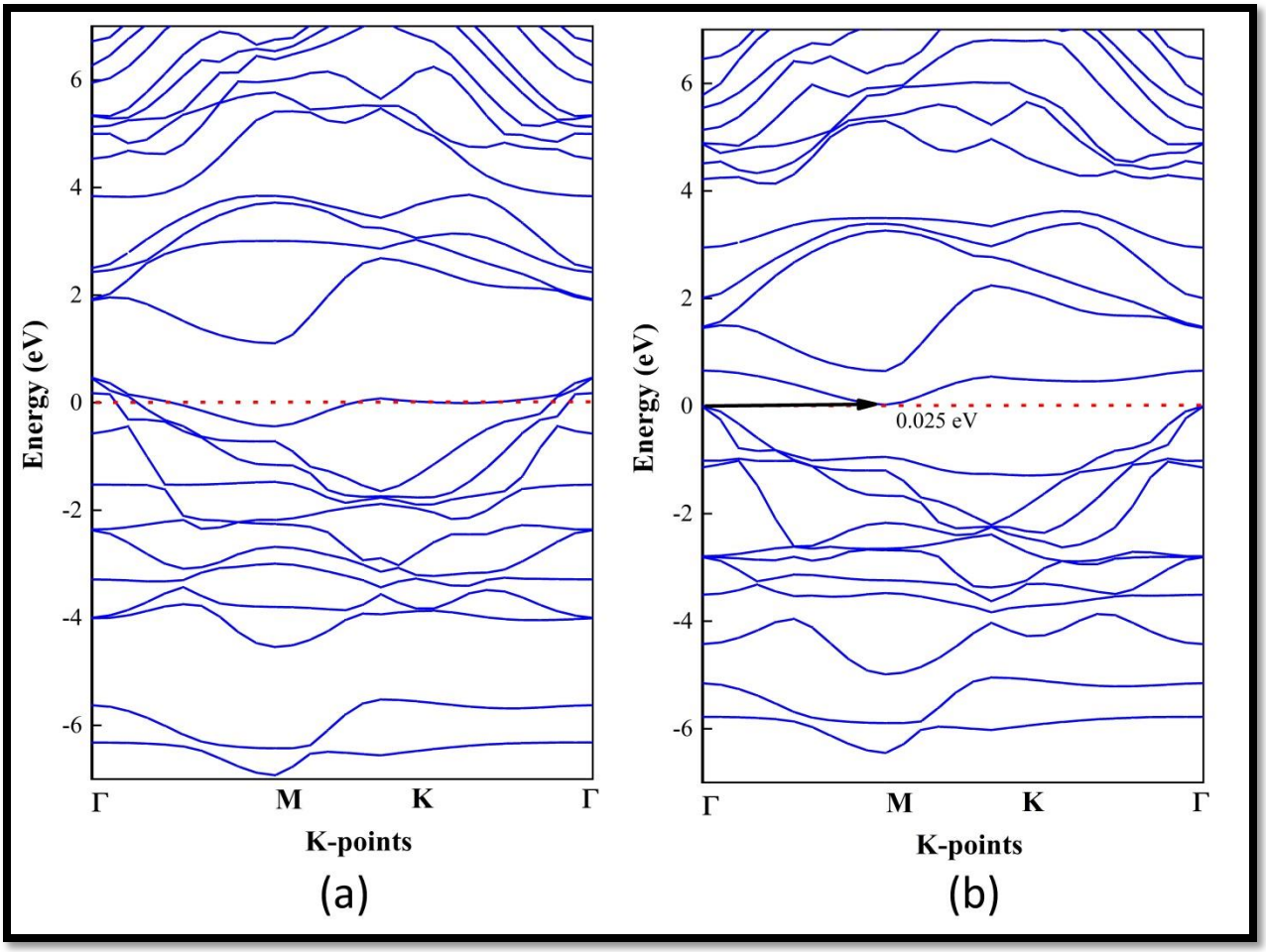

Fig. (4.14): The calculated band structures of HfSSe (a) Se (b) S monolayer after the adsorption of SO_2 gas.

Clearly, Fig. (4.15)(a) and (b) show that the DOS and PDOS for the SO_2 adsorbed on HfSSe-Se and HfSSe-S, but the DOS of SO_2 molecule contributed near the Fermi level is subtle and no apparent orbital hybridization is observable in the PDOS. Meanwhile, the electron sharing between the SO_2 molecule and HfSSe monolayer are lacking, which further supports the previous conclusion that the physical adsorption nature of this system. For the HfSSe monolayer (see Fig. (4.15)), the total DOS obviously changes around the Fermi level and strong orbital hybridization, indicating that the electronic properties of HfSSe can be drastically changed after SO_2 adsorption. SO_2 molecule and the monolayer are bound together

by the intensive orbital hybridization where the orbitals of (X=S, Se) atoms possess the similar states. The SO_2 adsorption on monolayer causes a small increase of the DOS around -2 eV near the Fermi level while another noticeable transformation occurs around 4.4 eV where the trend of DOS is more gradual here on with the enlarged area of DOS in the conduction band.

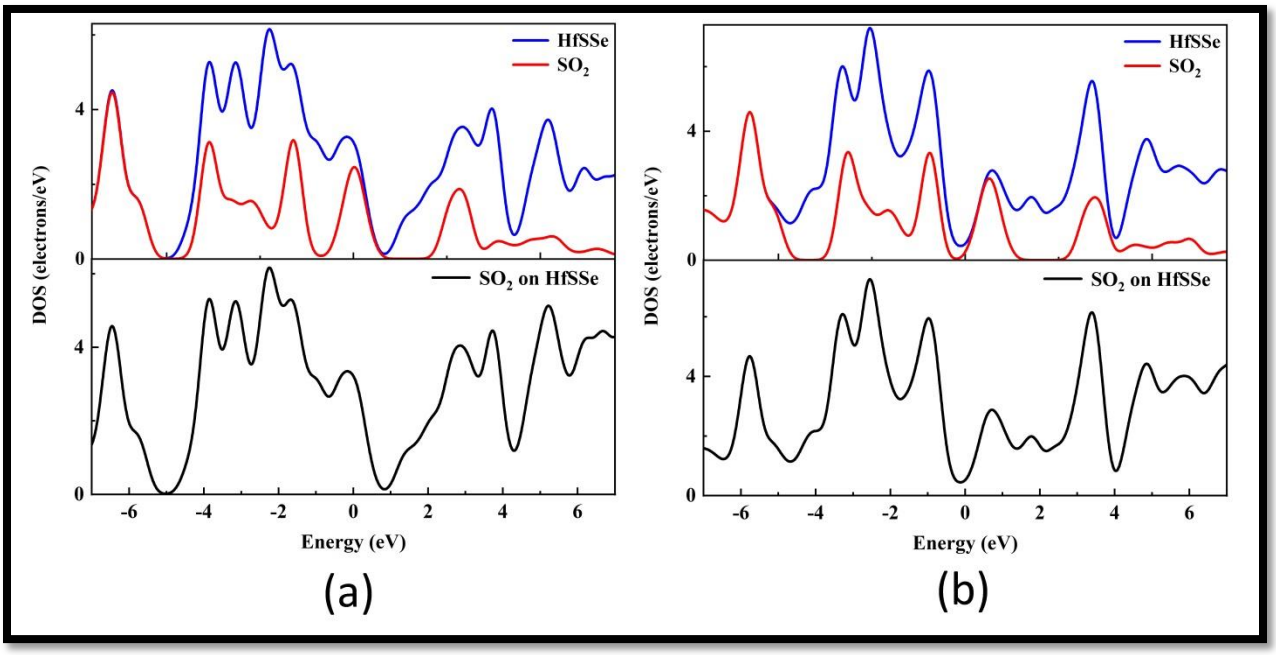

Fig. (4.15): DOS of HfSSe (a) Se and(b) S monolayer after the adsorption of SO_2 gas.

4.7 Optical Properties of Adsorbed molecules on monolayer

The optical characteristics of HfSSe of Se and S monolayer due to the adsorption of the prior gas molecules will be investigated next. In this part, we'll concentrate on the effect of adsorption on these monolayer. In the energy range up to 25 eV, the optical characteristics of adsorbed HfSSe of Se and S monolayer are calculated.

4.7.1. The Reflectivity

The coefficient of reflection, often known as reflectivity, describes how light reflects off different surfaces. This is commonly denoted by the letter R and is

defined as the ratio of reflected power to incident power on a surface. The ratio of incident light intensity that bounces back from a surface is known as reflectance. The reflectance, R, of a thin sheet at normal incidence is given by the following equation:

$$R=I_r/I_0 \quad (4.2)$$

Where I_r is intensity of reflected light and I_0 is the intensity of the incident light. Refraction causes the light waves to propagate with a smaller velocity than in free space. This reduction of the velocity leads to the bending of light rays at interfaces described by Snell's law of refraction. Refraction, in itself, does not affect the intensity of the light wave as it propagates constituting electrical energy, scattered or used to heat a material. The reflectivity curves of molecules adsorbed on HfSSe of Se and S monolayer are illustrated in Figs. (4.16). It can be seen that the maximum reflectivity of this monolayer after the adsorption of gas molecules is dependent on the type of gas as lists in Table (4.2). It can be seen that the largest static reflectivity is 60% for CO_2 adsorbed on HfSSe of S monolayer and the smallest static reflectivity is 16% for NO_2 adsorbed on HfSSe of S monolayer.

Overall, the maximum peak of HfSSe of S adsorbed with CO_2 molecule increases slightly at 8.99 eV with reflectivity of about 60%. Obviously, these percentages represent the maximum values of reflectivity, which is reaching 60% in the best case. Meanwhile, the position of strong peaks still in the UV region range (4.05- 8.57) eV, which is consistent with the absorption coefficient, that is shown in the preceding sections. The behavior of reflectivity curves is identical to that of absorption curves, with the exception of the number of peaks, which is more than three for all gas molecules. Nonetheless, Table (4.2) shows that the reflectivity values of the HfSSe monolayer are nearly identical to those of the Se and S monolayer.

Table (4.2): The calculated reflectivity of HfSSe of Se and S monolayer after the adsorption of different gas molecules.

Gas molecules	HfSSe-Se Monolayer	HfSSe-S Monolayer
CO	0.26	0.25
CO_2	0.44	0.60
NO	0.23	0.22
NO_2	0.17	0.16
SO_2	0.20	0.23

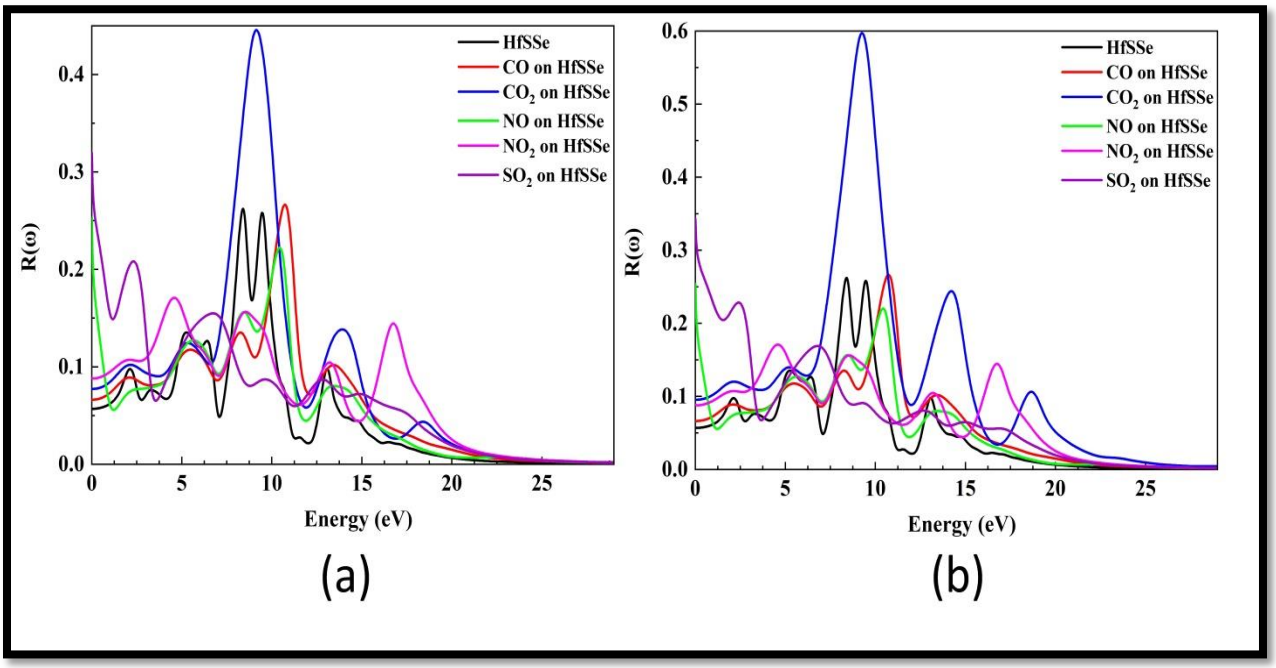

Fig.(4.16): The reflectivity as a function of energy of HfSSe :(a) Se and (b) S monolayer after the adsorption of CO,CO_2,NO,NO_2 and SO_2 molecules.

4.7.2. The Absorption Coefficient

The absorption coefficient provides useful data about optimum solar energy conversion efficiency. Figs. (4.17) shows the absorption coefficient curves of molecules adsorbed on HfSSe of Se and S monolayer. In principle, it is concluded that there are two absorption peaks in the pristine monolayer, the first at lower energy than the other which is higher from the former. However, the edge absorption of pristine Se monolayer begins in mid-infrared (IR) region, whereas edges absorption of pristine S and Se monolayer are in the visible region, the absorption coefficients are ranging between $10^4\,cm^{-1}$ and $10^5\,cm^{-1}$. After the adsorption of gas molecules on HfSSe of Se and S monolayer, a very distinctive and inviting spectacle may be perceived by means of the absorption coefficient of the adsorbed system as plotted in Figs. (4.17). The main phenomena that can be seen from this Figure are; the locations of the beginning of absorption and maximum peaks, number of peaks, and the height of these peaks. The beginning of absorption of adsorbed SO_2 on monolayer starts in the far IR region (2 meV) and the other molecules start in the near IR region between 0.413 eV and 0.823 eV. On the other hand, the value of CO_2/HfSSe of S monolayer maximum peak absorption is the largest, whose value is $3.01\times10^4\,cm^{-1}$ is positioned at 8.99 eV, followed by the absorption peak of CO_2/HfSSe of Se monolayer ($2.39\times10^4\,cm^{-1}$ at 9 eV) and then the absorption peaks CO/HfSSe of Se monolayer ($1.69\times10^4\,cm^{-1}$ at 11.10 eV) as listed in Table (4.3). Clearly, the absorption peaks values increase and the locations of absorption maximum peaks are shifted to lower energy values depending on the type of gas molecules in the deep UV region, except the CO and SO_2 molecules adsorbed on HfSSe monolayer, which is shifted to higher energy values. Remarkably, it turns out that the values of the absorption coefficient of these systems are equivalent to the perovskite, which is supposed to be the main component of solar cells. The other observation that worth paying attention is the

CO_2, NO_2, and SO_2 molecules adsorbed on the HfSSe monolayer result in new absorption peaks seem in the UV region. Therefore, it is easy to say that adsorption in these systems led to an increase in the number of maximum peaks of these systems, which insinuate that the absorption coefficients of molecules adsorbed on these monolayer have been earnestly improved. It can be seen from above, that we can benefit from the molecules adsorbed on HfSSe monolayer in the photoelectric and optoelectronic devices especially in the UV range.

Table (4.3): The maximum peak values of absorption coefficient (in cm^{-1}) of HfSSe of Se and S monolayer after the adsorption of gas molecules.

Gas Molecules	**HfSSe-Se Monolayer**	**HfSSe-S Monolayer**
CO	1.69×10^4	1.70×10^4
CO_2	2.39×10^4	3.01×10^4
NO	1.39×10^4	1.38×10^4
NO_2	1.30×10^4	1.33×10^4
SO_2	1.14×10^4	1.09×10^4

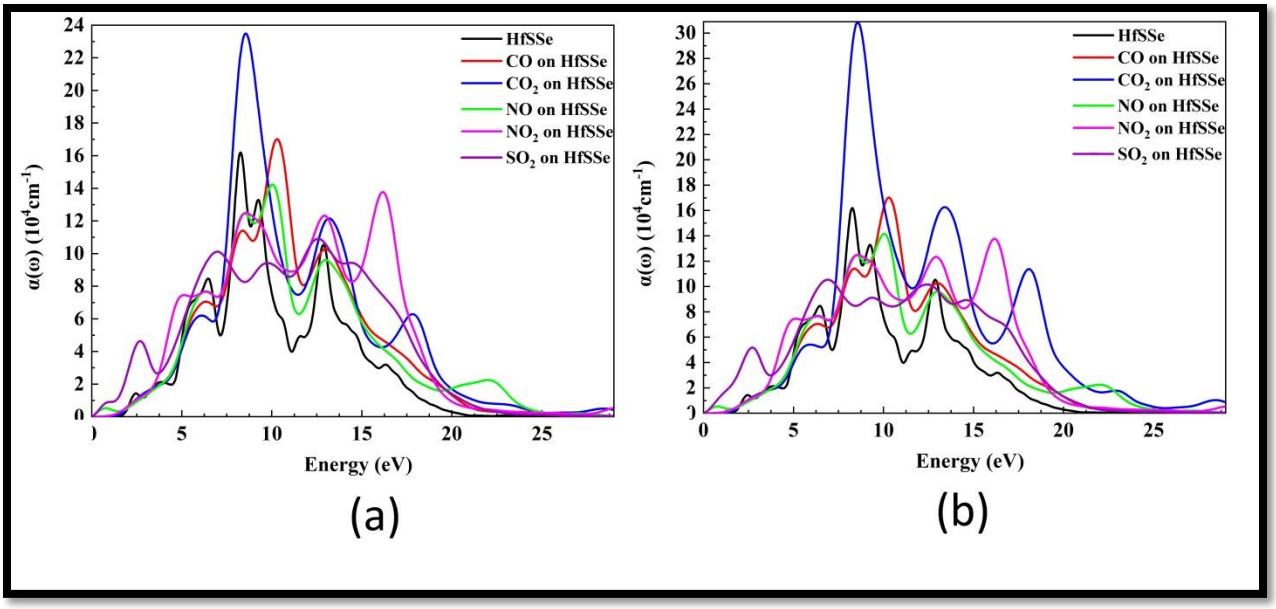

Fig.(4.17): The absorption coefficient as a function of photon energy of HfSSe:(a) Se and (b) S monolayer after the adsorption of CO,CO_2,NO,NO_2 and SO_2 molecules.

4.7.3. Refractive Index

When light enters a substance, its refractive index influences how much light is twisted, or refracted [18]. Figs(4.18) show the refractive indices of monolayer as a function of photon energy, from which the static refractive index of monolayer is calculated. The static refractive indices of adsorbed systems almost similar between Se and S, except for SO_2 molecule adsorbed of HfSSe-Se monolayer, whose value is 2.36 is alowest to 1.66 of HfSSe -S as displayed in Table (4.4). In general, it is apparent that there is a similarity between the real dielectric function and the refractive index curves, where the behavior of these two curves are completely identical with different values only.

Table (4.4): The maximum values of refractive index of HfSSe of Se and S monolayer after the adsorption of gas molecules.

Gas molecules	HfSSe-Se Monolayer	HfSSe-S Monolayer
CO	1.70	1.71
CO_2	2.11	2.50
NO	1.80	1.81
NO_2	2.22	2.12
SO_2	2.36	1.66

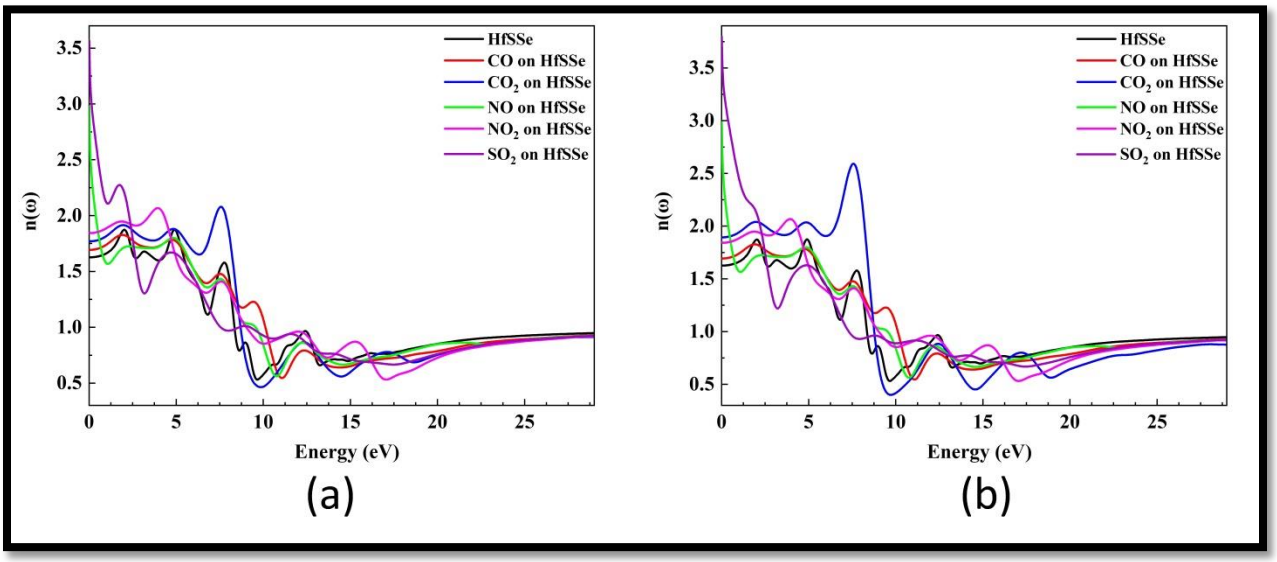

Fig.(4.18): The refractive index as a function of energy of HfSSe:(a) Se and (b) S monolayer after the adsorption of CO,CO_2,NO,NO_2 and SO_2 molecules.

4.7.4. Dielectric Function

Any system with 2D sheets can utilize the optical dielectric function to characterize its optical characteristics. The dielectric function of gas molecules adsorbed on HfSSe of Se and S monolayer is shown in Figs. (4.19) as a function of photon energy. The real (Re) and imaginary (Im) components of the dielectric function are determined in this section utilizing polarized light perpendicular to the

monolayer surface plane. The preceding section indicated that each component of the dielectric function of pure monolayer has a single peak, implying that there is only one transfer between the valence and conduction bands. Furthermore, because of the large real static dielectric constant that occurs at zero energy, our results suggested that pristine monolayer exhibit higher electronic polarizability. The actual static dielectric functions of adsorbed systems decrease after adsorption when compared to the pristine monolayer, with the exception of adsorbed CO_2 on HfSSe of the S monolayer, which has the highest value (5.61). The lowest value (2.11) is for the adsorbed SO_2 molecule on HfSSe of the S monolayer as shown in the table (4.5), which correlates to the reflectivity findings of the gas CO_2 molecule, as we shall see later . A quick look on Figs. (4.19) and(4.20),leads us to another deduction, which is there is more than one peak in the adsorption systems with gas molecules. This mean that there is more than one electronic translation from valance band to the conduction band. Also, it can be seen from the Figs. (4.19) and (4.20), that the adsorption of gas CO_2 molecule on HfSSe monolayer has three maximum peaks. Additionally, their behavior is similar to pristine monolayer state with respect to the presence of negative values of the real dielectric function, our perception is that at these negative values, these monolayer behave as metal within this range of photon energy. Its behavior is similar to the real part counterpart in terms of the increase in the peak number and the dwindle in the value of maximum peak compared with the peak of the pristine monolayer. Totally, the maximum peaks of the real dielectric function are always lower than the maximum peaks of imaginary dielectric function counterpart, which is different from pristine monolayer. It is important to allude that the highest peak of adsorbed systems belonging to adsorbed gas on HfSSe of S monolayer as depicted in the Figs. (4.19)and (4.20). Clearly, the maximum peaks of the real dielectric function are occurred in the UV region, whereas the most maximum peaks of the imaginary

dielectric function are happened in the UV region, excluding some cases that are occurring in the visible region. On the other hand, it is revealed from the results that the adsorption of gases leads to shifting the maximum peaks to lower energies as shown in Table(4.5).

Table (4.5): The maximum peak locations of real (Re) and imaginary (Im) dielectric functions of HfSSe of Se and S monolayer at the photon energy (in eV) after the adsorption of gas molecules.

Gas molecules	**HfSSe-Se Monolayer**		**HfSSe-S Monolayer**	
	Re	**Im**	**Re**	**Im**
CO	2.80	2.31	2.91	2.11
CO_2	3.71	4.91	5.61	8.90
NO	2.51	2.12	2.91	2.14
NO_2	4.01	3.13	3.90	3.15
SO_2	2.30	4.10	2.11	4.13

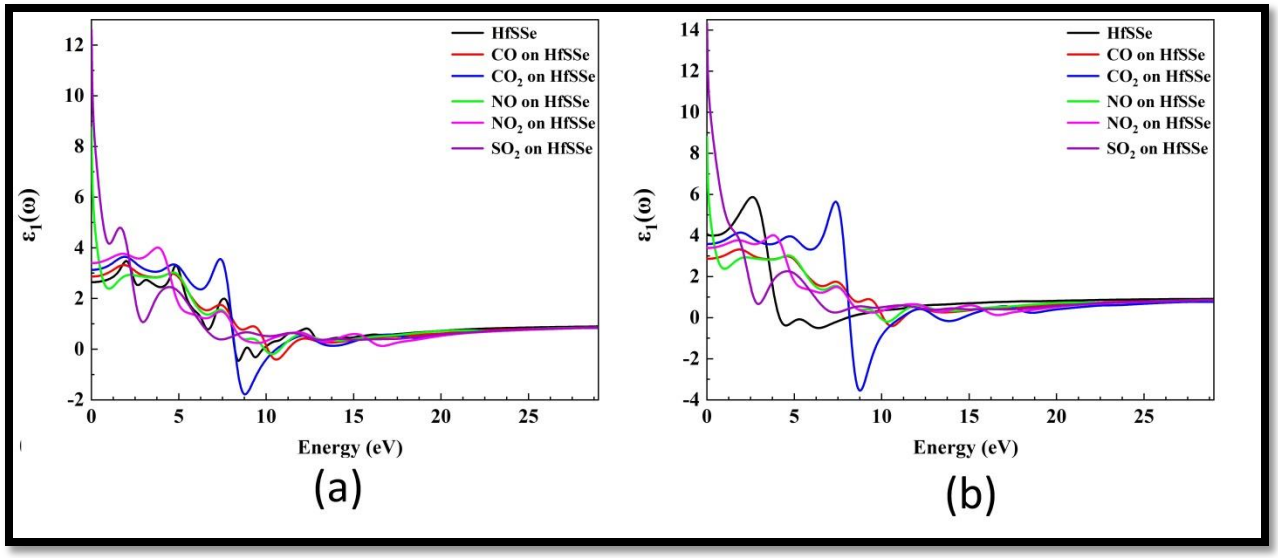

Fig.(4.19): Dielectric function Real as a function of photon energy of HfSSe :(a) Se and (b) S monolayer after adsorption of CO,CO_2,NO,NO_2 and SO_2 molecules.

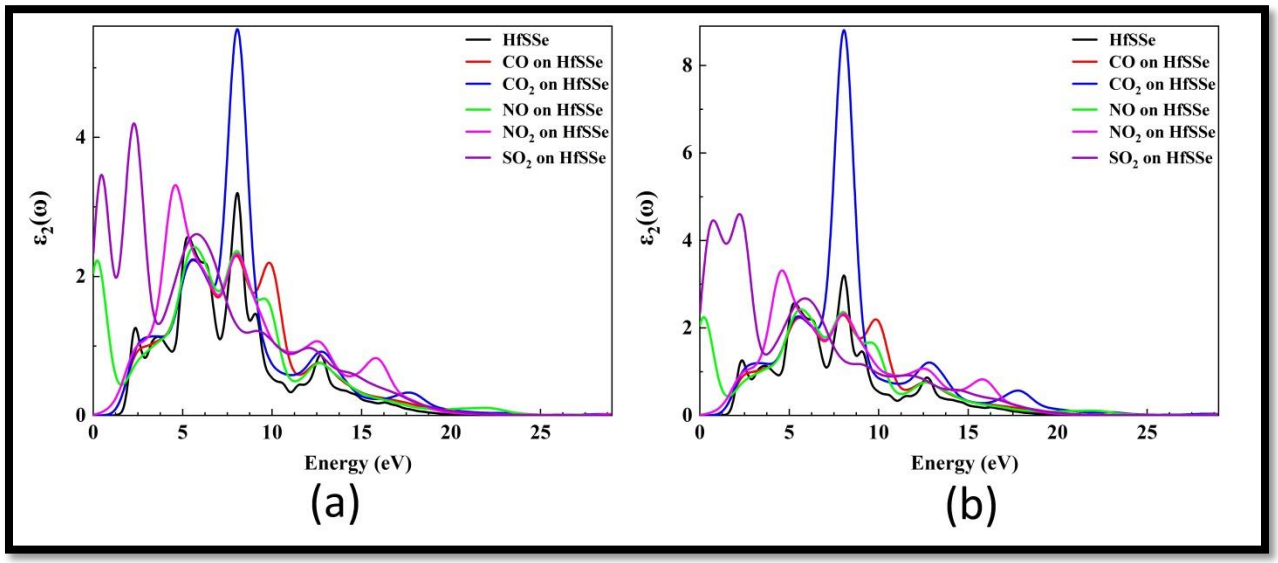

Fig.(4.20): Dielectric function Imaginary as a function of photon energy of HfSSe :(a) Se and (b) S monolayer after adsorption of CO,CO_2,NO,NO_2 and SO_2 molecules.

4.7.5. The optical Conductivity

Figs (4.21) illustrates the optical conductivity of the HfSSe (S, Se) monolayer as a function of photon energy following gas adsorption. In general, the computed

optical conductivity indicates that there are multiple peaks and minima throughout the energy range investigated, as shown in Table (4.6). The optical conductivity of the adsorbed system, as displayed in Figs. (4.21), may be used to experience a highly distinctive and beautiful sight when gas molecules adsorb on HfSSe of Se and S monolayer. The number of peaks, the height of these peaks, and the locations of maximal peaks are the key phenomena shown in these figures. Depending on the composition of gas molecules in the UV region, optical conductivity values generally decrease and maximal optical conductivity peaks are pushed to higher energy values. Adsorbed molecules on the HfSSe monolayer, on the other hand, cause additional UV peaks to appear. As a result, it's straightforward to conclude that increased conductivity in these systems resulted in a rise in the number of maximum peaks, implying that the conductivity of adsorbed molecules on this monolayer has significantly enhanced. Clearly, the optical conductivity are ranging between 1.89×10^{15} sec^{-1} for SO_2/HfSSe-Se monolayer and 8.97×10^{15} sec^{-1} for CO_2/HfSSe-S monolayer. Table (4.6) show that the largest value of optical conductivity is 8.97×10^{15} sec^{-1} for CO_2/HfSSe-S monolayer, followed by the optical conductivity of CO_2/HfSSe-Se monolayer (5.99×10^{15} sec^{-1}) and then the NO/HfSSe-Se monolayer (2.71×10^{15} sec^{-1}). Also, it can be seen from Table (4.6) that the values of conductivity of HfSSe-S monolayer are larger than that of HfSSe-Se monolayer. Moreover, the photoconductivity and hence optical conductivity of materials increase as a result of absorbing photons [19].

Table (4.6): The maximum values of conductivity of HfSSe of Se and S monolayer after the adsorption of gas molecules.

Gas molecules	HfSSe-Se Monolayer	HfSSe-S Monolayer
CO	2.61	2.53
CO_2	5.99	8.97
NO	2.71	2.62
NO_2	1.97	1.99
SO_2	1.89	1.99

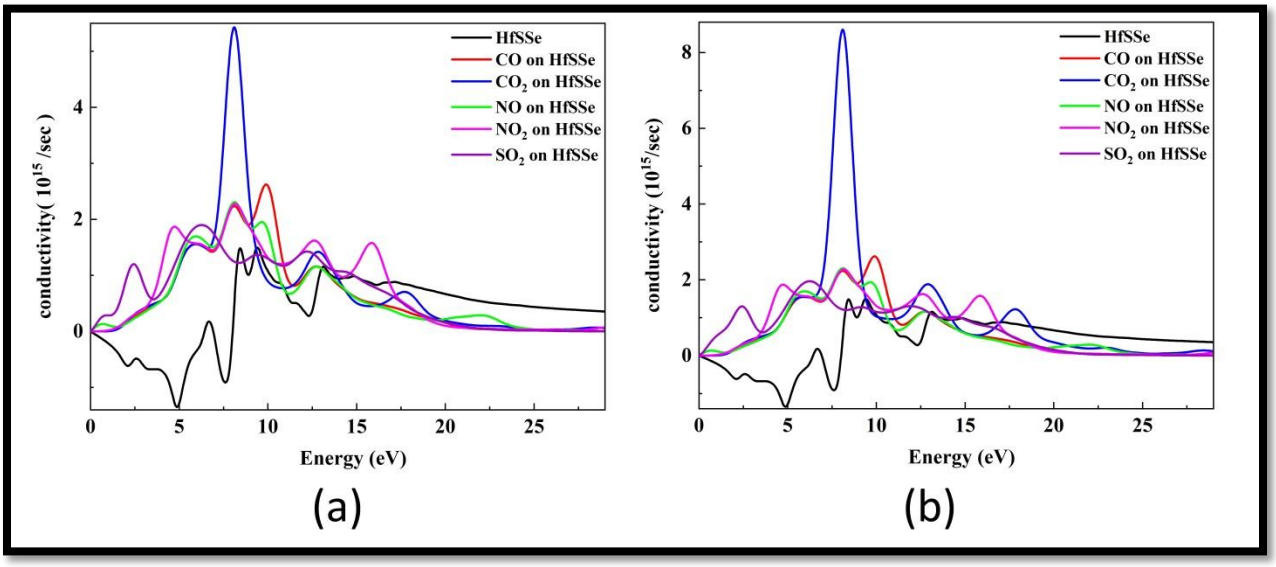

Fig.(4.21): The optical conductivity as a function of photon energy of HfSSe:(a) Se and(b) S monolayer after the adsorption of CO,CO_2,NO,NO_2 and SO_2 molecules.

4.7.6. The loss Energy Function

The electron energy loss function is an important optical parameter. Figs. (4.22) shows the energy loss function as a function of photon energy. Prominent

peak is found at range (15.2-20.3) eV, which indicates rapid reduction in the reflectance. As can be noticed from Figs. (4.22) ,that the molecules adsorbed on HfSSe of Se and S monolayer with gas molecules lead to lower peaks relative to the pristine monolayer peak, excluding adsorbed CO_2 on HfSSe-S monolayer that has a sharp peak equal to 2.91 at 15.2 eV and adsorbed NO_2 on HfSSe-S monolayer, which has a sharp peak equal to 2.59 at 18.54 eV as shown in Table (4.7) and Figs. (4.22). It should be noted that the behaviour of loss function curves are similar to the absorption and reflectivity peaks that discussed earlier. Clearly, after the adsorption of molecules on HfSSe monolayer, there is more than one peak but the most maximum peaks located in vacuum UV region except CO_2/HfSSe-S monolayer which has a maximum peak in the extreme UV range. In contrast, adsorbed CO molecule on HfSSe-Se monolayer has the lowest value of loss function (1.60).

Table (4.7): The maximum values of loss function of HfSSe of Se and S monolayer after the adsorption of gas molecules.

Gas molecules	**HfSSe-Se Monolayer**	**HfSSe-S Monolayer**
CO	1.60	1.65
CO_2	2.10	2.91
NO	1.70	1.60
NO_2	2.45	2.59
SO_2	1.93	1.92

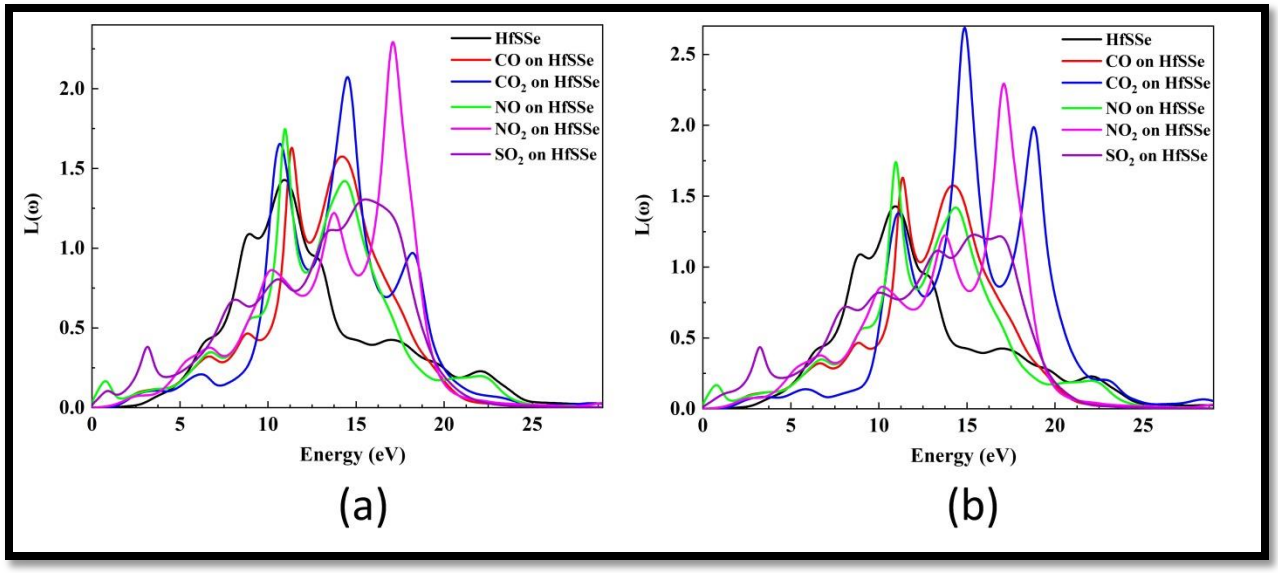

Fig.(4.22): The loss function as a function of energy of HfSSe:(a) Se and (b) S monolayer after the adsorption of CO,CO_2,NO,NO_2 and SO_2 molecules.

.

Chapter Five
Conclusions And Future Works

Conclusions

It has been concluded from the present work that:

1. HfSSe monolayer is semiconductor with an indirect band gap equal 0.620eV with the VBM and CBM located on the Γ–M path.
2. The absorption coefficients of HfSSe monolayer are comparable to the perovskite solar cells, because it is value can reach 10^6 cm^{-1}.
3. The adsorption of gas molecules occurs at simple difference sites on the studied monolayer.
4. The adsorption energies are negative values, which indicate the exothermic nature energetically favorable upon adsorption gas molecules.
5. The adsorption of gas molecules on HfSSe monolayer undergoes physisorption interaction thus can be used to detecting gas molecules.
6. There is no distortion in the structure of HfSSe monolayer in the case of adsorption of gas molecules.
7. Adsorbed gas molecules on the HfSSe monolayer lead to a change in the electronic properties of this monolayer.
8. The energy band gap of HfSSe monolayer is more sensitive to the molecule gas molecules than other monolayer.
9. There are many main peaks in all DOS.
10. The DOS in the valence and conduction bands of the molecules adsorbed on monolayer are significantly altered upon adsorption of gas molecules.
11. The optical properties of HfSSe monolayer can be modified by the adsorption of gas molecules.
12. The absorption peaks values increase and the locations of absorption maximum peaks are shifted to lower energy values depending only in CO_2 gas molecule.

13. The highest optical conductivity occurs in the adsorbed CO_2 molecules on HfSSe-S monolayer.
14. The refraction indices of HfSSe between Se and S monolayer are almost the same in values except adsorbed SO_2 of HfSSe-Se is (2.36) large than HfSSe-S is (1.66).
15. There is more than one maximum peak of dielectric functions in the adsorption systems with gas molecules.
16. The maximum value of reflectivity in the adsorbed systems does not exceed 60% in all cases.
17. The reflection peaks of monolayer occur in the UV region range (4.05- 8.57 eV), which is consistent with the absorption coefficient.
18. The highest peak of loss function occurs in 2.91 at the photon energy 10.11 eV in the case of the adsorption of CO_2 on HfSSe-S monolayer.
19. The findings presented in this work inspire new experiments to design and synthesize the potential HfSSe monolayer based optoelectronic devices.
20. The calculations provide an effective method to modulate the electronic and optical properties of the HfSSe monolayer for device applications.

Future Work

The following studies can be suggested for future work:

1. Studying the effects of high temperatures and pressure on the electronic structure and optical properties of adsorbed gas molecules on the HfSSe monolayer using DFT calculations.
2. Investigating the vibrational, electrical, and magnetic properties of adsorbed gas molecules on the HfSSe monolayer using DFT calculations.

3. Investigating the effect of doping on the electronic and optical properties of adsorbed gas molecules on the HfSSe monolayer using DFT calculations.
4. Studying the effect of some defects on the adsorbed gas molecules on the HfSSe monolayer using DFT calculations.

References

[1] Wang QH, Kalantar-Zadeh K, Kis A, Coleman JN, Strano MS. Electronics and optoelectronics of two-dimensional transition metal dichalcogenides. Nature nanotechnology. 2012;7(11):699–712.

[2] Johari P, Shenoy VB. Tuning the electronic properties of semiconducting transition metal dichalcogenides by applying mechanical strains. ACS nano. 2012;6(6):5449–56.

[3] Mak KF, Shan J. Photonics and optoelectronics of 2D semiconductor transition metal dichalcogenides. Nature Photonics. 2016;10(4):216–26.

[4] Qin D, Yan P, Ding G, Ge X, Song H, Gao G. Monolayer PdSe 2: A promising two-dimensional thermoelectric material. Scientific reports. 2018;8(1):1–8.

[5] Perkins FK, Friedman AL, Cobas E, Campbell PM, Jernigan GG, Jonker BT. Chemical vapor sensing with monolayer MoS2. Nano letters. 2013;13(2):668–73.

[6] Voiry D, Yang J, Chhowalla M. Recent strategies for improving the catalytic activity of 2D TMD nanosheets toward the hydrogen evolution reaction. Advanced materials. 2016;28(29):6197–206.

[7] Lee J, Park JY, Cho EB, Kim TY, Han SA, Kim T, Liu Y, Kim SK, Roh CJ, Yoon H. Reliable piezoelectricity in bilayer WSe2 for piezoelectric nanogenerators. Advanced Materials. 2017;29(29):1606667.

[8] Lu AY, Zhu H, Xiao J, Chuu CP, Han Y, Chiu MH, Cheng CC, Yang CW, Wei KH, Yang Y. Janus monolayers of transition metal dichalcogenides. Nature nanotechnology. 2017;12(8):744–9.

[9] Zhang J, Jia S, Kholmanov I, Dong L, Er D, Chen W, Guo H, Jin Z, Shenoy VB, Shi L. Janus monolayer transition-metal dichalcogenides. ACS nano. 2017;11(8):8192–8.

[10] Guan Z, Ni S, Hu S. Tunable electronic and optical properties of monolayer and multilayer Janus MoSSe as a photocatalyst for solar water splitting: a first-principles study. The Journal of Physical Chemistry C. 2018;122(11):6209–16.

[11] Hu T, Jia F, Zhao G, Wu J, Stroppa A, Ren W. Intrinsic and anisotropic Rashba spin splitting in Janus transition-metal dichalcogenide monolayers. Physical Review B. 2018;97(23):235404.

[12] Mleczko MJ, Zhang C, Lee HR, Kuo HH, Magyari-Köpe B, Moore RG, Shen ZX, Fisher IR, Nishi Y, Pop E. HfSe2 and ZrSe2: Two-dimensional semiconductors with native high-κ oxides. Science advances. 2017;3(8):e1700481.

[13] Singh D, Ahuja R. Enhanced optoelectronic and thermoelectric properties by intrinsic structural defects in monolayer HfS2. ACS Applied Energy Materials. 2019;2(9):6891–903.

[14] Zhang Y, Yuan S, Feng X, Li H, Zhou J, Wang B. Preparation of Nanofibrous Metal–Organic Framework Filters for Efficient Air Pollution Control. Journal of the American Chemical Society. 2016 May;138(18):5785–8.

[15] Jappor HR, Khudair SAM. Electronic properties of adsorption of CO, CO2, NH3, NO, NO2 and SO2 on nitrogen doped graphene for gas sensor applications. Sensor Letters. 2017;15(5):432–9.

[16] Huang B, Li Z, Liu Z, Zhou G, Hao S, Wu J, Gu BL, Duan W. Adsorption of Gas Molecules on Graphene Nanoribbons and Its Implication for Nanoscale Molecule Sensor. The Journal of Physical Chemistry C. 2008 Sep;112(35):13442–6.

[17] Schedin F, Geim AK, Morozov S V., Hill EW, Blake P, Katsnelson MI, Novoselov KS. Detection of individual gas molecules adsorbed on graphene.

Nature Materials. 2007 Sep;6(9):652–5.

[18] Xia W, Hu W, Li Z, Yang J. A first-principles study of gas adsorption on germanene. Phys Chem Chem Phys. 2014 Sep;16(41):22495–8.

[19] Pang Q, Li L, Gao D li, Chai R peng, Zhang C ling, Song Y ling. Tuning the electronic and magnetic properties of germanene by surface adsorption of small nitrogen-based molecules. Physica E: Low-dimensional Systems and Nanostructures. 2017 Apr;88:237–42.

[20] Nagarajan V, Chandiramouli R. NO2 adsorption behaviour on germanene nanosheet – A first-principles investigation. Superlattices and Microstructures. 2017 Jan;101:160–71.

[21] Safari F, Moradinasab M, Fathipour M, Kosina H. Adsorption of the NH3, NO, NO2, CO2, and CO gas molecules on blue phosphorene: A first-principles study. Applied Surface Science. 2019 Jan;464:153–61.

[22] Sun X, Luan S, Shen H, Lei S. Effect of metal doping on carbon monoxide adsorption on phosphorene: A first-principles study. Superlattices and Microstructures. 2018 Dec;124:168–75.

[23] Jappor HR, Jaber AS. Electronic properties of CO and CO2 adsorbed silicene/graphene nanoribbons as a promising candidate for a metal-free catalyst and a gas sensor. Sensor Letters. 2016;14(10):989–95.

[24] Jappor HR. Electronic and structural properties of gas adsorbed graphene-silicene hybrid as a gas sensor. Journal of Nanoelectronics and Optoelectronics. 2017;12(8):742–7.

[25] Chen X, Tan C, Yang Q, Meng R, Liang Q, Cai M, Zhang S, Jiang J. Ab Initio Study of the Adsorption of Small Molecules on Stanene. The Journal of Physical Chemistry C. 2016 Jul;120(26):13987–94.

[26] Nagarajan V, Chandiramouli R. Adsorption behavior of NH3 and NO2 molecules on stanene and stanane nanosheets – A density functional theory

study. Chemical Physics Letters. 2018 Mar;695:162–9.

[27] Xu K, Huang Y, Chen B, Xia Y, Lei W, Wang Z, Wang Q, Wang F, Yin L, He J. Toward High-Performance Top-Gate Ultrathin HfS2 Field-Effect Transistors by Interface Engineering. Small. 2016;12(23):3106–11.

[28] Tsipas P, Tsoutsou D, Marquez-Velasco J, Aretouli KE, Xenogiannopoulou E, Vassalou E, Kordas G, Dimoulas A. Epitaxial ZrSe2/MoSe2 semiconductor vd Waals heterostructures on wide band gap AlN substrates. Microelectronic Engineering. 2015;147:269–72.

[29] Xu K, Wang Z, Wang F, Huang Y, Wang F, Yin L, Jiang C, He J. Ultrasensitive Phototransistors Based on Few-Layered HfS2. Advanced Materials. 2015;27(47):7881–7.

[30] Wang D, Meng J, Zhang X, Guo G, Yin Z, Liu H, Cheng L, Gao M, You J, Wang R. Selective direct growth of atomic layered HfS2 on hexagonal boron nitride for high performance photodetectors. Chemistry of Materials. 2018;30(11):3819–26.

[31] Yin L, Xu K, Wen Y, Wang Z, Huang Y, Wang F, Shifa TA, Cheng R, Ma H, He J. Ultrafast and ultrasensitive phototransistors based on few-layered HfSe2. Applied Physics Letters. 2016;109(21):213105.

[32] Kang M, Rathi S, Lee I, Li L, Khan MA, Lim D, Lee Y, Park J, Yun SJ, Youn DH. Tunable electrical properties of multilayer HfSe 2 field effect transistors by oxygen plasma treatment. Nanoscale. 2017;9(4):1645–52.

[33] Yan C, Gan L, Zhou X, Guo J, Huang W, Huang J, Jin B, Xiong J, Zhai T, Li Y. Space-confined chemical vapor deposition synthesis of ultrathin HfS2 flakes for optoelectronic application. Advanced Functional Materials. 2017;27(39):1702918.

[34] Li L, Wang W, Gan L, Zhou N, Zhu X, Zhang Q, Li H, Tian M, Zhai T. Ternary Ta2NiSe5 flakes for a high-performance infrared photodetector.

Advanced Functional Materials. 2016;26(45):8281–9.

[35] Perumal P, Ulaganathan RK, Sankar R, Liao Y, Sun T, Chu M, Chou FC, Chen Y, Shih M, Chen Y. Ultra-thin layered ternary single crystals [Sn (SxSe1− x) 2] with bandgap engineering for high performance phototransistors on versatile substrates. Advanced Functional Materials. 2016;26(21):3630–8.

[36] Wang D, Zhang X, Guo G, Gao S, Li X, Meng J, Yin Z, Liu H, Gao M, Cheng L. Large-Area Synthesis of Layered HfS2 (1− x) Se2x Alloys with Fully Tunable Chemical Compositions and Bandgaps. Advanced Materials. 2018;30(44):1803285.

[37] Ubaldini A, Jacimovic J, Ubrig N, Giannini E. Chloride-driven chemical vapor transport method for crystal growth of transition metal dichalcogenides. Crystal Growth & Design. 2013;13(10):4453–9.

[38] Binnewies M, Glaum R, Schmidt M, Schmidt P. Chemical vapor transport reactions–A historical review. Zeitschrift für anorganische und allgemeine Chemie. 2013;639(2):219–29.

[39] Hoat DM, Naseri M, Hieu NN, Ponce-Pérez R, Rivas-Silva JF, Vu T V, Cocoletzi GH. A comprehensive investigation on electronic structure, optical and thermoelectric properties of the HfSSe Janus monolayer. Journal of Physics and Chemistry of Solids. 2020;144:109490.

[40] Tamalampudi SR, Lu YY, Kumar R, Sankar UR, Liao CD. K. Moorthy B, C.-H. Cheng, FC Chou and Y.-T. Chen. Nano Lett. 2014;14:2800.

[41] Ferrari L, Kaufmann J, Winnefeld F, Plank J. Interaction of cement model systems with superplasticizers investigated by atomic force microscopy, zeta potential, and adsorption measurements. Journal of Colloid and Interface Science. 2010 Jul;347(1):15–24.

[42] Saffarzadeh A. Modeling of gas adsorption on graphene nanoribbons. Journal

of Applied Physics. 2010;107(11):114309.

[43] Yue Q, Shao Z, Chang S, Li J. Adsorption of gas molecules on monolayer MoS2 and effect of applied electric field. Nanoscale Research Letters. 2013 Oct;8(1):425.

[44] Zhou C, Zhu H, Wu Y, Lin W, Yang W, Dong L. Effect of external strain on the charge transfer: Adsorption of gas molecules on monolayer GaSe. Materials Chemistry and Physics. 2017 Sep;198:49–56.

[45] Sun X, Yang Q, Meng R, Tan C, Liang Q, Jiang J, Ye H, Chen X. Adsorption of gas molecules on graphene-like InN monolayer: A first-principle study. Applied Surface Science. 2017 May;404:291–9.

[46] Jappor HR, Habeeb MA. RETRACTED: Optical properties of two-dimensional GaS and GaSe monolayers. Elsevier; 2018.

[47] Chen GX, Li HF, Wang DD, Li SQ, Fan XB, Zhang JM. Adsorption of toxic gas molecules on pristine and transition metal doped hexagonal GaN monolayer: A first-principles study. Vacuum. 2019 Jul;165:35–45.

[48] Ye H, Liu L, Xu Y, Wang L, Chen X, Zhang K, Liu Y, Koh SW, Zhang G. SnSe monolayer: A promising candidate of SO2 sensor with high adsorption quantity. Applied Surface Science. 2019 Aug;484:33–8.

[49] Tian B, Huang T, Guo J, Shu H, Wang Y, Dai J. Gas adsorption on the pristine monolayer GeP3: A first-principles calculation. Vacuum. 2019 Jun;164:181–5.

[50] Kumar V, Roy DR. Single-layer stanane as potential gas sensor for NO2, SO2, CO2 and NH3 under DFT investigation. Physica E: Low-dimensional Systems and Nanostructures. 2019 Jun;110:100–6.

[51] Ghobadi N, Touski SB. The Electrical and Spin Properties of Monolayer and Bilayer Janus HfSSe under Vertical Electrical Field. 2020 Aug 25; Available from: http://arxiv.org/abs/2008.11361

[52] Zhao X, Wang M, Pei M, Xia C, Wang T, Yang Y, Dai X, Wei S. Electronic properties and controllable Schottky barrier of Janus HfSSe and graphene van der waals heterostructure. Solid State Communications. 2022;344:114686.

[53] Bensalem Salaheddine. Contribution to the study of physical properties of CZTX (X=S, Se) solar materials, Ph.D Thesis, Department of Physics, Faculty of Sciences, University Ferhat Abbas, Algeria. 2015.

[54] Fitts DD. Principles of quantum mechanics: as applied to chemistry and chemical physics. Cambridge University Press, USA; 1999.

[55] Demtröder W. Molecular physics: theoretical principles and experimental methods. Wiley-VCH Verlag GmbH&Co, USA.; 2007.

[56] Sakurai JJ, Napolitano J. Modern quantum mechanics. 2nd ed. Addison-Wesley, USA; 2011. 550 p.

[57] Kaxiras E. Atomic and electronic structure of solids. Cambridge University Press, USA; 2003.

[58] Jensen F. Introduction to Computational Chemistry Second Edition. Department of Chemistry, University of Southern Denmark, Odense, Denmark; 2011.

[59] Sahni V. Quantal Density Functional Theory. In: Quantal Density Functional Theory II. Berlin, Heidelberg: Springer Berlin Heidelberg; 2009. p. 35–51.

[60] Young DC. A Practical Guide for Applying Techniques to Real-World Problems. Wiley–Interscience New York, USA; 2001.

[61] Rogers DW. Computational Chemistry using the PC. John Wiley & Sons, Ltd, UK; 2003.

[62] Koch W, Holthausen MC. A chemist's guide to density functional theory. Wiley-VCH, UK; 2001. 300 p.

[63] Lipkowitz KB, Larter R, Cundari TR. Reviews in computational chemistry,

Volume 21. 2005.

[64] Reimers JR. Computational methods for large systems : electronic structure approaches for biotechnology and nanotechnology. Wiley, UK; 2011.

[65] Sherrill CD. Introduction to Electronic Structure Theory. Georgia Institute of Technology; 2002.

[66] Hutter J. Lecture notes in computational chemistry electronic structure theory,Physical Chemistry Institute. University of Zurich, Switzerland,. 2005;

[67] Lipkowitz KB, Larter R, Cundari TR, Emeritus E, Boyd DB. Reviews in Computational Chemistry, Volume 19. John Wiley & Sons, Inc., Hoboken, New Jersey.; 2003.

[68] Bose DN, Pal S. Photoconductivity, low-temperature conductivity, and magnetoresistance studies on the layered semiconductor GaTe. Physical Review B. 2001 May;63(23):235321.

[69] Hehre WJ. A guide to molecular mechanics and quantum chemical calculations. Vol. 2. Wavefunction Irvine, CA; 2003.

[70] Dorsett H, White A. Overview of molecular modelling and ab initio molecular orbital methods suitable for use with energetic materials. Defense Science and Technology Organization Salisbury (Australia); 2000.

[71] Jensen F. Introduction to computational chemistry. Department of Chemistry, University of Southern Denmark, Odense, Denmark: John Wiley & Sons, Ltd, UK; 2017.

[72] Hohenberg P, Kohn W. Inhomogeneous Electron Gas. Physical Review. 1964 Nov;136(3B):B864–71.

[73] Levine IN. Quantum chemistry. New Jersey, USA,: Pearson Prentice Hall; 2009. 751 p.

[74] Cramer CJ. Essentials of computational chemistry: theories and models. John

Wiley & Sons, Ltd, UK; 2013.

[75] Parr RG, Yang W. Density-functional theory of atoms and molecules. Oxford University Press, UK; 1989. 333 p.

[76] Perdew JP, Burke K, Ernzerhof M. Generalized Gradient Approximation Made Simple. Physical Review Letters. 1996 Oct;77(18):3865–8.

[77] C. Wagner. Exchange energy and potential using the Laplacian of the density. University Muncie, Indiana, USA; 2012.

[78] Segall MD, Lindan PJD, Probert MJ, Pickard CJ, Hasnip PJ, Clark SJ, Payne MC. First-principles simulation: ideas, illustrations and the CASTEP code. Journal of Physics: Condensed Matter. 2002 Mar;14(11):2717–44.

[79] Asmatulu R, Nuraje N, Mul G. Chapter 1. Introduction to Green Nanostructured Photocatalysts. In Cambridge, England: RSC Publishing; 2015. p. 1–12.

[80] Mohammed AH. Tuning the optical energy band gap of sol-gel-based titanium dioxide nanocomposite particles incorporated with ITO, fullerene, and SWCNT. Mechanical Engineering, Wichita State University, USA; 2016.

[81] Nuraje N, Kudaibergenov S, Asmatulu R. Solar Energy Storage with Nanomaterials. In: Producing Fuels and Fine Chemicals from Biomass Using Nanomaterials. CRC Press; 2013. p. 95–118.

[82] Dagenais K, Chamberlin M, Constantin C. Modeling Energy Band Gap as a Function of Optical Electronegativity for Binary Oxides. Journal of Young Investigators. 2013;25(3):73–8.

[83] Asahi R. Visible-Light Photocatalysis in Nitrogen-Doped Titanium Oxides. Science. 2001 Jul;293(5528):269–71.

[84] Kittel C. Introduction to solid state physics. 8th ed. Wiley, USA; 2005. 680 p.

[85] J. R. Hook HEH. Solid State Physics. 2nd editio. John Wiley and Sons Inc;

1995.

[86] Lu AJ, Pan BC. Nature of Single Vacancy in Achiral Carbon Nanotubes. Physical Review Letters. 2004 Mar;92(10):105504.

[87] Elfurawi U. Optical and Electronic Properties of PbS Colloidal Nanocrystals, Ph. D Thesis, University of Nottingham, UK. 2012.

[88] Abed Al- Abbas SS, Muhsin MK, Jappor HR. Tunable optical and electronic properties of gallium telluride monolayer for photovoltaic absorbers and ultraviolet detectors. Chemical Physics Letters. 2018 Dec;713:46–51.

[89] ABDI AB. Probing Electronic and Vibronic States in CdTe Self-Assembled Quantum Dots and CdS Nanowires using Room Temperature Resonant Raman Scattering. University of Cincinnati,Arts and Sciences : Physics; 2006.

[90] Zhang J. Control of Electronic Coupling and Optical Properties in Quantum Dot Solids, Ph. D Thesis, Faculty of Physics, University of München, China. 2010.

[91] Abed Al-Abbas SS, Muhsin MK, Jappor HR. Two-dimensional GaTe monolayer as a potential gas sensor for SO2 and NO2 with discriminate optical properties. Superlattices and Microstructures [Internet]. 2019;135(September):106245. Available from: https://doi.org/10.1016/j.spmi.2019.106245

[92] Singh JB. Analytical and Structyral Analysis of Iron Oxides Using Material Studio. School of Material Science and Nanotechnology, National Institute of Technology, Kurukshetra- 136119; 2015 p. 3139502.

[93] Jappor HR, Habeeb MA. Tunable electronic and optical properties of GaS/GaSe van der Waals heterostructure. Current Applied Physics. 2018 Jun;18(6):673–80.

[94] Fox M. Optical Properties of Solidsphy. Oxford University Press Inc., New

York, USA; 2001.

[95] Dresselhaus MS. Solid State Physics Part II Optical Properties. 1994.

[96] Xu K, Zhang Z, Wang Z, Wang F, Huang Y, Liao L, He J. Short channel field-effect transistors from ultrathin GaTe nanosheets. Applied Physics Letters. 2015 Aug;107(15):153507.

[97] Zhuang HL, Hennig RG. Single-Layer Group-III Monochalcogenide Photocatalysts for Water Splitting. Chemistry of Materials. 2013;25(15):3232–8.

[98] Susoma J, Karvonen L, Säynätjoki A, Mehravar S, Norwood RA, Peyghambarian N, Kieu K, Lipsanen H, Riikonen J. Second and third harmonic generation in few-layer gallium telluride characterized by multiphoton microscopy. Applied Physics Letters. 2016 Feb;108(7):073103.

[99] Huang S, Tatsumi Y, Ling X, Guo H, Wang Z, Watson G, Puretzky AA, Geohegan DB, Kong J, Li J, Yang T, Saito R, Dresselhaus MS. In-Plane Optical Anisotropy of Layered Gallium Telluride. ACS Nano. 2016 Sep;10(9):8964–72.

[100] Liu T, Chen Y, Zhang M, Yuan L, Zhang C, Wang J, Fan J. A first-principles study of gas molecule adsorption on borophene. AIP Advances. 2017 Dec;7(12):125007.

[101] Abbasi A, Sardroodi JJ. Adsorption of O3, SO2 and SO3 gas molecules on MoS2 monolayers: A computational investigation. Applied Surface Science. 2019 Mar;469:781–91.

[102] Luo H, Cao Y, Zhou J, Feng J, Cao J, Guo H. Adsorption of NO2, NH3 on monolayer MoS2 doped with Al, Si, and P: A first-principles study. Chemical Physics Letters. 2016;643(2):27–33.

[103] Mao Y, Long L, Yuan J, Zhong J, Zhao H. Toxic gases molecules (NH3, SO2 and NO2) adsorption on GeSe monolayer with point defects

engineering. Chemical Physics Letters. 2018 Aug;706:501–8.

[104] Abdulameer MJ, Abed Al-Abbas SS, Jappor HR. Tuning optical and electronic properties of 2D ZnI2/CdS heterostructure by biaxial strains for optical nanodevices: A first-principles study. Journal of Applied Physics. 2021;129(22).

[105] Guo S, Yuan L, Liu X, Zhou W, Song X, Zhang S. First-principles study of SO2 sensors based on phosphorene and its isoelectronic counterparts: GeS, GeSe, SnS, SnSe. Chemical Physics Letters. 2017 Oct;686:83–7.

[106] Zhang J, Yang G, Tian J, Wang Z, Tang Y, Ma D. Effect of atom adsorption on the electronic, magnetic, and optical properties of the GeP monolayer: A first-principle study. Applied Surface Science. 2019 May;475:863–72.

[107] Niu F, Cai M, Pang J, Li X, Zhang G, Yang D. A first-principles study: Adsorption of small gas molecules on GeP3 monolayer. Surface Science. 2019 Jun;684:37–43.

[108] Tian J, Liu L, Xia S, Diao Y, Lu F. Optoelectronic properties of two-dimensional GaN adsorbed with H, N and O: A first-principle study. Physics Letters A. 2019 Jun;

[109] Liang XY, Ding N, Ng SP, Wu CML. Adsorption of gas molecules on Ga-doped graphene and effect of applied electric field: A DFT study. Applied Surface Science. 2017 Jul;411:11–7.

[110] Zhang X, Dai Z, Li W, Liang N, Wu X. Theoretical Calculation of the Gas-Sensing Properties of Pt-Decorated Carbon Nanotubes. Sensors. 2013;13:15159–71.

[111] Niu F, Cai M, Pang J, Li X, Yang D, Zhang G. Gas molecular adsorption effects on the electronic and optical properties of monolayer SnP3. Vacuum. 2019 Oct;168:108823.

[112] Ma D, Wang Q, Li T, He C, Ma B, Tang Y, Lu Z, Yang Z. Repairing sulfur

vacancies in the MoS2 monolayer by using CO, NO and NO2 molecules. Journal of Materials Chemistry C. 2016 Jul;4(29):7093–101.

[113] Ouyang T, Qian Z, Hao X, Ahuja R, Liu X. Effect of defects on adsorption characteristics of AlN monolayer towards SO2 and NO2: Ab initio exposure. Applied Surface Science. 2018;462:615–22.

[114] Cox PA. Introduction to quantum theory and atomic structure. UK: Oxford University Press; 1996. 90 p.

[115] Tamalampudi SR, Lu YY, Kumar U. R, Sankar R, Liao CD, Moorthy B. K, Cheng CH, Chou FC, Chen YT. High Performance and Bendable Few-Layered InSe Photodetectors with Broad Spectral Response. Nano Letters. 2014 May;14(5):2800–6.

[116] Late DJ, Liu B, Matte HSSR, Rao CNR, Dravid VP. Rapid Characterization of Ultrathin Layers of Chalcogenides on SiO2/Si Substrates. Advanced Functional Materials. 2012;22(9):1894–905.

الخلاصة

تم استخدام نظرية الكثافة الوظيفية (DFT) لدراسة الخصائص الالكترونية و البصرية و الامتزاز لجزيئات الغاز (CO , CO_2 , NO , NO_2 , SO_2) على الطبقة الاحادية HfSSe (Se,S) . في البداية , تم حساب خصائص الطبقة الاحادية HfSSe البكر تم تقدير فجوة النطاق ل HfSSe (Se,S) لتكون (0.626 eV) التي تسمح بسلوك اشباه الموصلات . يمكن ان تصل معاملات الامتصاص ل HfSSe البكر الى 10^6 cm^{-1}, وهي مماثلة للخلايا الشمسية لبيروفسكايت . تظهر النتائج ان امتزاز الغازات يحدث في مواقع مختلفة على الطبقة الاحادية التي تمت دراستها . ومع ذلك , فأن جميع طاقات الامتزاز سلبية وامتزاز جزيئات الغاز على هذه الطبقة الاحادية يخضع لتفاعل الامتزاز الفيزيائي , وبالتالي يمكن استخدامها للكشف عن جزيئات الغاز . وقد تم التوصل الى ان التفاعلات بين الطبقة الاحادية المذكورة اعلاه وجزيئات الغاز هي تتاثر بنية نطاق الطاقه للطبقة الاحادية بشكل كبير . و بالاضافة الى ذلك , فان هياكل الحزمة للطبقة الاحادية HfSSe (Se , S) بعد امتزاز غاز NO تكون موصلة . بالاضافة الى ذلك , فأن هياكل الحزمة في الطبقة الاحادية HfSSe بعد امتزاز غاز SO_2 , فجوات الحزمة في الانظمة الممتزه في HfSSe للSe هي موصلة و فجوة الحزمة في HfSSe لل S هي (0.025 eV) . يمكن ان تكون الخصائص البصرية لهذة الطبقة الاحادية يمكن تعديلها عن طريق امتزاز جزيئات الغاز . معامل الانكسار للطبقة الاحادية HfSSe لل S اكبر من تلك الموجودة في الطبقة الاحادية HfSSe لل Se , وتصل الى 2.50 و 2.31 للغازات ال CO_2 و SO_2 , على التوالي . من ناحية اخرى , تحدث قمم انعكاس الطبقة الواحدة في نطاق منطقة الاشعة فوق البنفسجية التي تتفق مع معامل الامتصاص . الى جانب ذلك , لا تتجاوز القيمة القصوى للانعكاسية في الانظمة الممتزة 60% . وقد تم التوصل الى ان ال HfSSe احادي الطبقة هو الاكثر ملائمة كمستشعر لغاز CO , CO_2 , NO , NO_2 , SO_2 بسبب وجود عملية الامتزاز . و اخيرا , توفر الحسابات طريقة فعالة لتعديل الخصائص الالكترونية والبصرية للطبقة الاحادية HfSSe لتطبيقات الاجهزة البصرية والنانوية .

جمهورية العراق
وزارة التعليم العالي والبحث العلمي
جامعة بابل
كلية التربية للعلوم الصرفة
قسم الفيزياء

تأثير امتزاز بعض الجزيئات على الخصائص الإلكترونية والبصرية للطبقة الأحادية HfSSe

رسالة مقدمة إلى
مجلس كلية التربية للعلوم الصرفة جامعة بابل كجزء من متطلبات نيل درجة الماجستير في التربية / الفيزياء

من قبل
غفران فلاح ابراهيم حسن
بكالوريوس تربية علوم (فيزياء)
جامعة بابل 2013م

بأشراف
أ. **د. شروق صباح عبد العباس**

1444هـ 2022م